

**Study on Metabolic Behavior of Pesticides in
Aquatic Plants: Uptake, Translocation and
Metabolism by Water Milfoil**

(水生植物における農薬の代謝挙動に関する研究：
フサモにおける取込み、植物内移行、代謝を中心に)

Daisuke Ando

**The United Graduate School of Agricultural Sciences,
Tottori University**

Doctoral Thesis

2019

Table of Contents

	Page
Abbreviations.....	1
1. Introduction	3
1.1 . Importance of Pesticide Risk Assessment for Water Milfoil.....	3
1.2 . General Knowledge of Pesticide Behavior in Terrestrial and Fresh Water Aquatic Plants	5
1.3 . Object of The Study.....	13
2. Fate Comparison of Pesticides Between Terrestrial and Fresh Water Aquatic Plants	15
2.1. Behavior of Insecticide Metofluthrin.....	15
2.1.1. Metabolism of Metofluthrin in Cabbage.....	17
2.1.2. Metabolism of Metofluthrin in Water Milfoil.....	41
2.1.3. Fate Comparison Between Cabbage and Water Milfoil	49
2.2. Behavior of Fungicide Mandestrobin	50
2.2.1. Metabolism of Mandestrobin in Wheat.....	51
2.2.2 Metabolism of Mandestrobin in Water Milfoil.....	73
2.2.3. Fate Comparison Between Wheat and Water Milfoil	80
2.3. Conclusion	81
3. Development of Experimental Design to Investigate Uptake, Translocation and Metabolism of Chemicals by Water Milfoil.....	82
4. Uptake, Translocation, and Metabolism of Phenols by Water Milfoil: Kinetic Analysis and Correlation With Physicochemical Properties.....	95
5. Fate of Flumioxazin in Aquatic Plants, Two Algae, Duckweed and Water Milfoil.....	115
6. Overall Summary, Discussion and Conclusion.....	141
7. References	148
8. Acknowledgement.....	167
9. Synopsis	168
10. The List of Published Articles as Base of The Doctoral Thesis	170

Abbreviations

ABC transporter: ATP (adenosine triphosphate)-binding cassette transporter

ADME: absorption, desorption, metabolism and excretion

AR: the applied radioactivity

BCF: bioconcentration factor

BMF: biomagnification factor

CYP: cytochrome P450

DEPT: distortionless enhancement by polarization transfer

DOM: dissolved organic matter

DT₅₀: degradation half-life time

EC₅₀: 50% effect concentration

EC: European Commission

ECOD: 7-ethoxycoumarin-*O*-deethylase

EFSA: European Food Safety Authority

EROD: 7-ethoxyresorufin-*O*-deethylase

EU: European Union

FAO: Food Agriculture Organization of the United Nations

GSH: glutathione

¹H-¹H COSY: correlation spectroscopy

HCH: hexachlorohexane

HMBC: hetero-nuclear multiple-bond connectivity

HPLC: high-performance liquid chromatography

HRMS: high resolution mass spectrometry

HSQC: hetero-nuclear single quantum coherence

LC-ESI-MS: Liquid chromatography-electrospray ionization-mass spectrometry

LOD: limit of detection

log *K*_{ow}: logarithm of octanol/water partition coefficient

LSC: liquid scintillation counting

NOE: nuclear overhauser effect difference

NOEC: non-observed effect concentration

NOESY: NOE correlated spectroscopy

PCB: polychlorinated biphenyl

QoI: quinone outside inhibitor

ROS: reactive oxygen species

SOM: superoxide dismutase

TLC: thin-layer chromatography

TMS: tetramethylsilane

TRR: the total radioactive residue

TSCF: transpiration stream concentration factor

US: United States

FAMIC: Food and Agricultural Materials Inspection Center

PEC: predicted environmental concentration

1. Introduction

1.1. Importance of Pesticide Risk Assessment for Water Milfoil

Synthetic pesticides are chemical products which contribute to our continuous supply of agricultural food products by controlling harmful insects, fungus and weeds, and have been recognized as one of the important measures to encounter growing concerns for food shortage accompanying global population growth. Also, non-agricultural use of insecticides for household and public hygiene helps us to improve our living standards, and especially in developing countries, to refuge from infection such as malaria and dengue diseases mediated by mosquito or other vectors. While providing considerable profits, pesticides may cause adverse effects for crop consumers or users, workers, bystanders and wild lives, hence, safety for each of them must be assured. In addition, since they are directly sprayed or applied at outdoor environment, pesticides may unintentionally enter into fresh water aquatic ecosystem by spray drift, run-off, drainage or accidental spills. From such aspect, risk evaluation for aquatic ecology is necessary and has been gaining much attention in recent years.

The fresh water aquatic ecosystem consists of wide variety of aquatic organisms including aquatic plants as primary producers, animal planktons and larger fish or other predators, establishing sustainable trophic food chain and nutrient circulation through complex interactions in the aquatic community. Among them, aquatic plants are very important for production/circulation of oxygen and nutrient which securely provide precious food and shelter for many aquatic biota (Scheffer 1988; Maltbny et al. 2009; Lewis 1995). They play key functions in biochemical cycles, through, for example, organic carbon production, phosphorous mobilization, the transfer of other trace elements, siltation of particulate matter as carbon sinks. They also directly influence the hydrology and sediment dynamics of fresh water ecosystems through their effects on water flow and particle trapping and re-suspension (Marion and Pailisson 2002; Madesen et al. 2001).⁵⁻⁶ Because of their significance, adverse effects on aquatic plants will give serious impacts to deteriorate the overall aquatic ecosystem.

Herbicides and plant-growth regulators, from the aspect of their specific mode of actions uniquely designed for plants, may cause substantial damages toward non-target aquatic plant species. In the risk assessment for fresh water aquatic plants in EU, the acute toxicity data (EC₅₀) for two algae and one macrophyte such as *Lemna* sp. had been required to determine fundamental adverse effect to aquatic plants (EC 2002) (for comparison, test with one and four algae is normally required in Japan and US registration, respectively, although additional species are required in case by case basis, thus, EU intends to cover wider aquatic plants for the risk assessment). However, the limited assessment with these suspended or floating species may not be sufficient to cover entire aquatic flora, due to the sediment-rooted macrophytes may potentially be exposed to chemicals not only from the water but additionally from the bottom sediment *via* root uptake, especially in the case pesticides preferentially bound to the sediment (Lewis 1995; Belgers et al. 2007; Cedergreen et al. 2004b; Turgut and Fomin 2002). From such affairs, in the latest aquatic guidance issued by EFSA in 2013, the risk assessment for submerged-rooted macrophytes, water milfoil as representative, was newly included as additional toxicity test species to be evaluated, if both algae and *Lemna* are highly susceptible to the chemical or if chronic sediment exposure is to cause concerns.

As indicated, there are two major routes that water milfoil may be exposed to pesticides; shoot exposure *via* water column and root exposure *via* sediment, and these events could occur simultaneously. And after the pesticides entered into the macrophyte, they will be translocated within the plant from root to shoot and *vice versa* with receiving metabolism/detoxification. While toxicological effect of pesticides are widely investigated, the information of metabolic behavior in aquatic plants is limited. And especially, there are few studies focused to clarify the uptake, translocation and metabolism of pesticides individually after shoot and root exposures. Since such knowledge is essential for understanding toxicity mechanism of the pesticides and for detailed risk evaluations, we developed an experimental design and studied the behavior of simple chemicals and a herbicide.

1.2. General Knowledge of Pesticide Behavior in Terrestrial and Fresh Water Aquatic Plants

To understand the behavior of pesticides in water milfoil, basic knowledge from terrestrial and fresh water aquatic plants are important. In this section, the information is briefly summarized, focusing on uptake, translocation and metabolism supplemented by abiotic factors affecting on the processes.

Terrestrial Plants

Foliar Uptake

The application of a pesticide is generally classified into foliar and soil treatments. The behavior of pesticide in the former treatment has been investigated extensively, not only experimentally but also theoretically by many researchers, but fewer investigations are available for the latter. The foliar uptake is initiated by penetration of pesticide through cuticle and sometimes stomata, followed by apoplastic, symplastic transport or phloem translocation, whereas root hairs play the most important part in absorption of pesticide from soil (Field and Dastgheib 1996). The cuticle is a complex structure consisting of a pectin layer that binds the cutin to the epidermal cell walls and a layer of epicuticular wax on the outside, and this structure as well as thickness depends on plant species (McFarlane 1995; Bianchi 1995), which often causes difference in pesticide retention on plant surface among plant species. The aerial surfaces of all higher plants carry a partial or continuous coverage of amorphous wax and that formation of crystalline wax is frequently embedded on amorphous layers (Baker 1982). The wax mainly composed of long-chained organic acids, aldehydes, hydrocarbons, primary/secondary alcohols, β -diketones (these up to C_{35}), these alkyl esters and triterpenoids (Bianchi 1995; Baker 1982). As general acceptance, the penetration of pesticide through the epicuticular wax or cuticle tends to increase with enhancing the hydrophobicity of the chemicals which is often described by $\log K_{ow}$. Although appropriate $\log K_{ow}$ is certainly the prerequisite property, it is not the only factor determines the foliar penetration, but molecule size, concentration, surface tension, deposit area, crystalline nature and so on also contribute significantly (Baker et al. 1992; Stevens et al. 1988; Wang and Liu 2007).

On the other hand, hydrophilic chemicals are also known to diffuse through the cuticle *via* polar pathway, so-called ‘aqueous pores’ which appear to be located around guard cells, glandular trichomes or clacking (Schönherr 2002, 2002, 2006; Schlegel et al. 2005). In addition to the above observations, the pesticide permeation through plant surface is critically affected by formulation or adjuvant which usually promotes and in some cases suppresses, depending on the type of its physicochemical character, contents and application ratio (Katagi 2008).

By the way, concomitantly or before the penetration, pesticides undergo sunlight-induced decomposition as the initial degradation process. Generally, most pesticide molecules have a substituted aromatic ring being connected with some lone-pair electrons or unsaturated bonds such as carbonyl or carbamoyl group, thus, exhibit a UV-vis absorption spectrum at >290 nm and gain solar energy to be shifted to the excited state (Katagi 2004; Burrows et al. 2002). Unless the energy of the excited molecule is lost by heat or light emission, it undergoes various reactions in the molecule. When carbonyl bond exists, C-C bond cleavage generates the ketyl radical (Norrish type I), or the carbonyl carbon in the excited state abstracts hydrogen from a neighboring alkyl group (Norrish type II) (Katagi 2004). The homolytic/heterolytic bond cleavage provides various photoproducts, while re-bond causes geometrical/optical isomerization or intramolecular rearrangement such as photo-Fries type rearrangement and cyclization or creating a new bond between nearby functional group *via* intramolecular transference (Katagi 2004; Remucal 2014). Even if the pesticide does not absorb the sunlight, the indirect reactions with ROS such as hydroxyl radical, $^1\text{O}_2$, ozone, peroxides and etc., deeply involve in the degradation (Katagi 2002; Burrows et al. 2002; Remucal 2014). And all these direct/indirect photodegradation profiles are influenced by surrounding medium, structural/physicochemical heterogeneity of plant surface, formulation type and state of the pesticides, where most of the pesticide photodegradation studies were conducted in the solubilized form in organic or aqueous solution, and studies in the solid state are limited which may exhibit difference in light absorption spectrum, restricted structural rotation, and give unique degradates (Katagi 2004).

Root Uptake

In addition to the foliar uptake, pesticides in soil can be taken up by plants. A

pesticide solute taken up can be transported to shoot along the transpiration stream at the xylem vessel, the water vapor at shoot as a driving force. To reach the xylem vessels, two pathways has been proposed. One is the apoplastic pathway, *via* the cell wall space of the epidermis and cortex, then, across cell membranes at the endodermis region (Bromilow and Chamberlain 1995). In the species that develop an exodermal Casparian strip (Peterson 1988), the pesticide solute must also cross the membrane at the exodermis region. The other path is the symplastic route, crossing cell membranes of root hairs, epidermis or cortex and moving to stele by successive permeation through plasmodesmata and membranes. The balance between the pesticide distribution in the apoplastic-symplastic compartments determines the overall transport pattern (Bromilow and Chamberlain 1995). Among physicochemical properties, lipophilicity is believed as the most important factor for root uptake. Briggs et al. (1982) examined the root uptake of chemicals by barley in the hydroponic system and correlated TSCF (concentration of the chemical taken up from root to shoot through xylem sap against the root exposure concentration) with $\log K_{ow}$, and found the well-cited bell-shaped uptake curve which has a vertex at $\log K_{ow}$ 1.8 as the maximum, while the concentration in root kept increasing along with $\log K_{ow}$. This indicate that high lipophilic compounds irreversibly stick to root surface and become immobile. The similar trends are reported from many researchers by conducting hydroponic experiments, and even in the presence of soil, where the pesticide competitively distributes among soil particles or organic matters, pore water and root through adsorption/desorption (Hsu et al. 1990; Ryan et al. 1988). In this case, the bell-shaped curve shifts to lower or higher $\log K_{ow}$ region, e.g., to lower region when contents of organic matters that binds pesticide increases. On the other hand, Dettenmaier et al. (2009) obtained the sigmoid plot to conclude that substances having lower $\log K_{ow}$ with high water solubility are suitable for root uptake. Since the experimental method, test substance, test condition, plant species and etc. are not identical, it is likely that the definitive conclusion for the responsible chemical properties for root uptake are still questionable and require more studies (Doucette et al. 2009).

It should be noted that, in addition to the sunlight-induced photodegradation on the soil surface followed by leaching, pesticides receive degradation in soil in parallel to the root uptake. In soil, biotic degradation by microbes and abiotic reactions induced by the

physicochemical properties occur. Microbial metabolism cause various reactions such as reduction at olefins, nitro, sulfone and other groups, oxidation at alkyl and benzene rings, dehalogenation, radical-mediated chain reactions and etc. (Vicente and Yolanda 2004; Sassman et al. 2004; Ghadiri and Rose 2001; Itoh et al. 2000). The abiotic ones are mainly hydrolysis, reduction catalyzed by redox reactions (Macalady et al. 1986), and interestingly, nitration was also reported as unique reaction (Kodaka et al. 2003).

Translocation

With respect of the pesticide translocation in plants, general acceptance is that pesticides with moderate lipophilicity show good transferability, due to the excess degree in lipophilicity cause strong irreversible adhesion on plant components, while immoderately polarized chemicals are repulsed from intrusion into inner plant, both result in a poor systemicity (Tyree et al. 1979). Hsu et al. (1996) studied the translocation of chemicals in plants and showed the mobility isotherm correlating pK_a and $\log K_{ow}$ which suggested the highest migration potential around pK_a 3 to 8 and $\log K_{ow}$ 2. Similar trends have been proposed in other studies (Bromilow and Chamberlain 1995; Satchivi et al. 2006), and these physicochemical properties are likely the important factors controlling the mobility of chemicals.

Incidentally, if the penetration barrier into plant was ignored, namely the foliar and root uptake processes, then the requirement of $\log K_{ow}$ is diminished and solubility (or pK_a) can be the dominant factor for transferability since the apoplastic and symplastic paths are the major pathway of water or mineral transport in plants (Campbell and Reece 2002). In many cases for the plant metabolism study of pesticides, e.g., triazole fungicides e.g., buromuconazole (EFSA 2010), organophosphates, e.g., dimethoate and Tolclofos-methyl (EFSA 2017, 2018), strobilurins, e.g., mandestrobin (EFSA 2015), and so on, at pesticide-untreated parts of the plant, the pesticide-derived residues often consisted of metabolites transported from distant area and have relatively high water solubility, while a limited parent pesticide was translocated. The fact supports the importance of solubility in considering the translocation of metabolites generated at inner plants.

Metabolism

After or in parallel to the translocation, pesticides undergo metabolism by various enzymatic reactions in plants which generally be categorized into three stages: phase I as basic detoxification, II as conjugation with small biomolecules and III as the final step for sequestration into vacuole or incorporation into plant natural components like pectin, lignin and cellulose. Various reactions such as hydroxylation, oxidation, epoxidation, demethylation, dealkylation, dehalogenation and sometimes reduction are known as phase I reactions basically to increase the solubility of the xenobiotics for detoxification and these are believed to be mostly mediated by CYP, Flavin-containing monooxygenases, laccases and other oxygenases (Kreuz et al. 1996; Van Eerd et al. 2003). In phase II, plants show diverse conjugation at hydroxyl, amine, carbonyl groups or sometimes directly on aromatic ring of xenobiotics, with multiple natural small compounds, including saccharides, amino acids, organic acids, GSH and even other complex phytochemicals. Phase III, though it is still not well understood, is the terminal step to store and remove the metabolites to ‘sink,’ as alternative path to the strategy of animals excreting xenobiotics by urine or feces since plants do not have such functions. Because the above detoxification mechanisms, mostly in phase I and II, have some similarity to the reactions in mammalian hepatic systems, the term ‘green liver’ was adopted by Sandermann (1994). However, since not only the parent pesticide but also its degradates entered from plant surface and soil, mostly generated through the reactions by sunlight and by microorganisms or chemical reactivity in soil, respectively, are further metabolized in plants, it should be emphasized that the metabolites in plants are often more complicate and diverse.

Fresh water aquatic plants

Although it may not be directly applicable, the basic information summarized the above is useful to consider the behavior of pesticide in aquatic plants. On the other hand, compared to the terrestrial plants, the information is critically less for aquatic plants, especially for water milfoil. In this paragraph, we aimed to focus on the knowledge on water milfoil.

Shoot Uptake

Macrophyte cuticular membranes are generally thin (c.a. 20 nm versus ~4000 nm for terrestrial plants) (Denny 1980; Jeffree 2006), though their tissues likely contain comparable wax contents to terrestrials, e.g., 0.2% for *Myriophyllum spicatum* (water milfoil) on a wet weight basis (Gobas et al. 1991). The wax of macrophyte mainly consists of shorter *n*-alkyl lipids, length from C₂₀ to C₂₄, than the terrestrial plants (Gao et al. 2011), which may provide a higher fluidity. In addition, it was reported that the isolated cuticular wax of a fully submerged macrophyte, shining pondweed (*Potamogeton lucens*), is more permeable to water by a factor of 1000 than those of terrestrials (Schönherr 1976). These information indicate that low log K_{ow} chemicals are possibly enable to penetrate into the water milfoil. However, hydrophobic chemicals still tend to be accumulated by macrophyte surface as summarized elsewhere (Wolf et al. 1991; Turgut 2005; Arnot and Gobas 2006; Katagi 2010). For instance, Gobas et al. (1991) found the positive linear relationship between that the accumulation of chemical, expressed as BCF (calculated from the uptake (k_1) and depuration rate constants (k_2) as k_1/k_2), and log K_{ow} , and showed that the bioconcentration elevates as log K_{ow} value increases. Similar tendency was reported for waterweed and duckweed, except for the difference that the accumulation of hydrophilic chemicals at low log K_{ow} range, approximately below 1, lost the linearity and plateaued to exhibit the minimum uptake potential (Carvalho et al. 2007). And the accumulation degree of pesticides is generally attenuated by the presence of DOM that interact with the pesticide through ion exchange, hydrogen bond, charge transfer, π - π stacking and so on, reducing the availability of the pesticide in water column (Haizer et al. 1998).

The initial abiotic reactions in aquatic plant exposure are aqueous photolysis and hydrolyses. The relative contribution of each process highly depends on the chemical structure of the pesticide, and regarding the hydrolysis, most pesticides are stable at neutral aqueous condition at ambient temperature, so its contribution is usually limited, except for pesticides having hydrolytically labile ester linkage such as phosphorous, carbamate or pyrethroid types (Katagi 2002). The presence of DOM in the water could both assist and suppress the photolysis, serving as photosensitizer and as antioxidant, light screening or sink for ROS (Burrows et al. 2002). Incidentally, it is expected that the degradates, generated either by photolysis, hydrolysis or both, are less accumulative than

the parent pesticide for aquatic plants, due to the lower lipophilicity. However, this may not be the case when rearranged products are to be occurred, mainly by photolysis, since they possibly show comparable hydrophobicity as the parent, and especially, even higher for cyclization products (Dimou et al. 2004).

Root Uptake

In respect of the root uptake, for example, Carvalho et al. (2007) studied the root uptake by parrot feather having emergent shoot using the hydroponic system and obtained the bell shape relation between TSCF and $\log K_{ow}$, as observed for barley (Briggs et al. 1982), while the uptake amount was somewhat less in parrot feather. But in the case of submerged macrophytes, transpiration stream underwater must be much inactive and the TSCF concept may not be applied. To the best of our knowledge, the root uptake study of organic chemicals in sediment-inclusive test systems with submerged condition has been described only for *Myriophyllum spicatum* with one herbicide (Burešová et al. 2013), *Hydrilla verticillata* with three insecticides (Hinman and Klaine 1992), and for *Myriophyllum spicatum* with two herbicides and PCBs (Dipens et al. 2014). The last two studies measured the concentration of test chemicals in root and shoot by applying the special exposure system introducing the Teflon boundary to separate shoot and root regions, and selectively exposed the root of the macrophytes. These two studies showed agreement for the accumulated concentration of the test chemicals in root with literature that the accumulation increases along with $\log K_{ow}$, however, the translocated concentration in shoot differed from the typical trait (Briggs et al. 1982; Carvalho et al. 2007; Trapp 2000), namely the bell shape relationship, indicated the effects of sediment interaction and diminished level of transpiration stream underwater condition are considered.

Metabolism

With respect to the manner of metabolism of xenobiotics, aquatic plants prone to have similarities with terrestrial plants, namely, possess phase I and II (and III) systems. For instance, transcriptome analysis of alga and lemna revealed that they encode a variety of CYP families, peroxidase, oxidases which are presented in terrestrial plants (Bhattacharya et al. 2013; Wang et al. 2016). Though which family or species take part

in the pesticide metabolism is mostly unknown, as well as for terrestrial plants, it is expected that aquatic plants have the analogical potential. In fact, many hydroxylation reactions, which is the most basic one, on xenobiotics have been reported in a wide variety of aquatic plants including water milfoil (Katagi 2010; Ensley et al. 1994; Barber et al. 1995; Sharma et al. 1997; Wang et al. 2017). In the detoxification of organic compounds in algae and macrophytes, phase I metabolic reactions by pseudo-cytochrome P450 or its isozymes such as EROD (7-ethoxyresorufin-*O*-deethylase) and ECOD (7-ethoxycoumarin-*O*-deethylase) have been reported (Torres et al. 2008; Thies et al. 1996; Pflugmacher and Steinberg 1997; Pflugmacher et al. 1999). Similarly, phase II reactions against xenobiotics to generate glucose and GSH conjugates are known in aquatic plants (Pflugmacher et al. 1999; Pflugmacher and Snadermann 1998a; Pflugmacher et al. 2000). Thus, it is likely that aquatic plants have similar detoxification capacity to terrestrial plants. There may be the possibility that the metabolites of xenobiotics can be excreted back to water column, however, definitive evidence for such ability is not known. On the other hand, macrophytes possess vacuoles (Talarico 2002) and accumulation of some xenobiotics in the organ has been reported (Bondareva et al. 2012), which is the similar mechanism to terrestrial plants.

1.3. Object of The Study

In chapter 1, the importance of risk assessments of pesticides on water milfoil was described. Unlike algae and floating macrophytes, submerged, sediment-rooted macrophytes, water milfoil as representative, may be exposed to pesticides not only *via* water column, but *via* sediment as the additional route if the pesticide is absorbed to sediment. For robust hazard characterization(s) on water milfoil, it is essential to understand the behavior of pesticides in detail, namely, metabolic reactions in the plant following shoot/root uptake and translocation.

As fundamental knowledge, behaviors of chemicals in uptake followed by translocation and metabolism were briefly summarized for terrestrial and aquatic plants. From the literature review, it was considered that biotic and abiotic reactions at outer plant could largely affect the fate of pesticides prior to be taken up by plants, depending on the chemical structure of the pesticide. The uptake is likely a process highly dominated, but not totally, by the physicochemical parameters such as hydrophobicity, water solubility and acidity, which may be applicable for water milfoil. However, since the structural difference and limited transpiration stream under submergence, a definitive relationship between physicochemical natures and shoot/root uptake by water milfoil requires further studies. With respect of the metabolic reactions, aquatic plants likely possess phase I, II (and III) mechanisms which can widely be seen for terrestrial plants and considered mostly similar, however, since only a limited information is available for water milfoil, this is not conclusive.

On the contrary to the lack of knowledge on water milfoil, it is cardinal to understand the fate of pesticides, namely, uptake/translocation/metabolism (and excretion, though not expected), so called ADME in the pharmacological research, for detailed toxicological assessment on the species. Moreover, in the case when unexpected, toxic metabolites are generated from pesticides in water milfoil, there is a risk(s) for further bioaccumulation/biomagnification through ecological food-chain to give adverse effects on higher organisms. To gain insight into the behavior of pesticides in water milfoil as essential knowledge for robust hazard characterization, the author have studied and clarified the fate of various compounds including simple chemicals, fungicide, insecticide

and herbicide, particularly by applying a newly developed exposure system designed to selectively expose the chemical to either shoot or root of water milfoil *via* water medium or *via* sediment, respectively.

In chapter 2, cabbage/wheat and water milfoil were exposed to the insecticide metofluthrin, a synthetic pyrethroid for hygiene usages, and the fungicide mandestrobin, a strobilurin to control wide range of crop diseases, as model case comparisons to experimentally confirm the differences of pesticide behavior in terrestrial plants and water milfoil.

In chapter 3, to establish the new exposure system which enables to separately expose either shoot or root and to reveal each uptake followed by translocation and metabolism behavior, 3-phenoxybenzoic acid was applied as the model test compound and validated the method.

In chapter 4, to understand basic relations between uptake/translocation/metabolism and the physicochemical properties of exposure compounds, the behavior of simple phenols were examined using the developed exposure system. The kinetics analysis of each behavior was implemented and compared with various chemical indexes.

In chapter 5, the fate of the widely used herbicide flumioxazin on water milfoil was investigated. For comparison, two algae and one floating macrophyte were also exposed to the herbicide.

In chapter 6, the newly obtained results are summarized, the importance of the study and contribution to the risk evaluations on aquatic plants are discussed, then, the overall conclusion is given.

2. Fate Comparison of Pesticides Between Terrestrial and Fresh Water Aquatic Plants

As described in the previous chapter, one of the critical factors determining the overall fate of pesticides could be the external abiotic/biotic reaction(s) involved under each circumstance where the plant is exposed to the compound. For terrestrial plants cultivated on the ground, pesticides applied on plant and soil surfaces receive direct/indirect photolysis and reaction by microorganisms as the initial driving forces for degradation before or simultaneously with the foliar/root uptake up followed by translocation and metabolism at inner plant. On the other hand for aquatic plants in fresh water, in addition to the aqueous photolysis, chemical hydrolysis as well as some biotic reactions by suspending microorganism and periphyton could take major roles for the decomposition.

To experimentally clarify such possibilities, we examined and compared the behaviors of pesticides in terrestrial and aquatic plants, using cabbage and wheat as terrestrial representative and water milfoil. Metofluthrin was selected as one of the two test compounds, since it possesses isopropenyl and ester bonds which are considered susceptible to direct/indirect sunlight photolysis and hydrolytically instable, respectively, during the exposure. The other test substance chosen was mandestrobin. In contrast to metofluthrin, mandestrobin is stable in water, while it is known to be somewhat reactive to photolysis. The obtained experimental results showed dissimilar trends between terrestrial plants and water milfoil, demonstrating the importance of the external factors which substantially affected the overall behavior of pesticides in the test plants.

2.1. Behavior of Insecticide Metofluthrin

Metofluthrin (**1**) [SumiOne[®], Eminence[®]; 2,3,5,6-tetrafluoro-4-(methoxymethyl)-benzy (*EZ*)-(1*R*,3*R*)-2,2-dimethyl-3-(prop-1-enyl)cyclopropanecarboxylate], structure given in Table 1, is a pyrethroid insecticide for household and public hygiene usages developed by Sumitomo Chemical Co., Ltd., possessing a strong knockdown activity

especially against mosquitoes. Because of its high volatility (1.96×10^{-3} Pa) with a low mammalian toxicity, **1** can be used in the non-heated formulation such as fan-type, paper and resin emanators (Matsuo et al. 2005). The presence of the two optical centers at the cyclopropenyl ring and one geometrical isomerism at the propenyl side chain results in eight isomers, and **1** consists of the biologically active *1R-trans* isomers having a *E/Z* geometrical ratio of 1/8, abbreviated as **1-RTE** and **1-RTZ** (Matsuo et al. 2005). The extremely limited emission of **1** to the environment is most likely because it is mainly used in indoor. However, as there is no geographic restriction, outdoor use, **1** may directly or indirectly reach to a non-target environment such as water body, soils and terrestrial and aquatic plants by personal outside insect repellent and other outdoor use. In addition, with regards to biocide, the submission of the relevant data to an environmental fate has recently become inevitable irrespective of the use pattern especially in EU and EPA due to the possible contamination by sewage treatment plant effluent. From these aspects, it is important to obtain experimental data of **1** to show that it is benign to the environment.

Several studies of **1** showed the degradation behaviors of **1** in environment, as shown in Figure 1. The aerobic soil metabolism in two US soils has shown that ^{14}C labeled **1-RTZ** and **1-RTE** rapidly degrade at the similar half-lives 2.3–3.5 days *via* cleavage of the ester linkage to produce corresponding acid (**7**) and alcohol (**10**), followed by successive oxidation at the prop-1-enyl group and the benzyl carbon to form terephthalic acid (**9**) and dicarboxylic acid (**11**) derivatives, respectively (Kodaka et al. 2007). Further degradation of the metabolites resulted in production of carbon dioxide. The radioactivity was also detected as the soil bound residues which might derived from the high soil adsorption coefficient (K_{oc}) of **1-RTZ** determined as 3,553–6,142 (mL g^{-1} o.c.) by the batch equilibrium method (Kodaka et al. 2007). No enantiomerization and geometrical isomerization proceeded in the soils. Under illumination on the moisture-controlled soil, **1-RTZ** degraded with DT_{50} 8.1–12.0 days (Nishiyama et al. 2010; Nishimura et al. 2011). The photodegradation pathway was oxidation of the double bond at the prop-1-enyl moiety and cleavage of the ester linkage followed by further decomposition to polar compounds and mineralization to carbon dioxide. The major degradates detected were caronaldehyde (**4**) and carboxylic acid (**5**) derivatives which were possibly generated by decomposition from ozonide (**2**) and diol (**6**) produced by the

activated oxygen species, *i.e.* ozone and hydrogen peroxide, respectively. The photoisomerization hardly proceeded throughout the test duration (Nishimura et al. 2011). In the hydrolysis study, **1-RTZ** moderately degraded by the ester cleavage with the half-life 26.8 days at pH 9 and 25°C, while it was much stable at pH 5 and 7. For aqueous photolysis using Xenon arc lamp, **1-RTZ** and **1-RTE** rapidly dissipated with their half-lives 1.1–3.4 days at pH 7 mainly due to ester cleavage to produce **7** and **10**, and oxidation of the olefinic double bond to form **3** and **4** while isomerization was a minor route (Nishiyama et al. 2010).

Up to this date, metabolism studies of **1** by terrestrial and aquatic plants are not available. In addition to our purpose for the behavioral comparison between these plants, the information is necessary for the toxicological assessments in human and non-target species, and hence, the studies are useful. Cabbage was selected as a model plant because its broad and waxy leaves (Baker 1982) have potential to trap and minimize the loss of **1** by its rapid volatilization from leaf surface (Katagi 2004).

2.1.1. Metabolism of Metofluthrin in Cabbage.

MATERIALS AND METHODS

Chemicals

The non-radiolabeled metofluthrin (**1**) and their potential degradates as follows were synthesized in our laboratory according to the reported methods (Kodaka et al. 2007; Nishiyama et al. 2010; Nishimura et al. 2011). The structure of the compounds are referred to Table 1; 2,3,5,6-tetrafluoro-4-(methoxymethyl)benzyl (1*R*,3*R*)-2,2-dimethyl-3-(3-methyl-1,2,4-trioxolane-5-cyclopropanecarboxylate (**2**), 2,3,5,6-tetrafluoro-4-(methoxymethyl)benzyl (1*R*,3*R*)-2,2-dimethyl-3-(3-methyl-1,2-epoxy)cyclopropane carboxylate (**3**), 2,3,5,6-tetrafluoro-4-(methoxymethyl)benzyl (1*R*,3*R*)-2,2-dimethyl-3-formylcyclopropanecarboxylate (**4**), 2,3,5,6-tetrafluoro-4-(methoxymethyl)benzyl (1*R*,3*R*)-2,2-dimethyl-3-carboxycyclopropanecarboxylate (**5**), 2,3,5,6-tetrafluoro-4-(methoxymethyl)benzyl (1*R*,3*R*)-2,2-dimethyl-3-(1,2-propanediol)cyclopropane carboxylate (**6**), 2,3,5,6-tetrafluoro-4-(methoxymethyl)benzyl alcohol (**7**), 2,3,5,6-tetrafluoro-4-(methoxymethyl)benzoic acid (**8**), tetrafluoroterephthalic acid (**9**), (1*R*,3*R*)-

2,2-dimethyl-3-(*E,Z*)-propenylcyclopropanecarboxylic acid (**10**), (1*R*,3*R*)-2,2-dimethyl-3-carboxycyclopropanecarboxylic acid (**11**). The chemical purity of each standard was determined to be >95% by HPLC. Degradate **2** was prepared by the following method. Each 3 mg of **1-RTZ** or **1-RTE** was dissolved in 1 mL of *n*-hexane solution and cooled to <-40°C using dry ice/acetone prior to the ozone oxidation. Ozone gas produced at an approximate concentration of 20 g N⁻¹m⁻³ using an ozone generator (type 0N-1-2, Nippon Ozone, Co, Ltd.) was gently bubbled into the reaction mixture for 3 min at <-40°C, which resulted in the formation of white precipitate of crude **2**. After the solution returned to room temperature, **2** was successively purified by HPLC, the solvent was removed using evaporator and dried *in vacuo* to obtain colorless liquid whose chemical purity was determined to be >95%. The chemical structure of **2** was confirmed by various modes of NMR and LC-ESI-MS spectroscopies. **2** was stable in acetonitrile, *n*-hexane and chloroform for a few months at a freezer below 0°C, but rapidly decomposed to **4** and **5** in aqueous organic media. The following ¹⁴C labeled isomers of **1** were synthesized in our laboratory with the reported methods (Kodaka et al. 2007; Nishiyama et al. 2010; Nishimura et al. 2011); **1-RTZ** separately labeled at the α -position of 2,3,5,6-tetrafluoro-4-methoxymethylbenzyl ring (benzyl-¹⁴C) or the carbonyl carbon (carbonyl-¹⁴C) and **1-RTE** at the carbonyl carbon (carbonyl-¹⁴C) with the specific activity of 0.1654, 0.1651 and 0.1651 mCi mg⁻¹, respectively. β -Glucosidase (almond) and cellulase (*Aspergillus niger*) were purchased from Wako Pure Chemical Industries, Ltd. All the reagents and solvents used were of the analytical grade.

Chromatography

The reversed-phase HPLC analysis of metabolites within the leaf surface rinse and extract was conducted using a Hitachi LC module (model L-7000) equipped with a SUMIPAX ODS A-212 column (5 μ m, 6-mm i.d. \times 15 cm, Sumika Chemical Analysis Service, Ltd.) at a flow rate of 1 mL min⁻¹. The following gradient system was operated as the typical analysis with acetonitrile containing 0.05% formic acid (solvent A) and distilled water with 0.05% formic acid (solvent B); 0 min, %A/%B, 5/95; 0 to 3 min, 5/95, isocratic; 3 to 10 min, 45/55 at 10 min, linear; 10 to 70 min, 75/25 at 70 min, linear; 70 to 71 min, 5/95 at 71 min, linear; 71 to 80 min, 5/95, isocratic (HPLC method 1). For

the separation of four isomers of **2**, the gradient system as below was applied; 0 min, %A (acetonitrile)/%B (water), 53/47; 0 to 3 min, 53/47, isocratic; 3 to 43.7 min, 58/42 at 43.7 min, linear; 43.7-44 min, 75/25 at 44 min, linear; 44-51 min, 53/47 at 51 min, linear; 51 to 60 min, 53/47, isocratic (HPLC method 2). The chiral analysis was conducted with a Shimadzu LC-10AT HPLC system connecting two SUMIPAX DI-NO₂ columns (5 μm, 4 mm i.d.×25 cm, Sumika Chemical Analysis Service, Ltd.) and one CHIRALCEL OD-H column (5 μm, 4.6 mm i.d.×25 cm, Daicel Chemical Industries, Ltd.) in series using an isocratic eluent of *n*-hexane/ethanol, 1000/0.5 (v/v) at a flow rate of 0.9 mL min⁻¹. The radioactivity eluted was monitored with a Flow Scintillation Analyzer Radiomatic 500TR (Perkin Elmer Co., Ltd.) or Ramona (Raytest Ltd.) radiodetector equipped with a 500-μL liquid cell using Ultima-Flo AP[®] (Perkin Elmer, Co., Ltd.) as the scintillator. The detection limit of the HPLC analyses was 30 dpm. The typical retention times of **1-RTZ** and **1-RTE**, and their related reference standards are reported previously (Kodaka et al. 2007; Nishiyama et al. 2010; Nishimura et al. 2011).

One- or two-dimensional TLC was carried out for an analytical purpose using precoated silica gel 60F₂₅₄ thin-layer chromatoplates (20×20 cm, 0.25-mm thickness; E. Merck). The non-radiolabeled reference standards were detected by exposing the chromatoplates to ultraviolet light for direct visualization or spraying bromocresol green reagent to distinguish acidic compounds. Autoradiograms were prepared by transcribing the TLC plates to BAS-III_s Fuji Imaging Plate (Fuji Photo Film Co., Ltd.) for several hours. The radioactivity in each spot exposed onto imaging plate was detected by a Bio-Imaging Analyzer Typhoon (GE Healthcare). The solvent systems for 2D-TLC were chloroform/methanol, 9/1 (v/v) and toluene/ethyl acetate/acetic acid, 5/7/1 (v/v/v). For the analysis of **2**, *n*-hexane/toluene/acetic acid, 3/15/2 (v/v/v) was applied for 1D-TLC development. The typical R_f values of **1-RTZ** and **1-RTE**, and their related reference standards are reported previously (Kodaka et al. 2007; Nishiyama et al. 2010; Nishimura et al. 2011).

Spectroscopy

For NMR spectrometric analyses, one-dimensional (¹H-, ¹³C-, DEPT, NOE difference) and two-dimensional experiments (¹H-¹H COSY, HSQC, HMBC, NOESY)

were employed in *d*-chloroform including TMS using a Varian Mercury 400 (Varian Technologies Ltd.) spectrometer (400 MHz).

LC–ESI–MS analysis was conducted using a Waters Micromass ZQ spectrometer equipped with a Waters Separation Module 2695 and Photo Array Detector 2996 as a liquid chromatograph. For the conventional analysis of metabolites, the HPLC method 1 was applied with the analytical parameters controlled by the MassLynx software (version 4.00) as shown below: source temp., 100°C, desolvation temp., 350°C, capillary voltage 3.2 kV, cone voltage 10–40 V. For the analysis of **2**, source temp., 70 and desolvation temp., 300°C were selected to mitigate its thermal degradation and the gradient system as below was applied; 0 min, %A (acetonitrile)/%B (methanol/20 mM ammonium acetate (20/10, v/v))/%C (water), 5/30/65; 0 to 50 min, 20/30/50, linear.

Radioanalysis

Radioactivity in liquid surface rinse and extract from plant was determined by mixing each aliquot with 10 mL of Packard Emulsifier Scintillator Plus[®] and analyzed by LSC with a Packard Model 2900TR spectrometer. Background level of radioactivity in LSC was 30 dpm, which was subtracted from the dpm value of a measured sample. The ¹⁴C in the extracted residues and untreated plant portions were individually measured as ¹⁴CO₂ using a Packard Model 307 sample oxidizer. ¹⁴CO₂ produced was absorbed into 9 mL of Packard Carb[®]-CO₂ absorber, mixed with 15 mL of Packard Permafluor[®] scintillator and the radioactivity therein was quantified by LSC. The efficiency of combustion was determined to be greater than 95.8%.

Plant Material and Treatment

Cabbage (*Brassica oleracea var. capitata*, variety: Green Ball) was grown in a 1/5,000-are Wagner pot filled with Kasai soil (Hyogo, Japan) in a greenhouse at 25°C for day and 20°C for night, one plant in each pot, two pots for each test chemical (one pot for the leaf treatment and the other is for the soil treatment, prepared six pots in total). The application of each [¹⁴C] **1-RTZ** and **-RTE** to the cabbage plant was conducted at the head forming growth stage (BBCH 41, Figure 2) (Meier 2001). The typical surface area and weight of a cabbage leaf at the application stage were 176.6 cm² and 10.31 g, respectively. The characterization of Kasai soil is as described below: soil texture (%) sand 82.9, silt

8.9, clay 8.2; soil classification, sandy loam; organic carbon content (g/g) 1.7; pH (H₂O) 6.6; maximum water-holding capacity (g per 100 g of dry soil) 28.19.

The application dose of **1** to cabbage plants was 431 g a.i. ha⁻¹. This was determined by assuming that all the active substance sprayed once using a typical commercial can was directly/evenly applied onto cabbage, and calculated based on the total surface area of cabbage leaves: 4 g aerosol of the water-based formulation containing 0.1% (w/w) of **1** was sprayed onto a square-foot field in purpose of general insect repellent. Although the isomeric ratio of **1-RTZ** and **1-RTE** in the active ingredient is 8/1, the same dosing rate was used for each isomer in this study. For the leaf treatment, the dosing solution per leaf was prepared by mixing 0.167 MBq of each [¹⁴C] **1** isomer with 0.761 mg of the corresponding unlabeled material in 100 µL of acetonitrile (0.212 MBq mg⁻¹). The prepared dosing solution was topically applied onto the front side of one leaf using a microsyringe, and additional two leaves of the same cabbage were treated (three leaves per each test chemical). In respect of the soil treatment, the same application ratio to the cabbage plant was applied, assuming that the substance was directly applied on the soil surface. Calculated from the surface area of the Wagner pot (1/5,000-are), the dosing solution per pot was prepared by combining 1.667 MBq of each [¹⁴C] **1** with 0.862 mg of the unlabeled material in 1 mL of acetonitrile, and was applied onto 120 g of Kasai soil in a plastic bag using pipet and thoroughly mixed for 30 min. After evaporation of acetonitrile, it was gently put onto the soil surface (approximately 1 cm in height) of the Wagner pot where cabbage plants were grown. For both leaf- and soil-treated pots, water was carefully supplied until the last sampling.

Sampling, Extraction and Analysis

With respect to the leaf treatment, three cabbage leaves per pot were sequentially harvested at 2, 7 and 14 days after the treatment, one leaf at each sampling point for each radiolabel. The leaf was cut from the stem using scissors, and untreated leaves neighboring the sampled leaf or stem of the cabbage were sampled. For the soil treatment, both cabbage plant and soil were separately sampled at 14 days after treatment. The whole cabbage plant was obtained by cutting the stem just above the ground. The dried soil was vertically divided into three layers according to its depth (top, 0-2 cm; middle, 2-10 cm; bottom, 10-18 cm) and the root was removed from the soil. All

samples were immediately weighed and stored in a freezer (<-20°C) until analysis.

In the case of the leaf treatment, each sampled leaf was surface-washed and rinsed with 100 mL of acetonitrile and further extracted individually. The rinsed leaf was cut into small pieces and homogenized with 20 mL of methanol at 10,000 rpm and 0°C for 10 min using a homogenizer AM-8 (Nissei Ltd.). The homogenate was vacuum filtered to separate the extract and the plant residue. The residue remained after filtration was extracted again in the same manner, and the filtrate was combined. The process was repeated using methanol/water (4/1, v/v). Each aliquot of the surface rinse, methanol and methanol/water extracts was analyzed with LSC, HPLC and 2D-TLC. The extracted residues were air-dried and individually combusted for LSC analysis. The soil in the leaf-treated pot was sampled at the last day, mixed and directly analyzed by combustion analysis without any extraction. For the soil treatment, a portion of each soil layer was subjected to a combustion analysis to determine the residual amount of ¹⁴C. Approximately 50 g of the evenly mixed top layer soil for each label was transferred into 200-mL plastic centrifuge bottles and 100 mL of methanol was added. The bottle was mechanically shaken for 10 min with a Taiyo SR-IIw reciprocating shaker, and then centrifuged at 5,000 rpm at 4°C for 10 min using a himac CR20G high speed refrigerated centrifuge (Hitachi Ltd.). The extract was recovered from the bottle by decantation and the residues were repeatedly extracted twice in the same manner, and then the extracts were combined. The procedure was repeated using methanol/conc. HCl (100/1, v/v). After radioassayed by LSC, the extracts were concentrated using an evaporator and each 10,000 dpm was subjected to HPLC and 2D-TLC analyses. The soil residues after extraction were air-dried in open vessels at room temperature for several days and subjected to combustion analysis to determine the remaining radioactivity.

TRR in the test system of the foliar application was determined as a sum of ¹⁴C in surface rinse, extract and unextractable from the leaf, and untreated leaves and soil. The TRR recovered from the test system of the soil treatment was determined as a sum of ¹⁴C in extractable and unextractable fractions of top soil and the one in middle and bottom soil layers and untreated plant.

Identification of Metabolites

In general, the identity of the metabolites was confirmed by HPLC and 2D-TLC co-chromatographies with the non-radiolabeled reference standards. In addition, LC-ESI-MS and NMR analyses were carried out for identification of **2**. In order to identify conjugated metabolites, approximately 200,000 dpm of the extract was dissolved in 1 mL of 10 mM sodium acetate buffer at pH 5.0 and 10 mg of cellulase or β -glucosidase was added to the solution. The mixture was incubated in a BR-180LF BioShaker (TAITEC Co. Ltd.) at 37°C and 100 rpm. The aliquot of the reaction mixture was sampled sequentially till 7 days and directly analyzed with HPLC and 2D-TLC. With regards to the characterization of metabolites in the extract, the chemical derivatizations (acetylation and methylation) were performed. The leaf extracts including 100,000 dpm were taken and the solvent was dried up using an evaporator. The dried extract was re-dissolved in 500 μ L of pyridine/acetic anhydride (50/50, v/v) and allowed to stand overnight for acetylation, and in 500 μ L of methanol with dropwise addition of 20 μ L of 0.1% TMS-diazomethane in *n*-hexane and mixing for 4 min for methylation. The derivatized samples were directly analyzed by HPLC.

For the purpose of collecting a sufficient amount of **2** for LC-MS and NMR analyses, 0.167 MBq of [benzyl- 14 C] **1-RTZ** mixed with 10 mg of the non-radiolabeled material in acetonitrile was applied onto the surface of three cabbage leaves (BBCH 41). The plants were grown in the greenhouse for 7 days. After the sampling, the treated leaves were rinsed with acetonitrile and the rinsate was subjected to isolation of **2** using the HPLC method 2.

RESULTS

Distribution of 14 C in Plant and Soil

The distribution of radioactivity after the foliar application is summarized in Table 2. For the leaf treatment, the radioactivity recovered from the treated leaves was 31.4–71.1%AR after 14 days. The unrecovered 14 C was most likely lost by vaporization considering the vapor pressure (1.96×10^{-3} Pa) and Henry's law constant (2.1×10^{-4} m³ mol⁻¹) of **1**. The 14 C recovered by the surface rinse gradually decreased to 11.8–26.3%AR at the end of the study while that in the leaf extract concomitantly increased to 18.0–42.2%AR. Total amount of unextractable 14 C was less than 3.1%AR during the study

in any case. Little amount of radioactivity was translocated from the treated leaf to the untreated portions of plant. In respect of the soil treatment, the ^{14}C distribution is given in Table 3. The ^{14}C recovered from the test system was 39.6–60.4%AR after 14 days. Majority of the radioactivity remained in the top layer soil (0-2 cm) which amounted to 12.1–30.9%AR, while the ones in the middle (2-10 cm) and bottom (10-18 cm) layers were 13.1–16.1 and 4.8–9.9%AR, respectively. The uptake of ^{14}C from the soil to plant was negligible as 1.5–3.6%AR.

The metabolite distribution for the leaf treatments is summarized in Table 4. The representative HPLC chromatogram of the surface rinse fraction is shown in Figure 3. On the leaf surface, **1-RTZ** and **1-RTE** rapidly dissipated to <0.1%TRR at 14 days after treatment. **2**, **4** and **5** were detected as major metabolites whose maximum amounts reached to 25.4, 28.5 and 26.0%TRR, respectively, at 7 days after treatment. Degradate **2** was separated into four peaks by using the HPLC method 2, i.e., the retention times of **2a**, **2b**, **2c** and **2d** were 33.7, 31.7, 30.0 and 29.3 min, respectively, which indicated the presence of four species, at least. Other minor metabolites were less than 2.0%TRR. In the leaf extract, **1-RTZ** and **1-RTE** were detected at 0.4–18.6 and 9.4–18.5%TRR, respectively, during the test duration. The comparison of the metabolic profile has shown that it is relatively different between **1-RTZ** and **1-RTE**. In the case of **1-RTZ**, the major metabolite having an intact ester linkage was the glucose conjugate of **6** amounting to its maximum 12.3%TRR. **7** was detected at 12.2%TRR for the benzyl label while **10** or **11** was not detected in cabbage plant. For **1-RTE**, **4** and **5** were formed at 4.0 and 4.6%TRR, respectively, and none of the metabolites exceeded 7%TRR. To evaluate the isomeric ratio, the chiral HPLC analysis of **1-RTZ** and **1-RTE** remained on/in the leaf for the benzyl label was conducted, and demonstrated negligible isomerization to the other stereoisomers (<0.7%TRR). For the soil treatment, most of the radioactivity remained as the intact parent compound, except for [benzyl- ^{14}C] **1-RTZ** which produced **8** in 41.9%TRR at 14 days after treatment.

Identification of Metabolite 2

Approximately 180 and 250 ng of possible isomeric metabolites **2a** and **2b** were obtained, respectively, from the experiment for collecting enough amounts for their identification. The purified metabolites **2a** and **2b** were individually subjected to ^1H -

NMR and ^1H - ^1H COSY, and 1D- and 2D-TLC analyses. The chemical shifts of these metabolites are listed in Table 5. Each proton signal pattern was very similar between the two, but was clearly different from that of **1-RTZ** as its original two methine protons at the propenyl moiety shifted from 4.92 and 5.35 ppm to a lower magnetic field 5.11 and 5.62 ppm, respectively. With regards to ^1H - ^1H COSY spectrum, no cross signal was observed between the above two adjacent methine protons for **2a** and **2b**, which suggested the cleavage of C-C double bond (Figure 4, showed **2a** as representative). In the 1D-TLC analysis using an acidic solvent C, both **2a** and **2b** decomposed to caronaldehyde (**4**) and carboxylic acid (**5**) derivatives during the development. Therefore, the chemical structures of **2a** and **2b** were assumed to be ozonide derivatives possessing a 1,2,4-trioxolane ring. To identify the chemical structure as ozonide, **2** was synthesized from **1-RTZ** and **1-RTE** by ozonation. The modification of HPLC gradient system (method 2) enabled the synthetic **2** from **RTZ** and **RTE** isomers to be clearly separated into four isomers, namely, **2a-2d**. The observed ratio of the four isomers was **2a/2b/2c/2d** = 33/16/37/14 for **1-RTZ** and **2a/2b/2c/2d** = 40/21/28/11 for **1-RTE**. The ozonation was performed several times followed by isomeric ratio confirmations by HPLC, each experiment showed similar ratio to the one mentioned above, suggested preferred generation of **2c/2d** to **2a/2b** from **RTE** isomer, while the ratio from **RTZ** was mostly even. The comparison of ^1H -, ^1H - ^1H NMR spectra and TLC, HPLC co-chromatograms has clarified that **2a**, **2b**, **2c** and **2d** produced on the leaf surface were definitively identical with those of the synthesized standards. Using each synthetic isomers, the ^1H - and ^{13}C -NMR spectra are tabulated in Table 5. The overall trends of the spectra were similar within four isomers, while the chemical shifts related to protons H5 and H6 on the cyclopropane ring were clearly different. The four isomers all exhibited identical cross peaks with **1** in various modes of 2D-NMR analyses, which clearly demonstrated the preservation of the chemical structures of the parent compound, except for the cleavage of the C-C double bond at the prop-1-enyl moiety. In the LC-ESI-MS analysis, the pseudo ions of **2a-2d** were observed at $m/z = 409$ $[\text{M}+\text{H}]^+$, 426 $[\text{M}+\text{NH}_4]^+$ and 431 $[\text{M}+\text{Na}]^+$ in the positive ion mode, which indicated all products incorporated three oxygen atoms into **1**. Taking all above into account, these four products were determined to be a pair of diastereomers of the ozonide derivative whose asymmetric two carbons exist in the trioxolane ring. Successively, the HPLC-purified synthetic isomers **2a**, **2b** and the

mixture of **2c** and **2d** were subjected to NOE difference analysis to gain insights into their conformations. The NOE resonance was clearly observed between the protons H10 (5.34-5.36 ppm) and H11 (4.92-4.96 ppm) in the trioxolane ring for the mixture (**2c+2d**), while little or no resonance was observed for **2a** and **2b** which indicated the structural distance between these protons are closer for the former isomers compared to the latter (Figure 5), thus, their configurations were characterized as *trans* (*threo*) and *cis* (*erythro*), respectively.

Identification of Metabolites 3–7

The chemical structures of **3–5** and **7** were confirmed by HPLC and 2D-TLC co-chromatographies with the synthetic standards. For the glucose conjugate of **6**, the corresponding HPLC fraction was isolated and then incubated with cellulase or β -glucosidase. A new peak produced by the enzymatic hydrolysis was identified as **6**, as the aglycone, by the HPLC and 2D-TLC co-chromatographies with the reference standard. Interestingly, the enzymatically liberated **6** predominantly consisted from the single isomer detected at the retention time 20.9 min, whose reference standard has four isomers in total arrived at different regions at 20.9 to 22.2 min.

DISSCUSSION

Significant radiocarbon loss, i.e. maximum 25.6%AR within 2 days, was observed after the foliar application of **1-RTZ** and **1-RTE** onto the cabbage plant (Table 1), which indicated their immediate volatilization from the leaf surface due to the high vapor pressure. The volatilization of pesticides from leaf surfaces can be conveniently evaluated with Henry's law constant. The similar trend in volatility as **1** ($2.1 \times 10^{-4} \text{ m}^3 \text{ mol}^{-1}$) was observed for other pyrethroids possessing a high Henry's law constant such as fenpropathrin ($1.8 \times 10^{-4} \text{ m}^3 \text{ mol}^{-1}$), phenothrin ($1.4 \times 10^{-6} \text{ m}^3 \text{ mol}^{-1}$), permethrin ($1.9 \times 10^{-6} \text{ m}^3 \text{ mol}^{-1}$) and cypermethrin ($4.2 \times 10^{-7} \text{ m}^3 \text{ mol}^{-1}$), while those with low one tend to remain on the leaf surface for a relatively longer period like tralomethrin ($3.9 \times 10^{-15} \text{ m}^3 \text{ mol}^{-1}$) (Nambu et al. 1980; Mikami et al. 1985; Cole et al. 1982; Gaughan and Casida 1978; HHS 2003; Laskowski 2002).

Both *E/Z* geometrical isomers reacted with atmospheric O₃ on the leaf surface

produced diastereomeric **2** as the major initial degradates. There are many precedent experiments indicated the formation of ozonide as a degradation intermediate for pyrethroids, but the detection of ozonide was not definitive probably due to their instability after generation and during chromatographic/spectroscopic analysis. Ruzo et al. (1986) studied the ozonolysis of synthetic pyrethroids, phenothrin and halothrin, in several organic solvents or on thin films and detected their ozonide derivatives which were tentatively identified by chemical ionization–mass spectrometry (CI–MS) and ¹⁹F-, ¹³C- and ¹H-NMR spectroscopy. Nambu et al. (1980) studied the metabolism of phenothrin on bean foliage and proposed its ozonide form by its measured molecular weight by electron ionization–mass spectrometry (EI–MS) and, as supportive, detecting its typical degradates produced such as the caronaldehyde and carboxylic acid derivatives during the 1D-TLC development using an acidic solvent. However, both authors did not confirm the structures using synthetic standards and determined the stereostructures. Incidentally, the halogen-substituted pyrethroids, e.g. deltamethrin, likely form less amount of ozonide products (Ruzo et al. 1986) and the corresponding degradates in their plant metabolisms (Mikami et al. 1985; Cole et al 1982; Gaughan and Casida 1978). Difference of substituent groups at olefins is considered to be an important factor to determine the reactivity with ozone because an electron-withdrawing substituent reduces the electron density at the olefin to suppresses the 1,3-dipolar cycloaddition of ozone, while an electron-donating group enhances it (Pryor et al. 1985). Because **2** has two asymmetric carbons at the 1,2,4-trioxolane ring, there are four isomers, i.e., **2a-2d**, which could be generated. From the detailed analysis of synthetic ozonide by 1D-NOE measurement together with the spectrum pattern and chemical shifts/coupling constants from various NMR analyses, the diastereomeric configurations of **2** isomers were determined as *trans* (*threo*) for **2a** and **2b**, and *cis* (*erythro*) for **2c** and **2d**. In the ¹³C-NMR spectra, the chemical shifts of C1 and C6 attached to the ozonide ring shifted to lower field and C11 to higher field for **2a** and **2b** compared to those of **2c** and **2d**. This difference in the chemical shifts was in good agreement with the results reported by Griesbaum et al. (2004) who have conducted extensive analyses to determine the configuration of several ozonide derivatives by ¹³C-NMR.

Furthermore, **2a** and **2b** were more preferentially produced from **1-RTE** while **2c** and **2d** from **1-RTZ** by the ozonolysis. This result supports our diastereomeric

assignment, because the empirical trend in a selectivity has been theoretically examined, especially for bulky substituents, that *trans* alkenes are more likely to be transformed to *trans* secondary ozonide *via trans* primary ozonide and *syn* carbonyl oxide, and *cis* alkenes and *vice versa* (Bauld et al. 1968; Ponce et al. 1997; Bailey and Ferrell 1978; Murray et al. 1967). The production of four diastereomers in the ozonolysis at olefins can be explained from a generalized observation on ‘Criegee intermediate’ (Criegee 1975; Geletneky and Berger 1998) as summarized in Figure 6, which can be briefly expressed by 3 steps: 1) 1,3-dipolar cycloaddition of O₃ to olefin to produce a highly unstable primary ozonide, 2) dissociation of the primary ozonide to give the corresponding zwitterionic carbonyl oxide and carbonyl compounds, i.e. Criegee intermediate, 3) recombination of the Criegee intermediate *via* another 1,3-dipolar cycloaddition to produce more stable secondary ozonide. The step 2 should be the important path to produce four diastereomers on the cabbage leaf surface, in which the four patterns of nonhomologous random recombination of carbonyl oxide ions and carbonyl compounds produced from the primary ozonide may be deeply involved. Incidentally, the secondary ozonides are considered to be less toxic to mammal because they are highly likely to be unstable in mammalian tissue due to their rapid decomposition in aqueous solutions (Zaikov and Rakovsky 2009; Perry et al. 2006; Pryor 1991). Furthermore, an ozonide derivative of unsaturated lipid, methyl oleate, was orally administered to rat which resulted in low toxicity, probably due to its fast degradation by enzymes and biological antioxidants such as GSH transferase and vitamins or SOD, respectively (Pryor 1991).

In the leaf tissue, the sugar conjugate of **6** was only produced as a major metabolite in the leaves treated with **1-RTZ**. This may be explained by the selective epoxidation of **1-RTZ** to produce intermediate **3** under the function of enzymes probably by CYP, because CYP-catalyzed stereoselective epoxidation at olefin is a common reaction in living organisms such as lipid/hormone biosynthesis and xenobiotic detoxification (Guengerich 2003; Hayashi et al. 200; Vaz et al. 1998; Sauveplane et al. 2009). Although **3** was not detected from neither **1-RTZ** nor **1-RTE** in cabbage plant, the epoxide derivative of **1** is reported to be produced in rat and photodegradation on soil (Nishimura et al. 2011; Kaneko 210). Vaz et al. (1998) clarified that the epoxidation of olefins by CYPs from several origins proceeded favorably with (*Z*)-2-butene than its (*E*)-isomer.

Sauveplane et al. (2009) reported the CYP derived from *Arabidopsis thaliana*, which was heterologously expressed in yeast, showed highly selective conversion of (*Z*)-configured unsaturated fatty acids to mono- or di-*cis*-epoxide. Ando *et al.* extensively studied the configuration of the epoxy chrysanthemate derivatives of (*S*)-bioallethrin and phenothrin produced by mouse microsomal CYP (Ando et al. 1991; Class et al. 1991). They have clarified that the oxygen atom was inserted to the propenyl double bond from the *si* face to produce the 7,8-epoxy derivative and its configuration at C7 carbon, the adjacent one to the cyclopropane ring, was *R* and *S* from selective oxidation of *trans*- and *cis*-chrysanthemates, respectively. Additionally, epoxy hydrolases which transform epoxy derivatives into diols are also reported to be stereoselective. Soybean-derived epoxy hydrolase converts *cis*-epoxy fatty acids into *threo* diols by catalyzing *trans*-addition of water into oxirane carbon which has the *S*-chirality (Blee and Schuber 1992). Taking all above into consideration, a single isomer of aglycone **6** detected in the cabbage plant is most likely to be the *threo* isomer in *R-R* configuration which was produced *via* the intermediate *cis* isomer of **3** in *R-S* configuration, and its estimated pathway is proposed in Figure 7.

In summary, the proposed metabolic pathway of **1** in the cabbage plant is described in Figure 8. **1-RTZ** and **1-RTE** reacted with atmospheric O₃ on the leaf surface to form ozonide **2a-d** as the initial product, and successively decomposed to caronaldehyde **4** and carboxylic acid **5** derivatives *via* opening of the trioxolane ring. At inner plant, they were further converted to the polar metabolites *via* cleavage of the ester linkage to **7** or dihydroxylation to **6** at the olefinic carbon, possibly mediated by epoxide **3**, followed by conjugation with sugar. The isomerization on/in the cabbage leaf was a minor reaction.

Tables:

Table 1: The chemical structures of the test chemicals and reference standards.

Designation	Chemical structure	Designation	Chemical structure
RTZ-1		6	
RTE-1		7	
2		8	
3		9	
4		10	
5		11	

*: ^{14}C label position of carbonyl label, [carbonyl- ^{14}C]1-RTZ and -RTE.

†: ^{14}C label position of benzyl label, [benzyl- ^{14}C]1-RTZ.

Table 2: Distribution of radioactivity after foliar applications.

	%AR								
	[benzyl- ¹⁴ C] 1-RTZ			[carbonyl- ¹⁴ C] 1-RTZ			[carbonyl- ¹⁴ C] 1-RTE		
	2 D	7D	14D	2D	7D	14D	2 D	7D	14D
Surface	65.6	36.0	11.8	50.1	47.3	26.3	61.7	31.5	15.8
Extract									
Methanol	7.4	11.8	17.1	27.2	35.6	39.2	17.5	13.4	32.9
75%Methanol	1.0	4.0	0.9	3.5	2.3	3.0	0.6	7.3	2.5
Unextractable	0.5	2.2	1.6	0.6	0.6	2.6	2.1	3.8	3.1
Untreated plant	NA	NA	ND	NA	NA	ND	NA	NA	ND
Untreated soil	NA	NA	ND	NA	NA	ND	NA	NA	ND
Total	74.5	54.0	31.4	81.4	85.8	71.1	81.9	56.0	54.3

NA: Not available. ND: Not detected.

Table 3: Distribution of radioactivity after soil applications after 14 days.

	%AR		
	[benzyl- ¹⁴ C] 1-RTZ	[carbonyl- ¹⁴ C] 1-RTZ	[carbonyl- ¹⁴ C] 1-RTE
	Treated Soil		
Top layer	30.9	28.8	12.1
Methanol	23.8	21.7	10.0
Methanol/HCl	3.7	1.7	1.3
Unextractable	3.4	5.4	0.8
Middle layer	13.1	15.7	16.1
Bottom layer	4.8	13.7	9.9
Untreated Plant	3.6	2.2	1.5
Total	54.2	60.4	39.6

Layer: Top (0-2 cm), middle (2-10cm), bottom (10-18 cm).

Table 4: Distribution of **1** and its metabolites in treated cabbage leaves.

	%TRR								
	[benzyl- ¹⁴ C] 1-RTZ			[carbonyl- ¹⁴ C] 1-RTZ			[carbonyl- ¹⁴ C] 1-RTE		
	Days after exposure								
	2 D	7 D	14 D	2 D	7 D	14 D	2 D	7 D	14 D
Surface									
1-RTZ	45.0	6.8	ND	7.8	0.5	ND	ND	ND	ND
1-RTE	ND	ND	ND	ND	ND	ND	59.6	1.5	ND
2a	6.6	10.0	ND	2.3	9.1	2.1	1.7	6.9	3.0
2b	3.5	5.2	ND	1.4	5.3	2.0	1.0	4.2	1.7
2c and 2d	5.8	10.2	ND	2.3	7.9	3.6	1.5	3.2	2.1
4	21.3	12.0	6.6	28.5	11.3	2.5	9.7	21.9	4.6
5	2.9	13.3	26.0	12.8	17.5	14.1	1.8	13.6	14.7
Others ^{a)}	3.0	9.2	5.0	6.5	3.5	12.7	ND	4.9	3.1
Subtotal	88.1	66.7	37.6	61.6	55.1	37.0	75.3	56.2	29.2
Extract									
1-RTZ	1.0	0.4	8.5	15.7	18.6	1.5	ND	ND	ND
1-RTE	ND	ND	ND	ND	ND	ND	18.5	11.6	9.4
4	0.2	1.4	ND	2.4	1.0	ND	0.3	0.5	4.0
5	ND	ND	1.4	ND	ND	ND	ND	1.7	4.6
6 conjugate^{b)}	3.1	3.7	11.3	7.2	6.6	12.3	ND	ND	ND
7	0.5	8.7	12.2	NA	NA	NA	NA	NA	NA
Others ^{c)}	6.4	15.1	23.4	12.4	18.0	45.5	3.3	22.2	47.2
Subtotal	11.2	29.3	57.3	37.7	44.2	59.3	22.1	37.0	65.2
Unextractable	0.7	4.0	5.1	0.7	0.7	3.7	2.6	6.8	5.6
Total	100.0	100.0	100.0	100.0	100.0	100.0	100.0	100.0	100.0

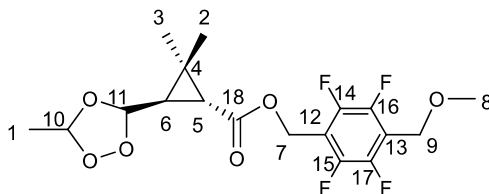
ND: Not detected. NA: Not available.

a) Consisted of multiple components, each of which amounted to <2.0%TRR

b) Sugar conjugate of **6**.

c) Consisted of multiple components, each of which amounted to < 7.0%TRR.

Table 5: ^1H - and ^{13}C -NMR chemical shifts of **2** isomers (**2a-2d**) in *d*-chloroform.



Isomer	Atom	^1H (ppm)	^{13}C (ppm)
2a	1	1.43 (3H, d, $J = 4.81$ Hz, $-\text{CH}_3$)	16.18
	2	1.23 (3H, s, $-\text{CH}_3$)	20.45
	3	1.24 (3H, s, $-\text{CH}_3$)	21.95
	4	-	26.81
	5	1.75 (1H, d, $J = 5.61$ Hz, cyclopropane-1)	30.49
	6	1.67 (1H, dd, $J = 5.21, 7.21$ Hz, cyclopropane-3)	31.56
	10	5.35 (1H, q, $J = 4.81$ Hz, trioxolane-3)	101.81
	11	4.92 (1H, d, $J = 7.21$ Hz, trioxolane-5)	104.16
2b	1	1.43 (3H, d, $J = 4.80$ Hz, $-\text{CH}_3$)	16.42
	2	1.26 (3H, s, $-\text{CH}_3$)	20.52
	3	1.27 (3H, s, $-\text{CH}_3$)	21.82
	4	-	26.61
	5	1.69 (1H, d, $J = 5.61$ Hz, cyclopropane-1)	30.26
	6	1.65 (1H, dd, $J = 5.61, 7.21$ Hz, cyclopropane-3)	31.00
	10	5.36 (1H, q, $J = 4.80$ Hz, trioxolane-3)	102.03
	11	4.93 (1H, d, $J = 7.21$ Hz, trioxolane-5)	103.92
2c	1	1.46 (3H, d, $J = 4.81$ Hz, $-\text{CH}_3$)	18.03, 18.24
2d	1	1.46 (3H, d, $J = 4.81$ Hz, $-\text{CH}_3$)	
2c	2	1.23 (3H, s, $-\text{CH}_3$)	20.45, 20.52
2d		1.25 (3H, s, $-\text{CH}_3$)	
2c	3	1.24 (3H, s, $-\text{CH}_3$)	21.95
2d		1.26 (3H, s, $-\text{CH}_3$)	
2c	4	-	26.77, 26.91
2d		-	
2c	5	1.71 (1H, d, $J = 5.21$ Hz, cyclopropane-1)	31.00, 31.56
2d		1.66 (1H, d, $J = 5.21$ Hz, cyclopropane-1)	
2c	6	1.74 (1H, dd, $J = 5.21, 7.21$ Hz, cyclopropane-3)	33.58, 33.71
2d		1.72 (1H, dd, $J = 5.21, 7.21$ Hz, cyclopropane-3)	
2c	10	5.34 (1H, q, $J = 4.81$ Hz, trioxolane-3)	101.86, 101.90
2d		5.34 (1H, q, $J = 4.81$ Hz, trioxolane-3)	
2c	11	4.96 (1H, d, $J = 7.21$ Hz, trioxolane-5)	103.78, 103.81
2d		4.96 (1H, d, $J = 7.21$ Hz, trioxolane-5)	
2a-2d^{a)}	7	5.24 (2H, s, benzyl)	54.02
	8	3.41 (3H, s, $-\text{OCH}_3$)	58.75
	9	5.24 (2H, s, benzyl)	61.62
	12	-	114.78
	13	-	117.17
	14, 15	-	144.12
	16, 17	-	146.48
	18	-	170.51

-: Not Available.

a) All the isomers **2a-2d** showed the identical chemical shifts for ^1H - and ^{13}C -NMR.

Figures:

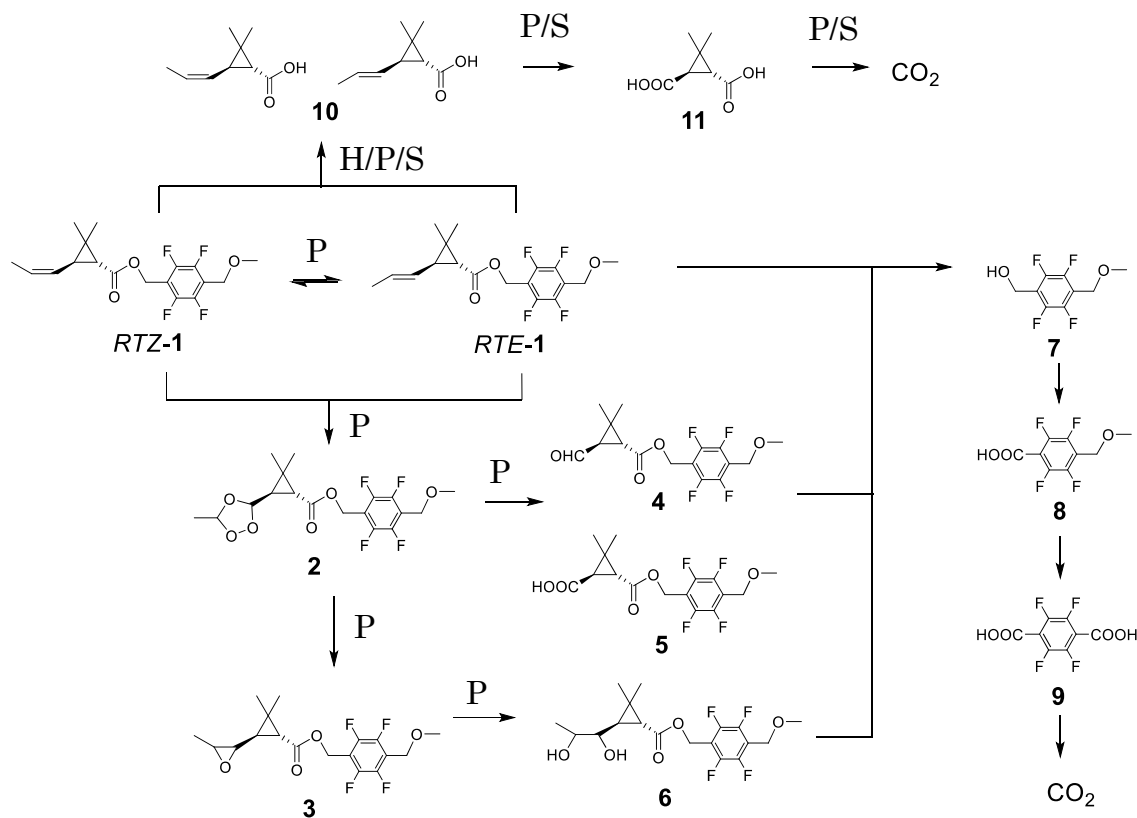


Figure 1: Degradation pathway of metofluthrin by hydrolysis/photolysis and in soil.
H: hydrolysis, P: photolysis, S: in soil.



Figure 2: Typical growth stage of cabbage at BBCH 41.

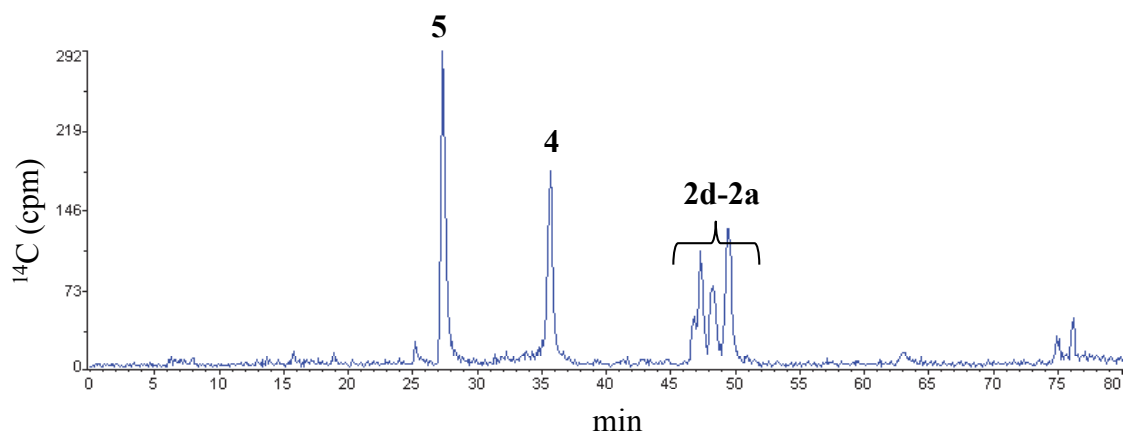


Figure 3: RP-HPLC chromatogram of the surface rinse of [carbonyl- ^{14}C] **1-RTZ** treated leaf after 7 days. Numbers above each peak indicate the corresponding metabolite.

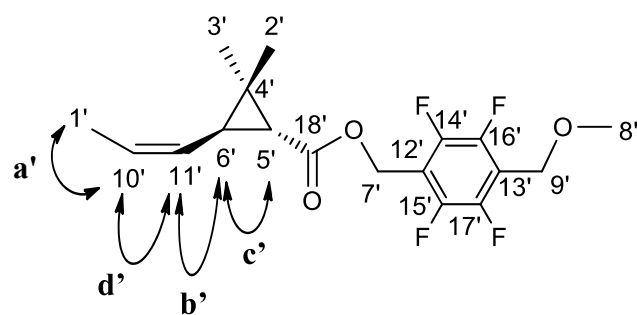
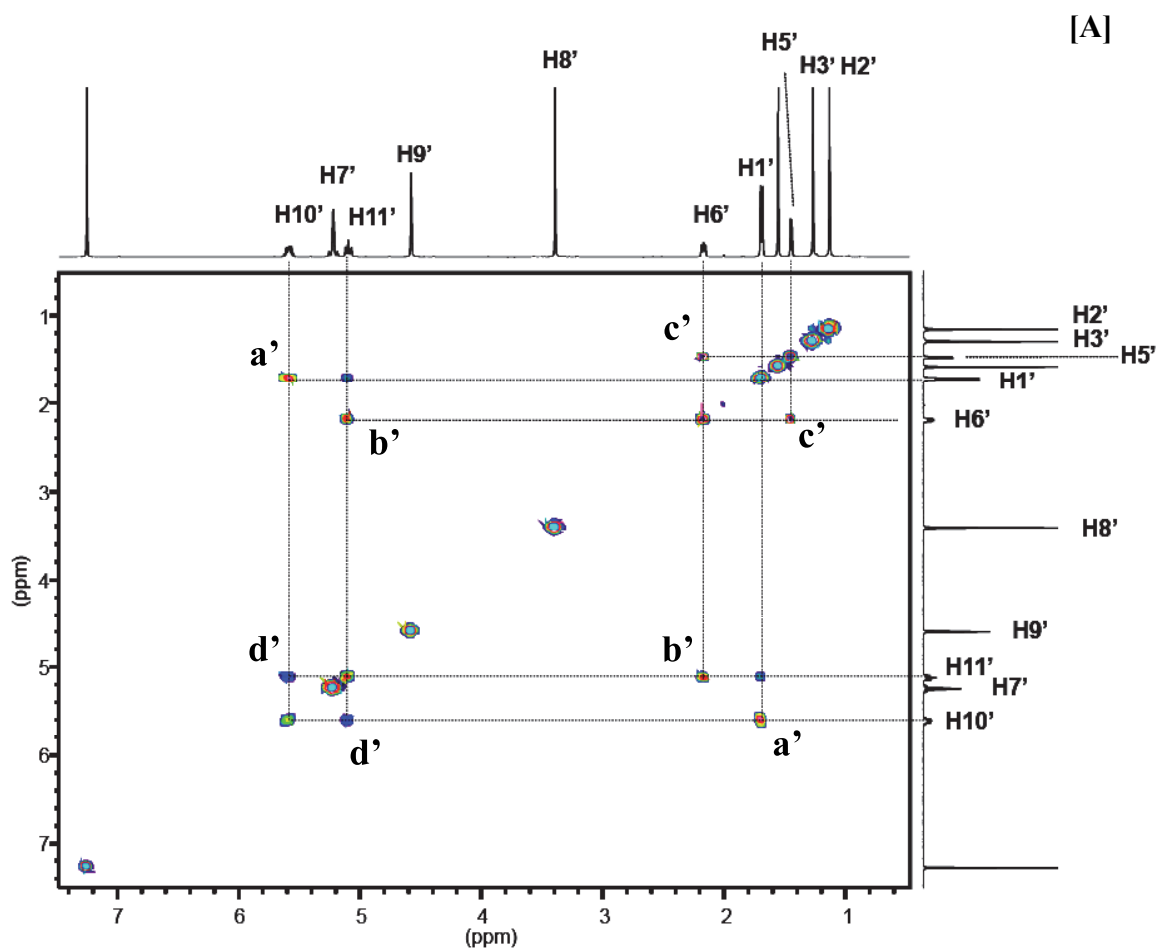


Figure 4: ¹H-¹H COSY spectrum of **2a** and **1-RTZ** in *d*-chloroform.
 [A] The spectrum of **1-RTZ**.

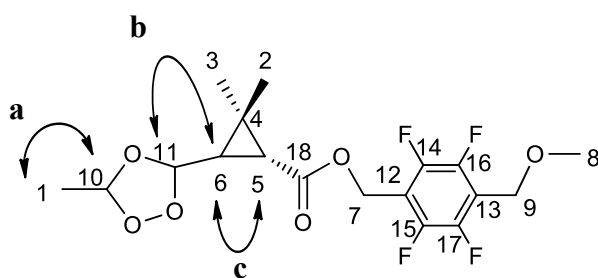
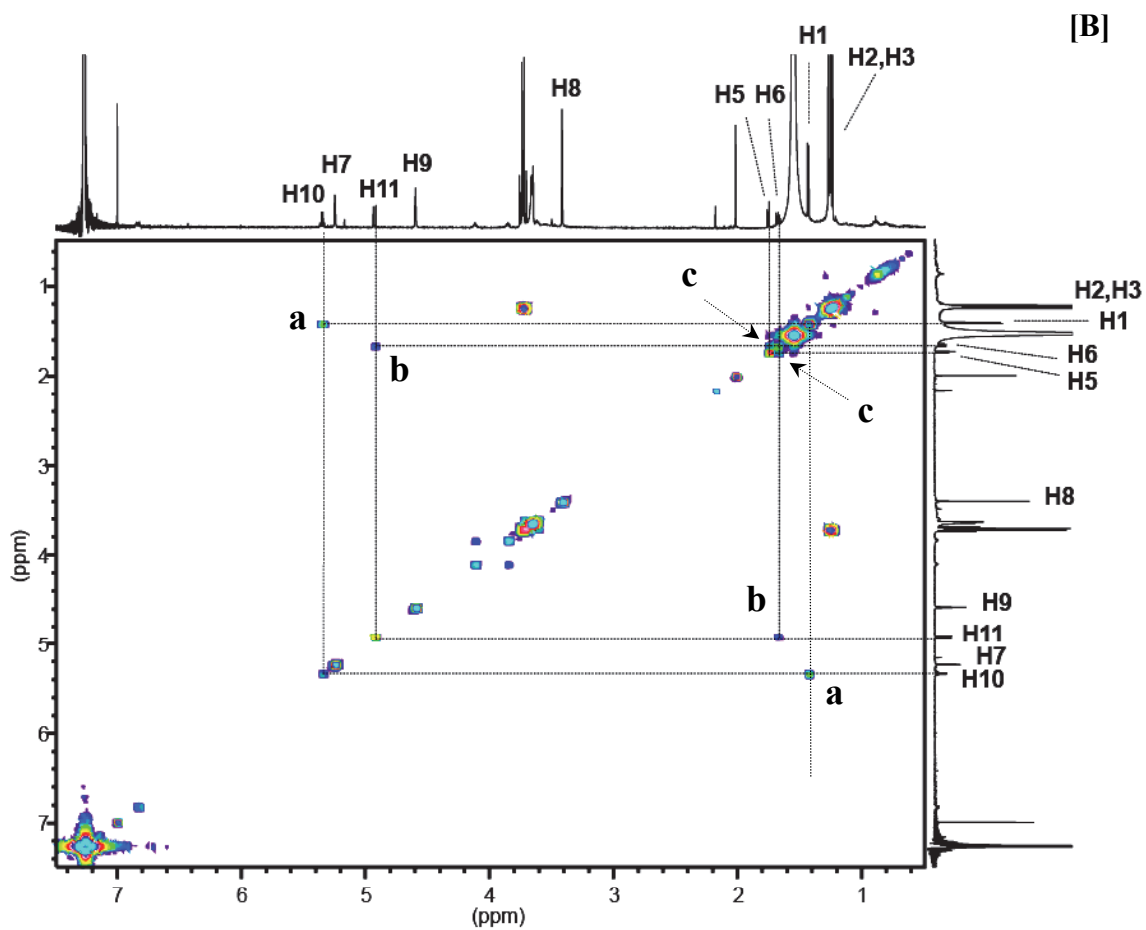


Figure 4 (continue): ^1H - ^1H COSY spectrum of **2a** and **1-RTZ** in *d*-chloroform.
 [B] The spectrum of metabolite **2a**.

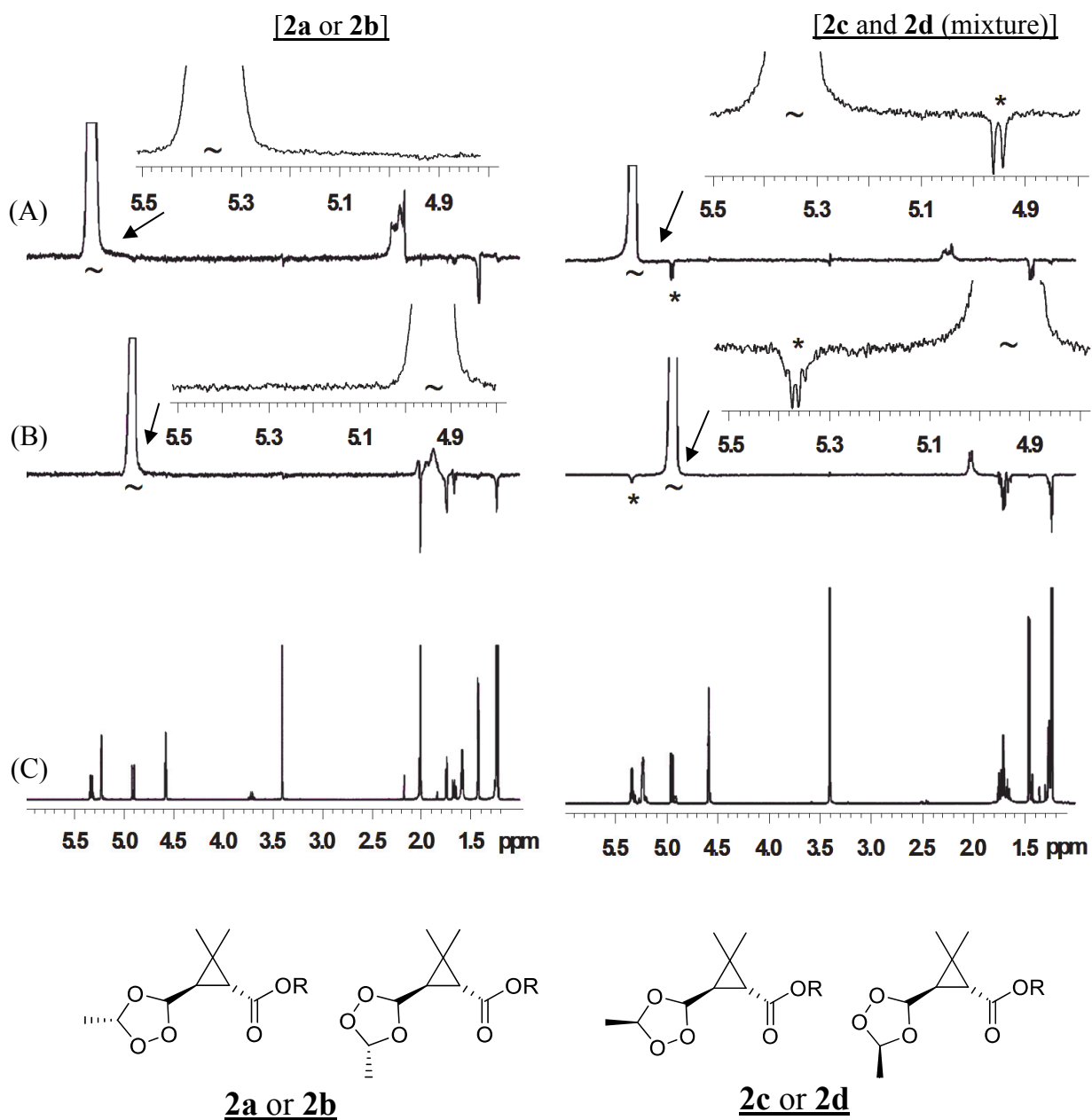


Figure 5: 1D-NOE spectra of **2** isomers in *d*-chloroform. (A, B) 1D-NOE spectra (5,000 scans, delay = 5.0 s, $\tau_m = 0.375$ s, LB = 0.5 Hz) of **2a** or **2b** (left) and mixture of **2c** and **2d** (right) after selective irradiation of proton at the ozonide ring. Enlarged views at around each arrows are shown above the NOE spectra. The irradiation targets are indicated by a tilde (~). The characteristic NOE response between the protons at the ozonide ring was observed only for the mixture of **2c** and **2d** by simultaneous irradiation of the proton signals at the ring (signals marked by an asterisk). (C) The conventional ^1H spectrum (16 scans) of **2a** or **2b** (left) and mixture of **2c** and **2d** (right).

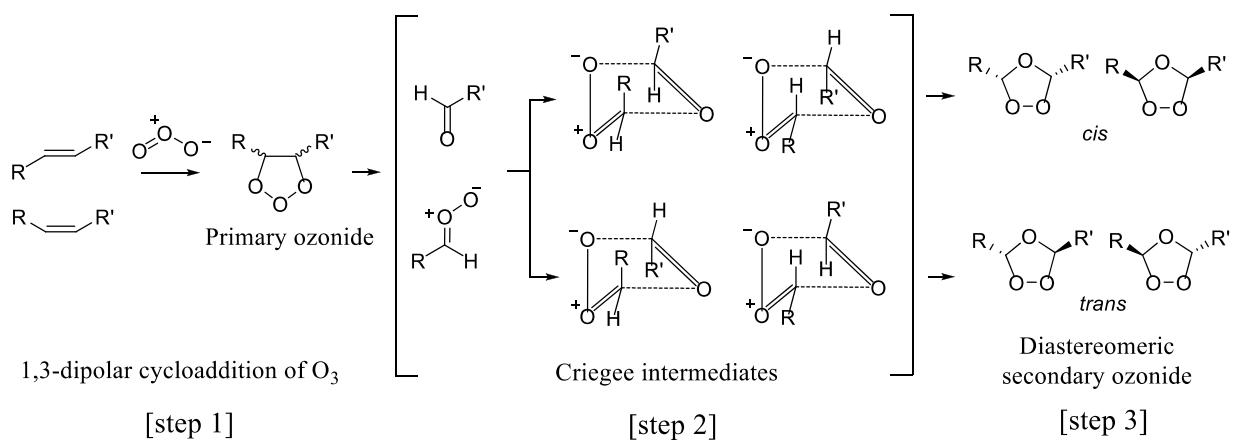


Figure 6: Scheme of diastereomer secondary ozonide production *via* Criegee intermediate.

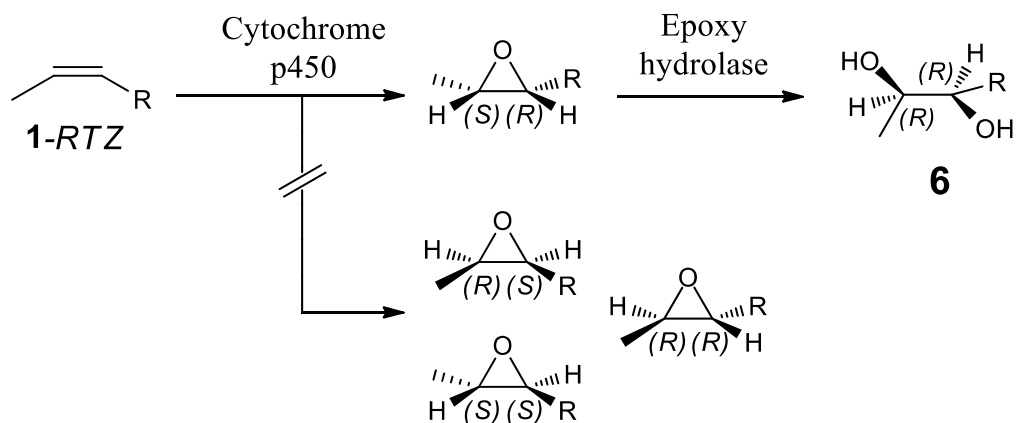


Figure 7: Proposed enzymatic dihydroxylation pathway of 1-RTZ.

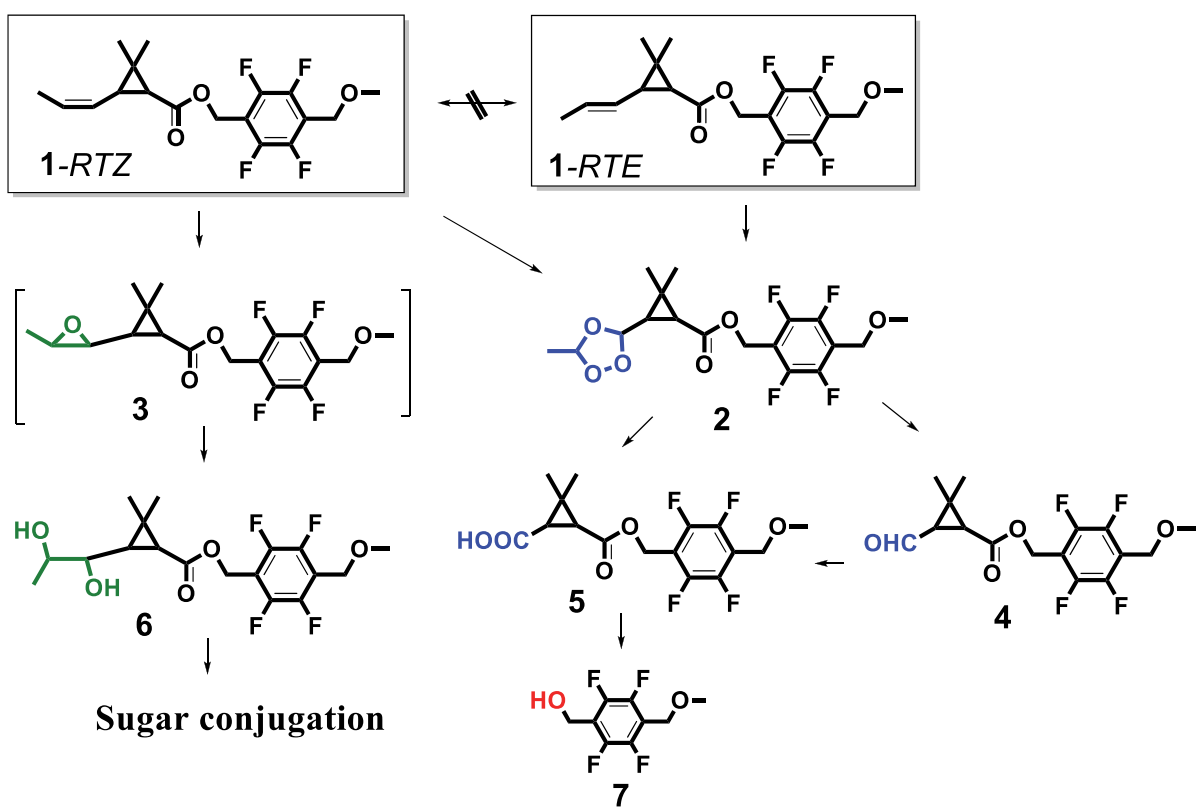


Figure 8: Proposed metabolic pathway of metofluthrin in/on cabbage plant.

2.1.2. Metabolism of Metofluthrin in Water Milfoil

Continuously to the cabbage metabolism study described in section 2.1.1, the behavior of metofluthrin in water milfoil was examined for comparison. From the results of cabbage, it was expected that the chrysanthemic acid moiety undergoes intensive, various metabolization in plant, which could provide unclear metabolic pathway for its moiety in water milfoil. Thus, only [benzyl-¹⁴C] label of metofluthrin has been applied as test material in this study, and as a result, the metabolic fate of the benzene moiety which has not observed in cabbage was revealed.

In this study, the same chemicals and analytical methods applied in the cabbage study were employed, unless otherwise noted. The same abbreviations used in the cabbage study for metofluthrin and its degradates are transcribed.

MATERIALS AND METHODS

Chemicals

The radiolabeled material [benzyl-¹⁴C]1-RTZ was used in this study. The non-radiolabeled substances applied were 1–9, each containing the benzyl ring moiety. The chemical structure of each substance is given in Table 1.

Chromatography

The Reversed-phase HPLC analysis of the test substance and its degradates was conducted using a LC-20A module (Shimadzu Ltd., Kyoto, Japan) equipped with a SUMIPAX ODS A-212 column. The two dimensional (2-D) TLC was conducted using chloroform/methanol = 9/1 (v/v/v) and toluene/ethyl acetate/formic acid = 5/7/1 (v/v/v) as the first and second eluents, respectively. The HPLC retention times and TLC R_f values of each reference compounds were described in the previous report (Nishiyama et al. 2010; Nishimura et al. 2011).

Spectroscopy

The HRMS analyses of metabolites were performed using Q-Exactive Focus (Thermo Fisher Scientific Inc.) mass spectrometer connected to the LC system. The

analytical parameters at the mass module controlled by the Xcalibur software (version 2.2) are shown below: sweep gas flow 10, source temp., 100°C, desolvation temp., 350°C, capillary voltage 3.5 kV, cone voltage 10-40 eV.

Plant Material and Treatment

Water milfoil (*Myriophyllum elatinoides*) was purchased from Aqua Rise Co. The plants were immersed into AAP (American Academy of Pediatrics) water medium (OECD 2002) at pH 7.0 ± 0.5 in a glass aquarium and acclimatized for 7 days in a climate chamber LH-220S (NK Systems Ltd.) under white fluorescent lighting ($120 \mu\text{E} \cdot \text{m}^{-2} \cdot \text{s}^{-10}$, 16 h per day).

The ^{14}C material dissolved in acetonitrile was mixed with the non-radiolabeled **1** to the isotopic ratio $^{14}\text{C}:^{12}\text{C} = 100:70$ as the dose solution. Then, the solution was injected to a 800 mL of the AAP medium in a glass beaker to prepare 0.7 ppm of **1** as the exposure concentration (radioactivity 1.67 MBq), to ensure sufficient detection of the radioactivity. To the exposure water, 10 water milfoil plants (length 11.2 ± 1.0 cm, roots 2–5 cm) were immersed and incubated in the climate chamber.

Sampling, Extraction and Analysis

Aliquot of the exposure water was sequentially sampled till 7 days and directly analyzed by LSC and HPLC. At Day 7, plants were sampled and extracted with 20 mL of acetone/water (3/1, v/v) using a homogenizer AM-8 (Nissei Ltd.) at 10,000 rpm and 0°C for 10 min. The homogenate was vacuum filtered and the plant residue was further extracted twice in the same manner. An aliquot of the extract was analyzed by LSC and HPLC. The post extracted plant residues were subjected to the combustion analysis.

Identification of Metabolites

In general, the identity of the metabolites was confirmed by HPLC and TLC co-chromatography with the non-radiolabeled reference standards. In order to clarify the presence of sugar-conjugated metabolites, approximately each 200,000 dpm of the exposure water and the plant extract was dried using evaporator, re-dissolved in 5 mL of 10 mM sodium acetate buffer (pH 5.0) and 3 mg of β -glucosidase was added to the

solution, then incubated at 37°C for 7 days. In addition, possible conjugated metabolites were isolated by the HPLC and TLC, then subjected to LC–ESI–MS analysis to clarify their molecular weight as secondary confirmation.

RESULTS AND DISCUSSIONS

¹⁴C Distribution

The ¹⁴C distribution in the exposure water during 7 days and in the plant at the last day are given in Tables 2 and 3, respectively. After the injection, the applied radioactivity recovered in the exposure water medium ranged from 41.2% to 84.3%AR and the accumulated ¹⁴C by water milfoil at Day 7 was 13.5%AR. As a particular behavior, the recovery in the medium steeply decreased to 41.2%AR after 0.5 day and continuously increased thereafter. The radioactive components detected in the water were mostly **7** and **8**, and the parent **1** did not remain at the last sampling point. These results suggested that **1** once adhered onto the plant surface and glass wall (approximately 10%AR was adsorbed on glass vessels in the previous photolysis/hydrolysis studies of **1** (Nishiyama et al. 2010; Nishimura et al. 2011) in a very rapid fashion, but most of it received ester hydrolysis to generate **7** and distributed back into the medium as supported by the fact that AR at Day 14 was 97.8% (water plus plant). In the previous studies, **7** was confirmed as the only degradate generated by aqueous hydrolysis (Nishiyama et al. 2010), while **4–7** were produced by photolysis and **8** only in the presence of soil (Nishimura et al. 2011). The ozonide **2** was not detected in both studies probably due to the unavailability of ozone in water (half-life: seconds to hours) (Von Gunten 2003), or immediate decomposition to **4–6**. In our study, **4–6** were transient and not significant in the water medium, thus, indicated that hydrolysis was the major factor for abiotic reaction. Incidentally, **7** was likely oxidized to **8** and further degraded into multiple products. As reviewed by Ghattas et al. (2017), various degradation reactions of organic compounds by microorganisms in aquatic environment are known. Because the water milfoil was subjected to the exposure without any sterilization of periphyton, it is assumed that water-suspended microbes or periphyton(s) on the water milfoil also contributed to metabolize **7** to **8**, then successively converted to multiple products. Other possibility is the participation of water milfoil by excreting **8** and other minor degradates following

metabolism at inner plant, however, this is unlikely since such excretion ability has not been confirmed so far.

In the plant, the parent compound **1** was not detected. The majority of the radioactive components was **12**, followed by **13**, **7**, **8** and other minor multiple metabolites, which amounted to: %AR/%TRR, 8.58/65.6, 1.4/10.0, 0.7/4.9, 0.7/4.8 and 1.2/9.3 (0.4/2.5 as maximum single component), respectively. These results indicated that the metabolites detected in the water milfoil have been derived from two routes, i.e. a route as **1** adsorbed on the surface of water milfoil penetrated into the plant and rapidly transformed to various metabolites, and the other route as hydrolysates/metabolite of **1** produced in the medium (and on the glass surface) were directly transported into plant and underwent further transformation.

Metabolite Characterization

The plant metabolite **12** and **13** released **7** as their aglycone by β -glucosidase hydrolysis, suggested their sugar-conjugated structures. Successive analysis by LC-MS gave the formic acid adduct of **12** in negative mode (Figure 1) at m/z 431.0975 $[M+HCOO]^-$ ($C_{16}H_{20}O_9F_4$, +1.048 ppm) accompanying the ^{14}C molecule 433.1006 ($C_{15}^{14}C_1H_{20}O_9F_4$, +0.738 ppm), which corresponded to the mono-glucose conjugate of **7**. The conjugate **13** showed its molecular ions (Figure 2) at 593.1515 $[M+HCOO]^-$ ($C_{22}H_{29}O_{14}F_4$, +2.628 ppm), 595.1547 ($C_{21}^{14}C_1H_{29}O_{14}F_4$, +2.548 ppm) and 547.1458 $[2M-H]^-$ ($C_{21}H_{27}O_{12}F_4$, +2.390 ppm), 549.1491 ($C_{20}^{14}C_1H_{27}O_{12}F_4$, +2.596 ppm) and characterized as di-saccharide conjugate of **7**. The observed conjugation with saccharides are widely known for terrestrial plants, as described in the chapter 1.

From the results, the behavior of metofluthrin in water milfoil is proposed in figure 3.

Tables:

Table 1: Chemical structure of the reference standards.

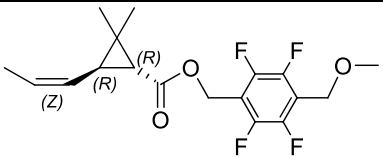
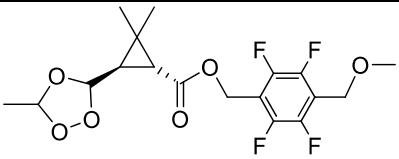
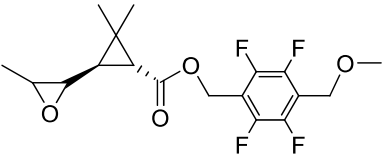
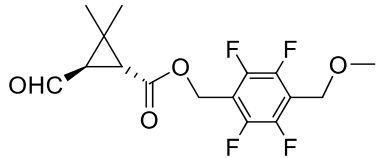
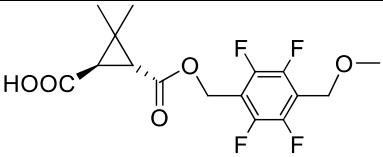
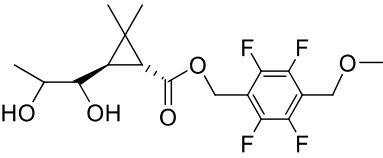
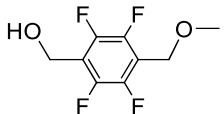
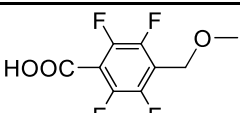
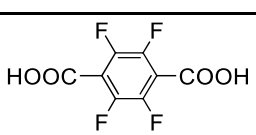
Designation	Chemical structure
RTZ-1	
2	
3	
4	
5	
6	
7	
8	
9	

Table 2: ¹⁴C distribution in the exposure water.

%AR				
	Days after exposure			
	0	0.5	2	7
<i>RTZ-1</i>	100.0	27.1	14.0	ND
4	ND	ND	1.7	ND
5	ND	ND	3.3	ND
6	ND	ND	0.9	ND
7	ND	14.1	45.4	57.7
8	ND	ND	5.1	20.6
Others*	ND	ND	1.8	6.0
Total**	100.0	41.2	72.2	84.3

ND: not detected.

*: the sum of multiple components, each <3.1%.

** : the unrecovered radioactivity was considered due to the absorption on plant and glass surfaces, which was re-distributed into the water by the ester hydrolysis.

Table 3: ¹⁴C distribution in the water milfoil at 7 day after the exposure.

%AR and %TRR		
	AR	TRR
Extract	12.8	94.6
<i>RTZ-1</i>	ND	ND
7	0.7	4.9
8	0.7	4.8
12	8.8	65.6
13	1.4	10.0
Others*	1.2	9.3
Unextractables	0.7	5.4
Total	13.5	100.0

ND: not detected.

*: The sum of multiple components, each <0.4%AR/2.5%TRR.

Figures:

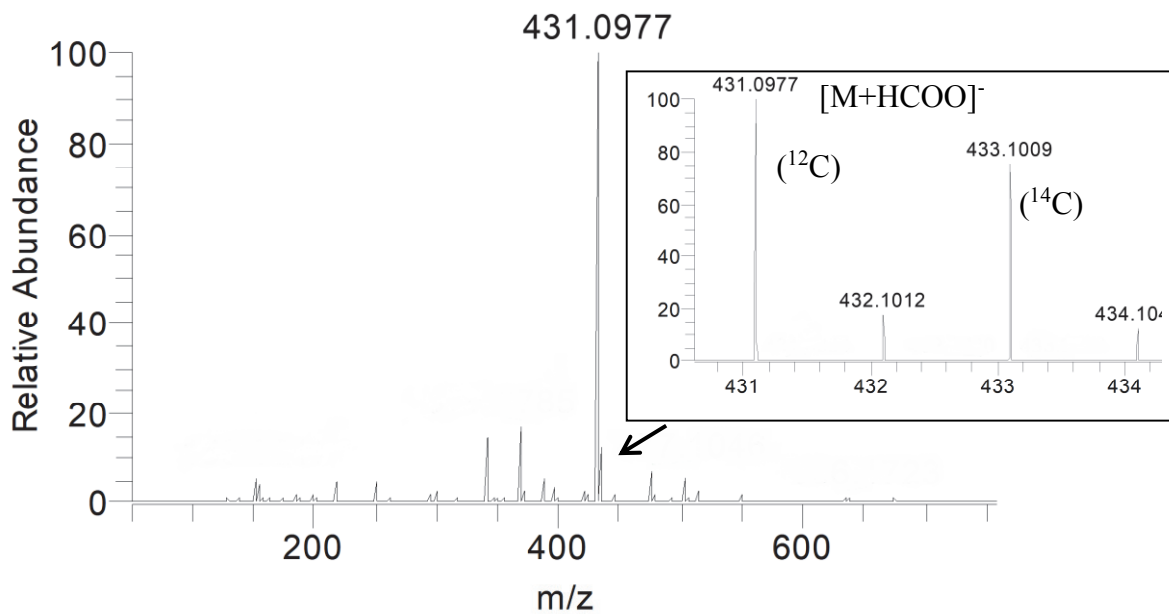


Figure 1: The mass spectrum of the metabolite 12.

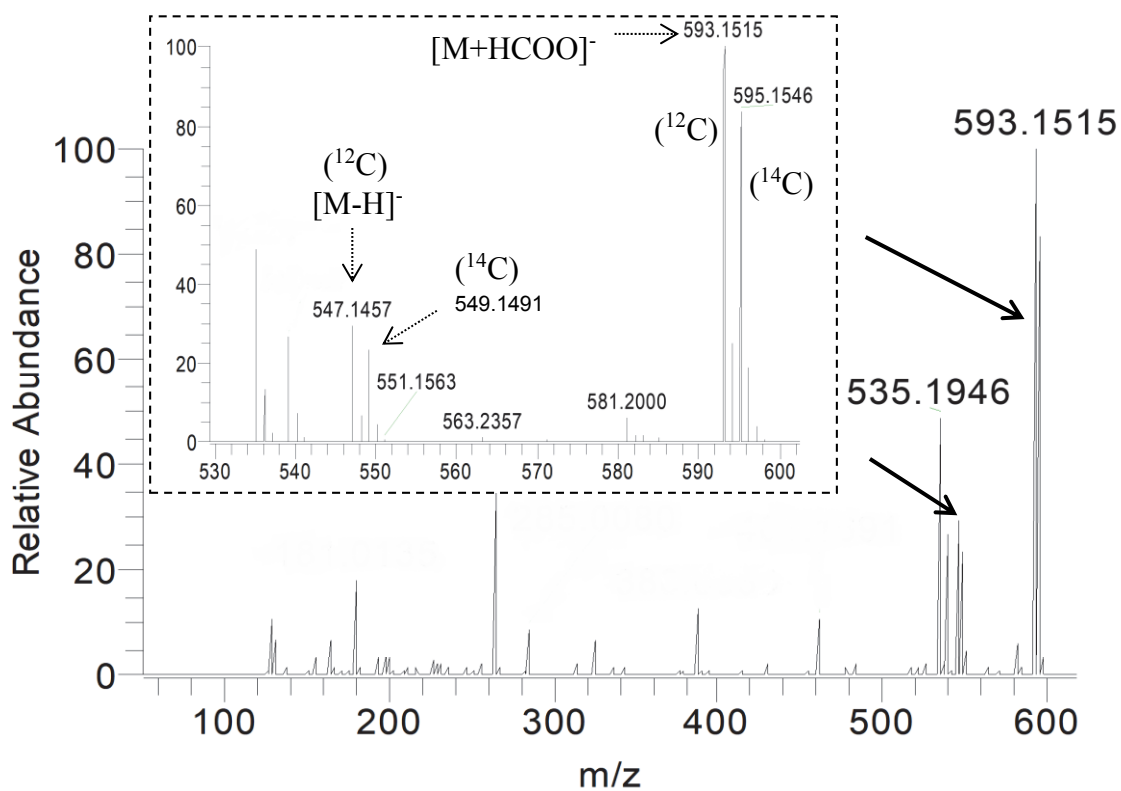


Figure 2: The mass spectrum of metabolite 13.

2.1.3. Fate Comparison Between Cabbage and Water Milfoil

The obvious differences experimentally demonstrated from the two metofluthrin studies can be summarized as:

1. As the initial degradation process, metofluthrin received ozonolysis followed by successive cleavage into the corresponding aldehyde and carboxylic acid on the cabbage surface, while aqueous hydrolysis and oxidation dominated in the water medium for water milfoil. These resulted in providing dissimilar metofluthrin-derived chemicals as the exposure species for each plant.
2. While the major species penetrated into cabbage were the hydrophobic metofluthrin and ester-conserving products, water milfoil likely accumulated less hydrophobic, high water-soluble chemicals, *viz.*, the ester cleaved products.
3. The metabolite distribution in plants were largely different between cabbage and water milfoil, both in quantity and variety. Saccharide conjugations commonly occurred, suggested the similar detoxification mechanism between these plants, but the target aglycones were different.

The above indicated the importance of chemical hydrolysis in the exposure of water milfoil for pesticides which are hydrolytically labile, causing difference in exposure chemical species, uptake, and eventually in metabolite distribution from terrestrial plants.

2.2. Behavior of Fungicide Mandestrobin

Mandestrobin, **1** [(*RS*)-2-methoxy-*N*-methyl-2-[α -(2,5-xylyloxy)-*o*-tolyl]-acetamide] is a new fungicide developed by Sumitomo Chemical Co., Ltd., possessing a 2-methoxy-*N*-methyl-acetamide substructure as a unique toxophore which is different from other strobilurin fungicides on the market and shows cross-resistant character with them. The fungicide was registered in various countries (*e.g.*, Japan, South Korea, EU, Canada, Australia and US) with the aim to control Sclerotinia rot, fruit tree scab and wide varieties of crop diseases by acting on mitochondrial respiratory chain complex III as QoI (Hirotoomi et al. 2016). **1** has an asymmetric center at the 2-carbon of the acetamide moiety and is manufactured as racemate form, thus, can be categorized as a chiral pesticide. For these groups, less or no bioactivity has often been identified on either one of the enantiomers. In the case of **1**, the *R* isomer possesses superior fungicidal activity to that of the antipode (Hirotoomi et al. 2016; EFSA 2015).

It is essential to examine and clarify the metabolic fate of a synthetic pesticide in crops to evaluate its toxicological risks for crop consumers who intake both the pesticide and its metabolites/degradates from agricultural commodities, as well as the fate in aquatic plants for detailed assessment on these species. Several research articles on metabolic profiles of strobilurin fungicides in crops have been published. For instance, azoxystrobin which was discovered at an early stage of synthetic strobilurin fungicide development history, having an enol ether/ester toxophore, like natural strobilurin A, is known to undergo cleavages of these linkages and the pyrimidine ring as major metabolic reactions combined with sunlight-driven *E/Z* isomerization at the olefin bond on plant surface (Joseph 1999; Balba 2007). Basically, the similar profiles have been reported for kresoxim-methyl and trifloxystrobin which have an oxime ether moiety as alternative to the enol function (Balba 2007). Unlike these precedent strobilurins, **1** which does not possess enol/oxime ether, ester or olefin functions may have a potential to undergo dissimilar metabolic pathway in plants. Besides, although there are several studies investigated the ecotoxicological effects of strobilurin fungicides on aquatic plants (Rodrigues et al. 2013), metabolism following uptake is not examined.

In this section, we report the metabolic behavior of **1** in wheat and water milfoil.

Wheat was selected as the major target species of **1** for crop protection. In the wheat study, two different [^{14}C]**1** separately radiolabeled at the phenoxy and benzyl rings were applied to clarify the fate of individual substructures. Due to the presence of the chiral center, **1** potentially undergo isomerization or enantioselective degradation/fractionation on and in plants either by abiotic and/or biotic reactions (Ma and Gan 2011; Albuquerque et al. 2018; Katagi 2012). To confirm such possibility, we quantitated the *R/S* enantiomeric composition of **1** after foliar application on wheat, as representative.

2.2.1. Metabolism of Mandestrobin in Wheat

MATERIALS AND METHODS

Chemicals

Two kinds of ^{14}C -radiolabeled **1** were prepared in our laboratory (Adachi et al. 2018). The compound was uniformly radiolabeled at the dimethylphenoxy and benzyl rings, abbreviated as [$\text{Ph-}^{14}\text{C}$]**1** (specific radioactivity; 120 mCi/mmol (4.44 GBq/mmol)) and [$\text{Bz-}^{14}\text{C}$]**1** (123 mCi/mmol (4.55 GBq/mmol)), respectively. The radiochemical purity of each ^{14}C compound exceeded 98.9% in reversed-phase high-performance liquid chromatography (HPLC) analysis. The *RS* isomeric ratio was confirmed to be 50:50 by the chiral HPLC analysis. Non-radiolabeled authentic standards of **1** (*R:S*, 50:50) and its metabolites were prepared in our laboratory (structures shown in Table 1). The structures of the compounds are given in Figure 1; (*RS*)-2-[2-(2-hydroxymethyl-5-methylphenoxy)methyl]phenyl]-2-methoxy-*N*-methylacetamide, **2**; (*RS*)-2-[2-(4-hydroxy-2,5-dimethylphenoxy)methyl]phenyl]-2-methoxy-*N*-methylacetamide, **3**; (*RS*)-2-[2-(5-hydroxymethyl-2-methylphenoxy)methyl]phenyl]-2-methoxy-*N*-methylacetamide, **4**; (*RS*)-3-{2-[1-methoxy-1-(*N*-methylcarbamoyl)methyl]benzyl-oxy}-4-methylbenzoic acid, **5**; (*RS*)-2-hydroxy-*N*-methyl-2-[α -(2,5-xyllyloxy)-*o*-tolyl]acetamide, **6**; (*RS*)-2-(2-hydroxymethylphenyl)-2-methoxy-*N*-methylacetamide, **7**. The compounds **6** and **7** were prepared according to the previous methods (Hirotoomi et al. 2016; Adachi et al. 2018). Other compounds were synthesized in our laboratory as follows with structural confirmation by HRMS with ESI mode and $^1\text{H-NMR}$ analyses;

Compound **2**: To **7** (1.50 g, 7.17 mmol) dissolved in tetrahydrofuran (THF, 30 mL), 4-methylsalicylic acid methyl ester (1.43 g, 8.60 mmol, Tokyo Chemical Industry), triphenylphosphine (2.26 g, 8.60 mmol, Tokyo Chemical Industry) and diisopropyl azodicarboxylate (1.74 g, 8.60 mmol, Tokyo Chemical Industry) were added and reacted under nitrogen atmosphere for 4 h with stirring at room temperature. The reaction mixture was evaporated and purified by silica gel column chromatography using toluene:acetone (2:1, v:v) to obtain the methyl ester of **2** (2.43 g, yield 94.8%, white solid). To 1.57 g (4.40 mmol) of the methyl ester product dissolved in dichloromethane (CH₂Cl₂, 20 mL), diisobutylaluminum hydride (1 mol/L in CH₂Cl₂, 13.2 mL, 13.2 mmol, Tokyo Chemical Industry) was added dropwise under nitrogen atmosphere at -78°C with stirring and reacted for 3 h. The reaction mixture was then poured into 2 M HCl with ice, and then extracted using CH₂Cl₂, dried with anhydrous magnesium sulfate and purified by silica gel column using hexane/ethyl acetate (2:1, v:v) to obtain **2** (692 mg, yield 47.7%, white solid). HRMS (ESI +): *m/z* 352.1511 [M+Na]⁺, -2.384 ppm error for C₁₉H₂₃O₄NNa.; ¹H-NMR (400 MHz, CDCl₃): δ 2.36 (3H, s, Ph-CH₃), 2.78 (3H, d, *J*=4.8 Hz, -CONHCH₃), 3.34 (3H, s, -OCH₃), 3.83 (3H, s, -COOCH₃), 4.54 (1H, d, *J*=12.4 Hz, -CH₂OH), 4.65 (1H, d, *J*=12.4 Hz, -CH₂OH), 4.97 (1H, s, -CH(OCH₃)CO-), 5.11 (1H, d, *J*=11.2 Hz, -CH₂O-), 5.37 (1H, d, *J*=11.2 Hz, -CH₂O-), 6.76~7.47 (8H, m, -CONHCH₃, Ph).

Compound **3**: *p*-xyloquinone (5.00 g, 36.7 mmol, Tokyo Chemical Industry) dissolved in 70 mL of diethyl ether was partitioned with 35 mL of sodium hydrosulfate (Tokyo Chemical Industry), washed with water and dried using anhydrous sodium sulfate to obtain *p*-xylohydroquinone (3.63 g, yield 71.6%, pale yellow powder). To the THF solution dissolving the hydroquinone (1.09 g, 7.90 mmol) and **7** (1.57 g, 7.50 mmol), triphenylphosphine (1.97 g, 7.50 mmol) and diisopropyl azodicarboxylate (1.52 g, 7.50 mmol) was added and reacted under nitrogen atmosphere for 18 h at room temperature with stirring. The reaction mixture was then evaporated and purified by silica gel column using hexane:ethyl acetate (2:1, v:v) to obtain **3** (550 mg, yield 22.3%, white solid). HRMS (ESI +): *m/z* 330.1690 [M+Na]⁺, -2.952 ppm error for C₁₉H₂₄O₄N.; ¹H-NMR (400 MHz, CDCl₃): δ 2.15 (3H, s, hydroquinone-CH₃), 2.19 (3H, s, hydroquinone-CH₃), 2.83 (3H, d, *J*=4.8 Hz, -CONHCH₃), 3.33-3.35 (3H, m, -OCH₃), 3.83 (3H, s, -

COOCH₃), 4.72 (1H, s, -OH), 4.99 (1H, d, $J=11.6$ Hz, -CH₂OH), 5.04 (1H, s, -CH(OCH₃)CO-), 5.38 (1H, d, $J=11.6$ Hz, -CH₂OH), 6.58 (1H, s, hydroquinone ring), 6.71 (1H, s, hydroquinone ring), 6.82~6.83 (1H, br, -CONHCH₃), 7.26~7.52 (4H, m, Ph).

Compound 4: To the ethanol solution (30 mL) dissolving 3-hydroxy-*p*-toluic acid (20 g, 131 mmol, Tokyo chemical Industry), 0.71 mL of concentrated sulfuric acid was added and refluxed for 13 h. After evaporation, 50 mL of water was added to the reaction mixture and pH was adjusted to 7 using sodium carbonate, and then, extracted with *tert*-butyl methyl ether. The organic solution was then dried using anhydrous sodium sulfate and evaporated to obtain 3-hydroxy-*p*-toluic acid ethyl ester (21.8 g, yield 92.2%, pale yellow liquid). 1.55 g of 3-hydroxy-*p*-toluic acid ethyl ester (8.60 mmol) and 1.50 g of **7** (7.17 mmol) was dissolved in 30 mL of THF. To the solution, triphenylphosphine (2.26 g, 8.60 mmol) and diisopropyl azodicarboxylate (1.74 g, 8.60 mmol) was added and reacted under nitrogen atmosphere for 3 h at room temperature with stirring. The reaction mixture was then evaporated and purified by silica gel column using hexane:ethyl acetate (3:2, v:v) to obtain ethyl ester of **5** (2.03 g, yield 76.1%, white solid). To the ethyl ester of **5** (1.89 g, 5.10 mmol) dissolved in CH₂Cl₂ (25 mL), diisobutylaluminum hydride (1 mol/L in CH₂Cl₂, 15.3 mL, 15.3 mmol) was added dropwise at -78 °C with stirring under nitrogen atmosphere and reacted for 3 h. The reaction mixture was poured into 2 M HCl with ice, and then extracted using CH₂Cl₂, dried with anhydrous magnesium sulfate and purified by silica gel column using hexane/ethyl acetate (2:1, v/v) to obtain **4** (940 mg, yield 56.0%, white solid). HRMS (ESI +): m/z 330.1695 [M+H]⁺, -1.498 ppm error for C₁₉H₂₄O₄N.; ¹H-NMR (400 MHz, CDCl₃): δ 2.25 (3H, s, Ph-CH₃), 2.83 (3H, d, $J=4.8$ Hz, -CONHCH₃), 3.35 (3H, s, -OCH₃), 4.61 (1H, brs, -CH₂OH), 4.99 (1H, s, -CH(OCH₃)CO-), 5.17 (1H, d, $J=12.4$ Hz, -CH₂O-), 5.45 (1H, d, $J=12.4$ Hz, -CH₂O-), 6.82~7.53 (8H, m, -CONHCH₃, Ph).

Compound 5: To the ethyl ester of **5** (1.30 g, 3.50 mmol) dissolved in ethanol (50 mL), 10 mL of 30% NaOH was added and reacted for 1.5 h at room temperature with stirring. The reaction solution was washed with diethyl ether and the aqueous solution was pH adjusted to 2 using concentrated HCl. The aqueous solution was extracted with ethyl acetate, and then, the organic layer was dried using anhydrous sodium sulfate and evaporated to obtain **5** (1.17 g, yield 97.1%, white solid). HRMS (ESI -): m/z 342.1341

[M-H]⁻, 1.435 ppm error for C₁₉H₂₀O₅N.; ¹H-NMR (400 MHz, CDCl₃) δ 2.27 (3H, s, Ph-CH₃), 2.59 (3H, d, *J*=4.8 Hz, -CONHCH₃), 3.30 (3H, s, -OCH₃), 5.00 (1H, s, -CH(OCH₃)CO-), 5.25 (1H, d, *J*=12.2 Hz, -CH₂O-), 5.45 (1H, d, *J*=12.2 Hz, -CH₂O-), 6.83 (1H, br m, -CONHCH₃), 7.28~8.12 (1H, m, -CONHCH₃, Ph).

In addition, 2,5-dimethylphenol (**8**) was purchased from Sigma Aldrich Co. The chemical structure of each compound is shown in Figure. 1. The chemical purity of each standard was >98%. All the reagents and solvents used in this experiment were of an analytical grade. The enzymes, β-glucosidase (EC 3.2.1.21., from almond, 37 units/mg) and Driselase (from *Basidiomycetes sp.*, cellulase >100 units/g, laminarinase >10 units/g, xylanase >3 units/g) were purchased from Oriental Yeast Co. Ltd. and Sigma Aldrich Co., respectively. All other chemicals were of a reagent grade and obtained from the commercial suppliers.

Chromatography

A reversed-phase HPLC system to analyze the test substance and its metabolites consisted of a series 1200 LC module (Agilent Technologies Inc.) or a L-7000 module (Hitachi Ltd.). The column used was a 5 μm, 150×6 mm, SUMIPAX ODS A-212 (Sumika Chemical Analytical Service, Ltd.). The following gradient system was employed at a flow rate of 1 mL/min; 0.1% formic acid (solvent A) and acetonitrile (Solvent B): 0-2 min, A%/B% (v/v), 95/5; 10 min, 70/30; 30 min, 65/35; 40 min, 0/100; 40-45 min, 0/100. The typical retention times of **1** and other synthetic standards were 42.2 (**1**), 33.4 (**2**), 36.4 (**3**), 35.8 (**4**), 37.5 (**5**), 39.2 (**6**), 17.1 (**7**), and 25.7 (**8**) min. In addition, three unknown metabolites with no corresponding reference standards were detected at 22.0 (**9**, **10**) and 26.5 (**11**) min, thus another HPLC condition was developed for the separation, quantitation and isolation of the co-eluted peaks **9** and **10**; a 4 μm, 4.6 mm i.d.×30 cm, Synergi Polar-RP column (Phenomenex Inc.) was applied with isocratic elution (acetonitrile with 0.1% formic acid:0.1% formic acid, 25:75 (v:v)). The chiral analysis for the *R* and *S* isomers of **1** was conducted with a LC-module Series 1100 (Hewlett Packard) using a 5 μm, 150×4.6 mm Chiralpak AD RH column (Daicel Chemical Industries) with an isocratic eluent of acetonitrile:water, 1:1 (v:v), at a flow rate 1 mL/min (retention time: *R* isomer/5.6 min, *S* isomer/7.1 min). The radioactivity in the

column effluent was measured using a Flow Scintillation Analyzer Radiomatic 525TR or 625TR (Perkin Elmer Co., Ltd.) with mixing Ultima-Flo A or M (Perkin Elmer, Co., Ltd.) as the scintillator. The detection limit of the HPLC analyses was 150 dpm (2.5 Bq).

TLC analysis was carried out for an analytical purpose using 20×20 cm, 0.25 mm thickness LK5DF thin-layer silica gel plates (Whatman). The non-radiolabeled reference standards were detected by exposing the chromatoplates to ultraviolet light for direct visualization. The radioactivity in each spot on the plate was detected by a AR2000 Imaging Scanner (Bioscan Inc.) The solvent systems for TLC were as follows: chloroform:methanol, 9:1 (v:v), R_f values 0.68 (1), 0.63 (2), 0.62 (3), 0.60 (4), 0.21 (5), 0.65 (6), 0.66 (7); ethyl acetate:methanol:acetic acid, 18:2:1 (v:v:v), R_f values 0.65 (1), 0.58 (2), 0.65 (3), 0.50 (4), 0.20 (5), 0.56 (7); hexane:isopropanol, 5:2 (v:v), R_f values 0.56 (1), 0.43 (2), 0.49 (3), 0.33 (4), 0.25 (5), 0.50 (7).

Radioanalysis

Radioactivity in the plant rinsates and extracts was determined by LSC with a model 2900TR spectrometer (Packard instrument Co.) or model LS6500 instrument (Beckman Coulter Inc.) after mixing each aliquot with Emulsifier Scintillator Plus or Ultima Gold (Perkin Elmer Co., Ltd.). The detection limit of LSC analysis was 40 dpm (0.67 Bq). The post extracted bound residues of plants were combusted using a model OX-500 or OX-700 Biological oxidizer with oxidizer LSC cocktail (RJ Harvey Instrument Co.). The radioactivity therein was quantitated by LSC. The efficiency of combustion was determined to be greater than 95.0%.

Spectroscopy

LC–ESI–MS analysis was conducted to characterize metabolites of **1** using a TQD tandem quadruple spectrometer equipped with an Acquity UPLC (Ultra Performance Liquid Chromatography) and an Acquity photodiode array detector (Waters Co.). The following parameters controlled by a MassLynx software (version 4.1, Waters Co.) were used for the typical analysis: source temperature 150°C; desolvation temperature 450°C; capillary voltage 3.2 kV; cone voltage 10–40 V; collision energy 5–20 V. The HPLC column eluent was diverted in the ratio 4:1 and introduced to the mass spectrometer and

radiodetector, respectively. For the confirmation of synthetic standards, HRMS was obtained using Q-Exactive Focus (Thermo Fisher Scientific Inc.) mass spectrometer by infusion injection. The analytical parameters at the mass module controlled by the Xcalibur software (version 2.2) are shown below: sweep gas flow 10, source temp., 100°C, desolvation temp., 350°C, capillary voltage 3.5 kV, cone voltage 10-40 eV. In addition, ¹H-NMR spectra of the standards were recorded in CDCl₃ using a Unity-400 spectrometer at 400 MHz (Varian Inc.) with TMS as an internal standard.

Plant Materials and Maintenance

The wheat 'Promontory' was purchased from Granite Seed (Lehi). The soil used for the wheat cultivation was a combination of local natural loamy sand from Rochester, MA, and a commercial potting soil (Metro Mix 360, SunGro Horticulture Distribution, Inc.) blended at a 9:1 ratio. The loamy sand was collected from a fallow field where no pesticide application was recorded in the previous three years. The soil used in the study had no detectable ¹⁴C-radioactivity exceeding the minimum quantifiable level. The pH of the soil mixture was adjusted from 4.5 to 6.2 by the addition of powdered limestone. The characterization of the soil was: soil texture, sand 71%, silt 22%, clay 7%; soil classification, sandy loam; organic carbon content 8.3%; pH 6.2; moisture, 29%. Wheat seeds (approximately 30 seeds per pot) were planted in each of the twenty seven pots (11-inch diameter). Wheat plants were grown in a greenhouse located at Smithers Viscient laboratory (Wareham) with the light cycle of 16 h day/8 h night. The temperature in a greenhouse was set at 28°C day/21°C night, and continuously monitored/recorded using a thermometer. The relative humidity in the greenhouse ranged from 19–85% for the duration of the study. The pots were watered with either well water or a dilute liquid fertilizer as necessary until harvest. The plants were fertilized with Peters 20-20-20 at a concentration of 200 mg/L.

Spray Application and Sampling

The spray application was conducted with 25% suspension concentrate (SC) formulation at the application rate of 300 g/ha. 4.6 mg of each radiolabeled **1** was individually mixed with 13.7 mg of the non-radiolabeled one for isotopic dilution (specific radioactivity of 200 kdpm/mg, 3.33 kBq/mg). Then, the blank formulation was

added to the mixture, along with water for concentration adjustment, to prepare 25% SC spray solution. The final concentration of **1** in the spray solution was 0.3 mg/mL. The formulation was sprayed onto the wheat at stem elongation stage (grown 37 days after seeding) using a hand pump sprayer from the top of plants. After the application, the radioactivity remaining in the bottle was recovered by rinsing with acetonitrile and the rinsate was assayed by LSC. After 7, 14 and 104 days, forage, hay and straw/grain were harvested from each 9 pots by cutting them individually at approximately 2–4 cm above the soil surface using a pruning scissors. Plant samples were removed from any adhering soil by gentle shaking or brushing and the total weight of each plant sample was recorded. The surface of each foliage was individually rinsed using acetonitrile, pulverized with dry ice, and then stored frozen until further extraction.

Extraction and Analysis

Each 10 to 30 g of pulverized plant from each 9 pots was placed into a plastic bottle and extracted with acetone:water (4:1, v:v, 10 mL/g plant) using a model 133 tissue homogenizer (Bio Spec Products Inc.) at high speed for one min. The sample was centrifuged at 3,000 rpm for 10 min to separate the extract from plant solids. The supernatant was removed and the extraction was repeated twice in the same manner, then the supernatants were combined. The remaining plant matrices were successively extracted with acetone/water/concentrated HCl (80:20:1, v:v:v, 10 mL/g plant) using the above procedures. The radioactivity in each extract was quantitated by LSC in duplicate and analyzed by HPLC. The extraction and LSC/HPLC analysis of each plant sample were performed within 1 month after the harvest. The unextractable residues were allowed to dry, and then subjected to combustion analysis. The unextractable residues of hay were further characterized by Driselase treatment (0.5–1.0 g of residues and 40 mg of enzyme dissolved in 10 mL of 0.1 M sodium acetate buffer pH 4.5 were incubated at 38°C, overnight), 0.1 M HCl and 0.1 M NaOH extractions (40°C, overnight). For straw, the unextractable residues were sequentially extracted using 0.1 M HCl (40°C, overnight), 6 M HCl (80°C, 4 h), 0.1 M NaOH (40°C, overnight) and 6 M NaOH (80°C, 4 h). The final ¹⁴C-bound residues in hay and straw were determined by combustion

analysis.

Metabolite Identification and Characterization

Identification of each metabolite was basically conducted by HPLC and TLC co-chromatographies with non-radiolabeled reference standards. To verify whether unknown metabolites **9–11** are conjugate or not, enzymatic and alkaline hydrolysis was representatively conducted using the [Ph-¹⁴C] hay extract. For the confirmation of glucose conjugate, approximately 200 kdpm (3.33 kBq) of the hay extract or 50 kdpm (833 Bq) of each HPLC-isolated unknown fraction was evaporated to dryness and dissolved in 1 mL of 10 mM acetate buffer at pH 5.0. To the mixture, 3 mg of β -glucosidase was added, mixed well and incubated in a BR-180LF BioShaker (TAITEC Co. Ltd.) at 37°C and 100 rpm. Aliquots of the mixture were sequentially sampled and analyzed by HPLC. For malonylglucose conjugates, the dried extract or each isolate was separately subjected to alkaline hydrolysis by adding 1 mL of 0.03 M NaOH as pretreatment prior to the enzymatic reaction. The mixture was reacted at the room temperature for 0.5 h, neutralized using 1 M HCl and the reaction mixture was subjected to HPLC and LC-MS analyses. Successively, 1 mL of 10 mM acetate buffer and 3 mg of β -glucosidase were added to the neutralized mixture and the reaction was periodically monitored by HPLC.

Estimation of Chemical Property

n-octanol/water Partition coefficient (K_{ow}) of **7** was predicted using Estimation Program Interface (EPI) Suite from the U.S. EPA (version 4.11) (EPA 2017).

RESULTS

Distribution of Radioactivity in Wheat

The actual application ratios of [¹⁴C]**1**, determined from the ¹⁴C remained in the post-spraying bottle, were 303 and 306 g/ha for phenoxy and benzyl label treatments, respectively. The recovered radioactivities in forage, hay, straw and grain for Ph/Bz label were 83.8/93.0, 90.3/96.2, 23.7/30.4 and 0.006%/0.008%AR, respectively. The distribution of ¹⁴C and constituents on/in foliage (forage, hay and straw), summarized in Table 2, was generally similar between the two radiolabels. The TRR in foliage was

calculated as the sum of ^{14}C in the surface rinse, extractable and unextractable. For foliage, the recovered radioactivity by the surface rinse decreased along with the cultivation period to 33.9–41.0 (3.542–4.570 ppm) in forage and 2.8–3.9%TRR (0.069–0.070 ppm) in straw. In the surface rinses, unaltered **1** was consistently the main component remained in forage and hay at 30.3–38.5%TRR (3.163–4.289 ppm) and 16.4–21.0%TRR (1.302–1.478 ppm), respectively, and then became minor as 0.3–0.5%TRR (0.005–0.012 ppm) in straw. As minor products, **2**, **3**, **4**, **5**, **6** and **7** were detected at their maximum of 1.1%TRR (0.020 ppm, straw), 0.1%TRR (0.003 ppm, straw), 0.4%TRR (0.007 ppm, straw), 0.2%TRR (0.004 ppm, straw), 0.5%TRR (0.031 ppm, hay) and 0.7%TRR (0.072 ppm, forage), respectively. Three polar unknowns **9–11**, which were later characterized as malonylglucose conjugates of **2–4**, were also observed at each below 0.4%TRR. Several other ^{14}C minor constituents also existed as minors, each amounting to less than 2.1%TRR for both radiolabels. With respect to the acetone/water and acetone/HCl extracts, the radioactivities therein were 50.0–58.6 and 2.0–3.2%TRR (forage), 61.1–70.6 and 2.2–4.7%TRR (hay) and 41.1–46.7 and 17.4–18.0%TRR (straw), respectively. In the sum of extracts, *i.e.* acetone/water and acetone/HCl, **1** declined from 12.5–29.6%TRR (13.950–3.091 ppm, forage) to 1.1–1.5%TRR (0.020–0.037 ppm, straw) along with the plant growth. The relevant metabolites observed in the extracts were **9**, **10** and **11** which reached their maximum values in hay as 11.0–12.3%TRR (0.688–1.108 ppm), 5.4–12.9%TRR (0.484–0.803 ppm) and 6.3–6.9%TRR (0.390–0.619 ppm), respectively. The maximum residual levels of **2**, **3** and **4** were 6.0–8.4%TRR (0.151–0.156 ppm, straw), 1.3–1.4%TRR (0.023–0.035 ppm, straw) and 1.7–2.7%TRR (0.032–0.069 ppm, straw), respectively. The benzyl label-specific degradate **7** amounted to the maximum of 11.3%TRR (0.281 ppm, straw), while the structural counterpart **8** unique to the phenyl label was not detected in any amount. There were no other ^{14}C components exceeding 7.3%TRR in the foliage extracts for both radiolabels. The unextractable residues of forage, hay and straw increased from 5.5–5.8%TRR (0.569–0.642 ppm, forage) to 32.5–37.6%TRR (0.696–0.810 ppm, straw) in parallel to the ^{14}C decrease on plant surface. The unextractable residues of hay and straw were attempted to be further characterized by

Driselase treatment and successive harsh extractions using HCl and NaOH solutions. By these procedures, the unextractable residues of hay released 1.5–3.5%TRR (0.091–0.319 ppm, Driselase), 1.4–1.5%TRR (0.090–0.133 ppm, 0.1 M HCl) and 2.3–5.8%TRR (0.208–0.362 ppm, 0.1 M NaOH), and finally, 0.4–1.3%TRR (0.037–0.081 ppm) remained as the bound residue for both radiolabels. From straw, the radioactivity recovered by acidic solvents (0.1 M and 6.0 M HCl) was less than 5.9%TRR (<0.123 ppm). Successive extractions using alkaline (0.1 M and 6.0 M NaOH) released more radioactivity (10.3–16.4%TRR, 0.210–0.304 ppm), but these fractions contained large amount of matrices which were unable to be analyzed chromatographically. The final radioactivity in bound residue of straw accounted for 0.6–1.1%TRR (0.014–0.020 ppm).

With respect to grain, the distribution of radioactivity and ^{14}C constituents is summarized in Table 3. The TRR in grain was calculated as the sum of ^{14}C in the extractable and unextractable because grain was extracted without surface rinse since it did not receive any direct ^{14}C spray due to the application timing prior to grain setting. The TRR of benzyl label specimen showed approximately seven times higher ^{14}C residues than that of phenoxy label (phenoxy: 0.012 ppm, benzyl: 0.089 ppm). The radioactivities in acetone/water and acetone/HCl extracts were combined and subjected to HPLC/TLC analyses due to the low residual level. For the phenoxy label, 67.0%TRR (0.008 ppm) was extractable. No radioactive components matched with the reference standards, but multiple constituents were detected in which the maximum single component amounted to 25.6%TRR (0.003 ppm). These products were not characterized further due to their extremely low radioactivity. For the benzyl label, 72.7%TRR (0.065 ppm) was extractable. The metabolites detected therein were **2**, **7** and **9/10** which amounted to 3.1%TRR (0.003 ppm), 60.6%TRR (0.054 ppm) and 1.3%TRR (0.001 ppm), respectively. Similarly with foliage, **8** was not detected. Several unknown ^{14}C constituents were observed, but were not further characterized due to their low TRR concentrations, <0.01 ppm. The unextractable residue accounted for 33.0 and 27.3%TRR which was equivalent to 0.004 and 0.024 ppm for phenoxy and benzyl labels, respectively.

RS Enantiomeric Ratio of 1 in Wheat

The *RS* isomeric ratio of **1** remaining in the rinsates and extracts of forage and hay was investigated by the chiral HPLC analysis. As representative, the chiral HPLC chromatogram of **1** in [Ph-¹⁴C] straw is shown in Figure 2. The *RS* ratio ranged from *R:S* = 50.1:49.9–50.4:49.6 in the surface rinsates and 50.2:49.8–44.1:55.9 in the extracts, mostly remaining as racemate. The results indicated that *RS* isomerization at the 2-carbon of acetamide as well as enantioselective degradation were insignificant at both surface and inner portions of wheat plant. Although the possibility of enantiomerization cannot be concluded unless the behavior of each isomer is clarified, the results are important evidences to support that fungicidal active *R* isomer would not predominantly convert to less effective *S* isomer and *vice versa* in crops after agricultural use.

Characterization of the Metabolites 9–11

The unknown metabolites **9–11** detected as major components in foliage extracts were further characterized in detail using the hay extract treated with [Ph-¹⁴C]**1**. When a portion of the original extract containing the unknowns was subjected to the enzymatic hydrolysis using β -glucosidase, **9**, **10** and **11** were slowly (deglycosylation not completed by 7 days) transformed to the corresponding aglycone, **2**, **3** and **4**, showing their possible identities as glucose conjugates (Figures 3A and B). By the LC-MS analysis of each unknown, the following ions were obtained in the negative ion mode ($C_{28}H_{35}NO_{12}$, Mw 577): *m/z* 690 [$M+CF_3COO$]⁻, 576 [$M-H$]⁻, 532 [$M-COOH$]⁻. As representative, the mass spectrum of **9** is shown in Figure 4A.

From these results, the structures of **9**, **10** and **11** were proposed as malonylglucose conjugates of **2**, **3** and **4**, respectively. As another hydrolysis experiment, the alkaline pretreatment was introduced prior to the enzymatic digestion in attempt to release possible endogenous malonyl moiety. By the pretreatment, individual malonylglucose conjugates in the hay extract were immediately converted to the corresponding new single peaks on HPLC chromatogram each eluted at approximately 3–4 min earlier retention time within 0.5 h (Figure 3C), and successive β -glucosidase hydrolysis released each

aglycone by 3 h (Figures 3D and E). The post-alkaline treatment products of **9–11** were also confirmed by LC-MS analysis. The following molecular mass and characteristic fragments were detected in the positive ion mode, revealed the glucose conjugate structures ($C_{25}H_{33}NO_9$, Mw 491): m/z 514 $[M+Na]^+$, 492 $[M+H]^+$, 330 $[M-glucose+OH+H]^+$, 312 $[M-glucose+H]^+$, 192 $[M-glucose-dimethylphenol+H]^+$. Figure 4B is shown as the representative of the demalonyl conjugate of **9**. These results demonstrated the elimination of the malonyl group from the glucose by the alkaline treatment while remaining each glycosidic linkage intact. As the results, **9**, **10** and **11** were fully characterized as **2-**, **3-** and **4-**malonyl glucosides, respectively.

DISCUSSIONS

Since the recovery of the applied radioactivities largely decreased at the final harvest (straw and grain), it is likely that **1** received photodegradation on plant surface and become mineralized/volatilized. Such tendency was previously confirmed in the photodegradation study of **1** (Adachi et al. 2018). The hydroxylated products **2**, **3**, **4**, carboxylated **5** and de-methylated **6** were considered as typical metabolites generated by enzymatic function(s) at inner plant tissues as phase I detoxification processes by cytochrome P450 and/or other oxygenases, and the malonylglucose conjugates **9–11** as phase II conjugation products by glucosyl/malonyl transferases (Siminzsky 2006; Sandermann 1994).

In the wheat surface rinse fractions aimed to analyze ^{14}C -residues on the plant surface where such phase I/II enzymes would hardly be accessible, not only **1** but also small amounts of **2–6** and the malonylglucose conjugates **9–11** were detected. Although epiphytic microbes present on the plant surface may have contributed to generate **2–6** (Van Eerd et al. 2003) the components in the rinse were regarded as the portions eluted from inner plant tissues during the surface wash since majority of these products were detected in the wheat extract, and the same theory could be applied for the existence of malonylglucose conjugates on the surface. This assumption is supported by the study of Myung et al. (2013). They investigated the structural change of epicuticular wax layer after washing the surface of wheat leaf using various organic solvents, and showed

that acetonitrile somewhat deteriorates the wax composition, although it was the most mild solvent they examined.

With respect to **7**, it is known as the major photodegradate rapidly generated *via* photo-induced homolytic bond cleavage at the benzyl ether bond (Haga and Takayanagi 1996; EFSA 2015; Achi et al. 2018), which is the reaction that could proceed on wheat surface by the sunlight. However, especially in straw, the degradate dominantly distributed inside the plant. Taking into account the hydrophilic nature of **7** ($\log K_{ow}$ -0.26; estimated using EPI Suite) which was generally considered unable to penetrate hydrophobic embedding epicuticular wax (Dettenmaier et al. 2009; Trapp 2007), it was assumed to be produced mainly by enzymatic reaction(s) at inside of wheat tissue. Besides, photodegradation of **1** induces photo-Claisen rearrangement and gives product through cleavage at the benzyl ether bond followed by recombination of **8** and the benzyl carbon of **7** (Adachi et al. 2018), but such products were not detected on/in wheat. The minor contribution of the photodegradation may be due to the sunlight screening effect by the morphological complexity of leaf surface and epicuticular wax layer, mostly consists of aliphatic hydrocarbons but also UV-absorptive unsaturated fatty acids, aldehydes/ketones, flavonoids and etc., preventing photolysis to proceed as **1** diffused within the layer (Katagi 2004).

Both in wheat foliage and grain, **8** or its particular derivatives, as possible counterpart of **7**, were not detected on/in wheat, which could be explained from their biotic (enzymatic) and abiotic (photolytic) processes. For biotic processes, the metabolism of dimethylphenols has been extensively studied in bacteria (Pho and Bayly 1980; Hopper and Chapman 1970; Hopper and Kemp 1980; Ewers et al. 1989). It was shown that the metabolism of **8** proceeds via oxidation of the methyl group at 5-position and the phenyl ring at 4-position to form 4-methylgentisic acid and successively undergoes benzene ring cleavage to produce various minor organic acids. In addition, phenolic compounds widely distributed as plant natural constituents in various higher plants are known to be incorporated into lignin in cell wall and anthocyanin in vacuole under the shikimate pathway (Mohr and Schopfer 1992). For abiotic process, by employing electron spin resonance (ESR) and radical trapping detection techniques, Adachi et al. (2018) succeeded to detect benzyl radical form of **7**, whereas, the counterpart phenoxy radical of **8** was undetectable. The authors concluded that the phenoxy radical

was unstable and rapidly decomposed to multiple components followed by mineralization *via* successive radical chain reactions interacting with other molecules or *via* self-decomposition. Thus, in summary, **8** is considered to be rapidly degraded into multiple degradates and incorporated to plant natural components once generated on and in plant. Such explanation could be supported by the results that foliage and grain of the phenoxy label treatment overall showed higher rates of multiple degradates and unextractables than the benzyl label.

The malonylglucose conjugates of hydroxylated **1** were likely generated by malonylation which is a well-known reaction in plants such as to stabilize labile biomolecules (Heller and Forkmann 1994) and to enhance solubility of xenobiotics to transport them into vacuole for detoxification (Taguchi et al. 2010). Similar to our finding, poor reactivity of malonylglucose conjugates against β -glucosidase is known for wide varieties of substrates including both natural products (e.g., isoflavones) and xenobiotics (Schmitt et al. 1985; Petroutsos et al. 2008; Ismail and Hayes 2005). The β -glucosidase from almond applied in this study is categorized in glycoside hydrolase (GH) family GH 1 (He 1997) and many β -glucosidases from GH 1, GH 3, etc., possess the similar reactive domain with highly conserved catalytic amino acid residues (Marana 2006; Cairns and Esen 2010; Rye and Withers 2000; Henrissat et al. 1995; Jenkins et al. 1995). The binding of glucose moiety at subsite -1 is considered to be strongly controlled by hydrogen bonds formed between the hydroxyl groups of glucose moiety at the 2-, 3-, 4- and 6-positions, where malonyl moiety bounds, and amino acid residues (Marana 2006; Cairns and Esen 2010; Vasella et al. 2002; Sansenya et al. 2011; Cicek et al. 2000; Verdoucq et al. 2004; Zechel et al. 2011; Matsuzawa et al. 2016). Such interactions are also believed to stabilize the deglycosylation transition-state (Marana 2006; Cairns and Esen 2010; Rye and Withers 2000; Henrissat et al. 1995; Jenkins et al. 1995; Vasella et al. 2002; Sansenya et al. 2011; Cicek et al. 2000; Verdoucq et al. 2004) and enables the key glutamine residue(s), or others, to function as catalytic acid/base and nucleophile (Marana 2006; Rye and Withers 2000; Sansenya et al. 2011; Zechel et al. 2011). Overall, based on the critical importance of hydrogen bonds formed at glucose OH groups including 6-OH, it is speculated that the decreased deglycosylation efficiency observed for malonylglucose was attributed to the malonyl additive causing unfavorable electrostatic repulsion or steric hindrance in forming proper hydrogen bond interactions.

In conclusion, the metabolic pathway of **1** in wheat is proposed in Figure 1. **1** penetrated into wheat tissue along with the growth period, and underwent extensive metabolism via phase I and II oxidation followed by incorporation into plant components (phase III). The *RS* isomerization or enantioselective degradation was considered unlikely in the wheat metabolism.

Tables:

Table 1: Chemical structures of reference standards.

Designation	Chemical structure
1	
2	
3	
4	
5	
6	
7	
8	

Table 2: ¹⁴C distribution and metabolites on/in foliage.

%TRR						
	Days after spray					
	Forage: 7 days		Hay: 14 days		Straw: 104 days	
	[Ph- ¹⁴ C]	[Bz- ¹⁴ C]	[Ph- ¹⁴ C]	[Bz- ¹⁴ C]	[Ph- ¹⁴ C]	[Bz- ¹⁴ C]
Surface Rinses	41.0	33.9	23.3	19.1	3.9	2.8
1	38.5	30.3	21.0	16.4	0.3	0.5
2	ND	ND	0.3	ND	1.1	0.4
3	ND	ND	ND	ND	ND	0.1
4	ND	ND	ND	ND	0.4	0.2
5	ND	ND	ND	ND	0.2	0.2
6	0.3	0.3	0.5	0.2	0.1	<0.1
7	NA	0.7	NA	ND	NA	0.5
9	0.3	0.2	0.2	0.3	0.11**	ND
10	0.1	0.2	0.2	0.1		
11	ND	0.2	ND	ND	ND	<0.1
others	1.8	2.0	1.1	2.1	1.7	0.9
Extractables*	53.2	60.6	65.8	72.8	58.5	64.7
1	12.5	29.6	5.3	6.3	1.1	1.5
2	ND	0.2	1.0	0.9	8.4	6.0
3	ND	ND	ND	ND	1.3	1.4
4	ND	ND	ND	ND	1.7	2.7
5	ND	ND	ND	ND	2.7	4.4
6	ND	2.5	0.2	0.6	0.6	0.4
7	NA	2.5	NA	1.5	NA	11.3
9	10.3	5.3	11.0	12.3	3.9**	2.8**
10	3.3	5.2	12.9	5.4		
11	6.1	4.1	6.3	6.9	1.2	ND
others	21.0 ^a	11.2 ^b	29.1 ^c	38.9 ^d	37.6 ^e	34.2 ^f
Unextractables	5.8	5.5	10.9^g	8.1^g	37.6^g	32.5^g
Total	100.0	100.0	100.0	100.0	100.0	100.0

ND: not detected. NA: not applicable.

*: the sum of acetone/water and acetone/HCl extracts.

** : 9 and 10 were not separated/quantitated using the secondary HPLC system.

a: consists of >7 components, each below 3.0%TRR.

b: consists of >5 components, each below 3.3%TRR.

c: consists of >8 components, each below 2.0%TRR.

d: consists of >8 components, each below 4.4%TRR.

e: consists of >8 components, each below 7.3%TRR.

f: consists of >7 components, each below 4.0%TRR.

g: further fractionated by harsh extractions.

Table 3. ¹⁴C distribution and metabolites in grain.

Grain	%TRR	
	[Ph- ¹⁴ C]	[Bz- ¹⁴ C]
Extractables *	67.0	72.7
1	ND	ND
2	ND	3.1
7	NA	60.6
9/10 **	ND	1.3
others	67.0 ^a	7.7 ^b
Unextractables	33.0	27.3
Total	100.0	100.0

ND: not detected. NA: not applicable.

*: the sum of acetone/water and acetone/HCl extracts.

** : not separated/quantitated using the secondary HPLC system.

a: consists of >3 components, each below 25.6%TRR.

b: consists of >5 components, each below 4.3%TRR.

Figures:

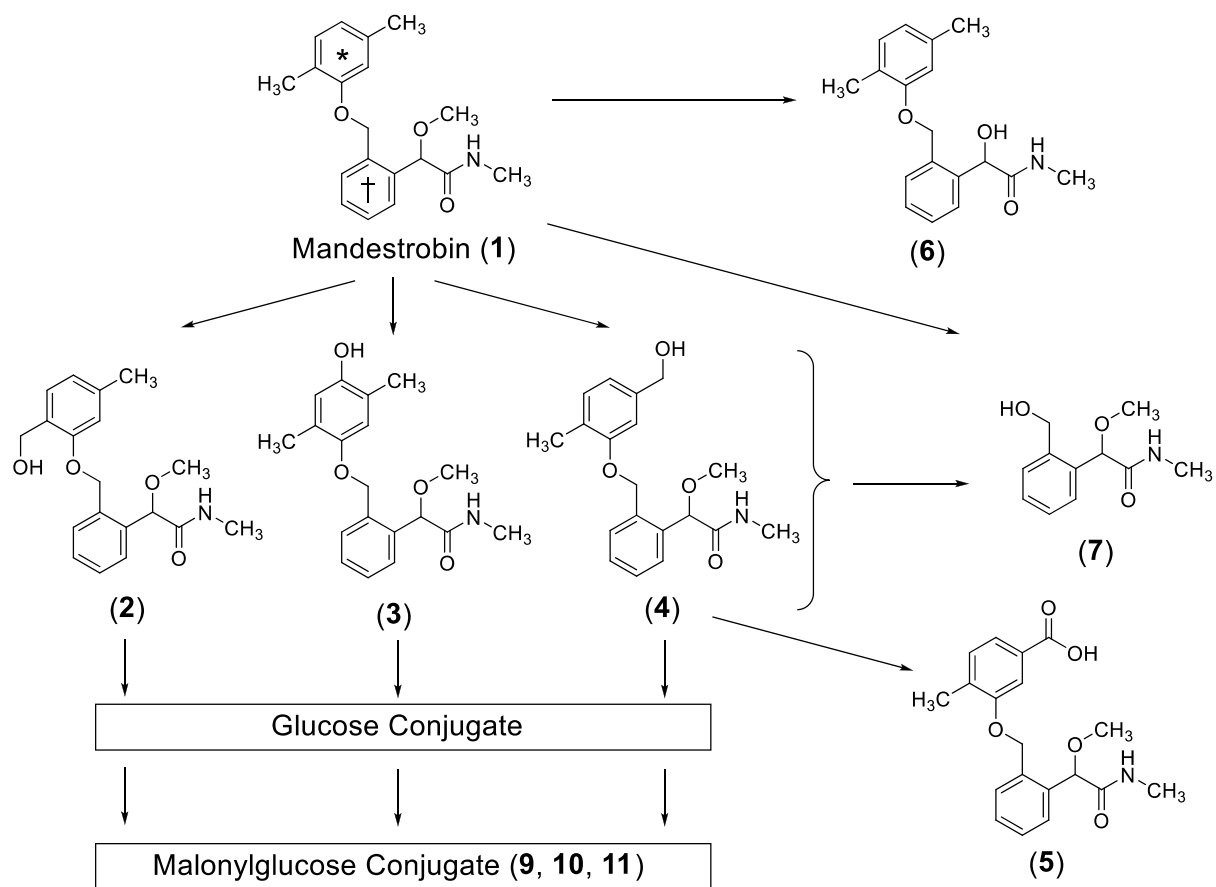


Figure 1: Proposed metabolic pathway of mandestrobin, **1**, on/in wheat plant after the foliar application. * and † in **1** indicate the radiolabeled positions of [Ph-¹⁴C]**1** and [Bz-¹⁴C]**1**, respectively.

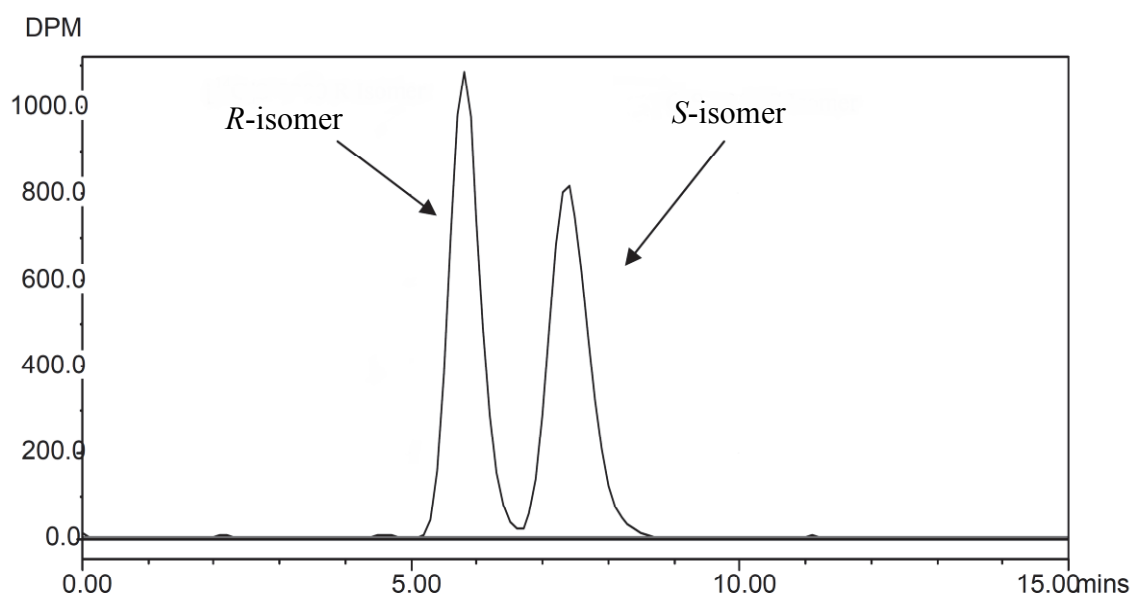
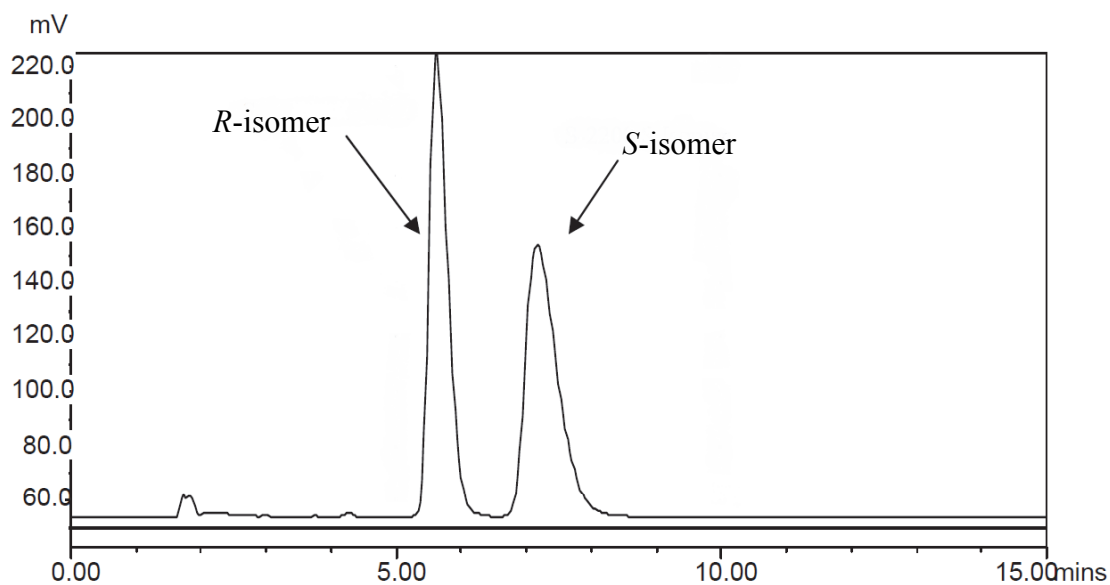


Figure 2: The chiral HPLC chromatogram of [Ph-¹⁴C] straw extract.
Top: Reference standards. Bottom: The straw sample.

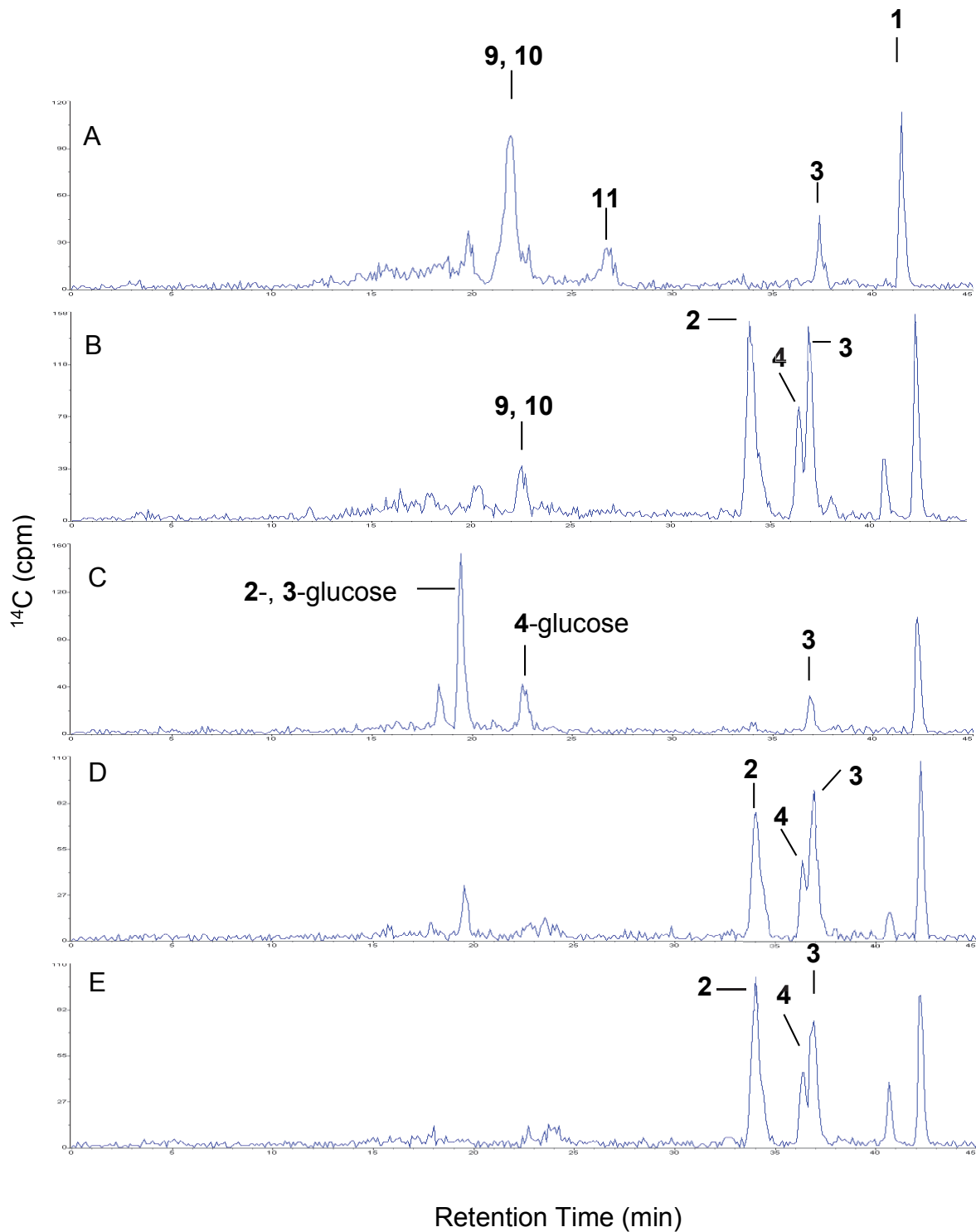


Figure 3: Hydrolytic behavior of [Ph- ^{14}C] hay extract analyzed by HPLC. A: original whole extract; B: 7 days after β -glucosidase treatment; C: 0.5 h after alkaline treatment; D: 1 h after β -glucosidase treatment following 0.5 h alkaline hydrolysis; E: 3 h after β -glucosidase treatment following 0.5 h alkaline hydrolysis

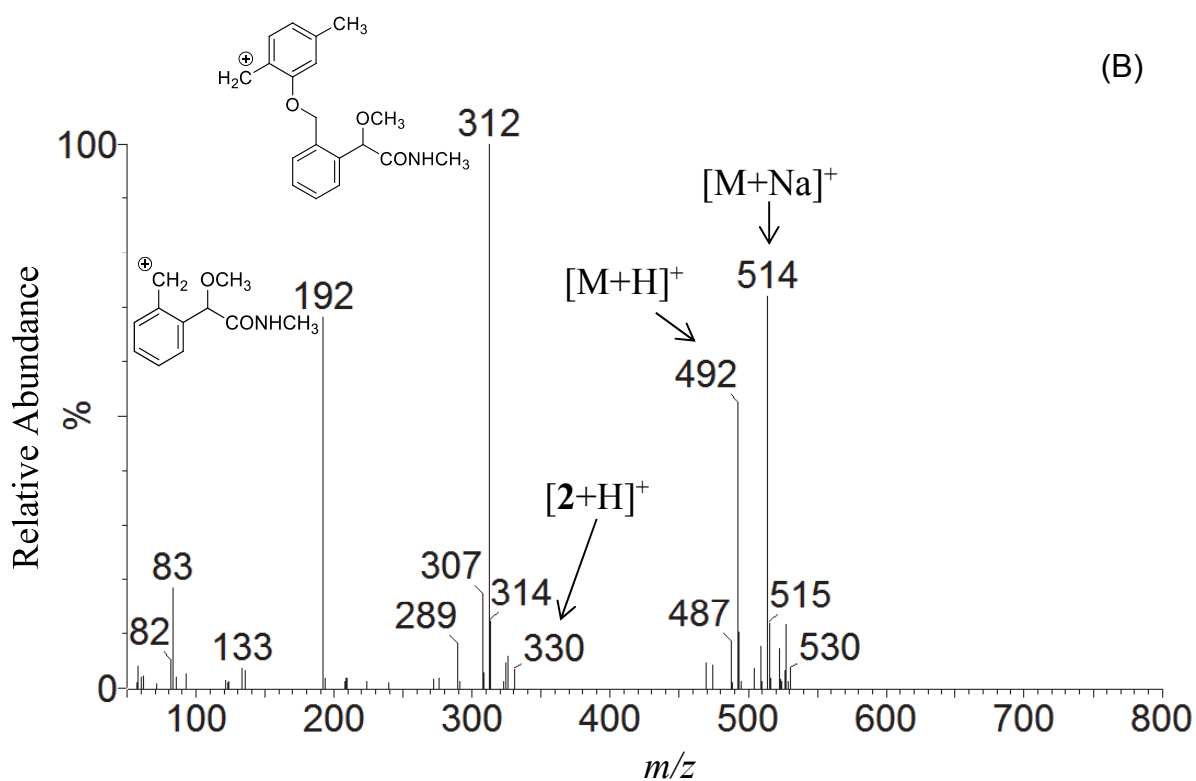
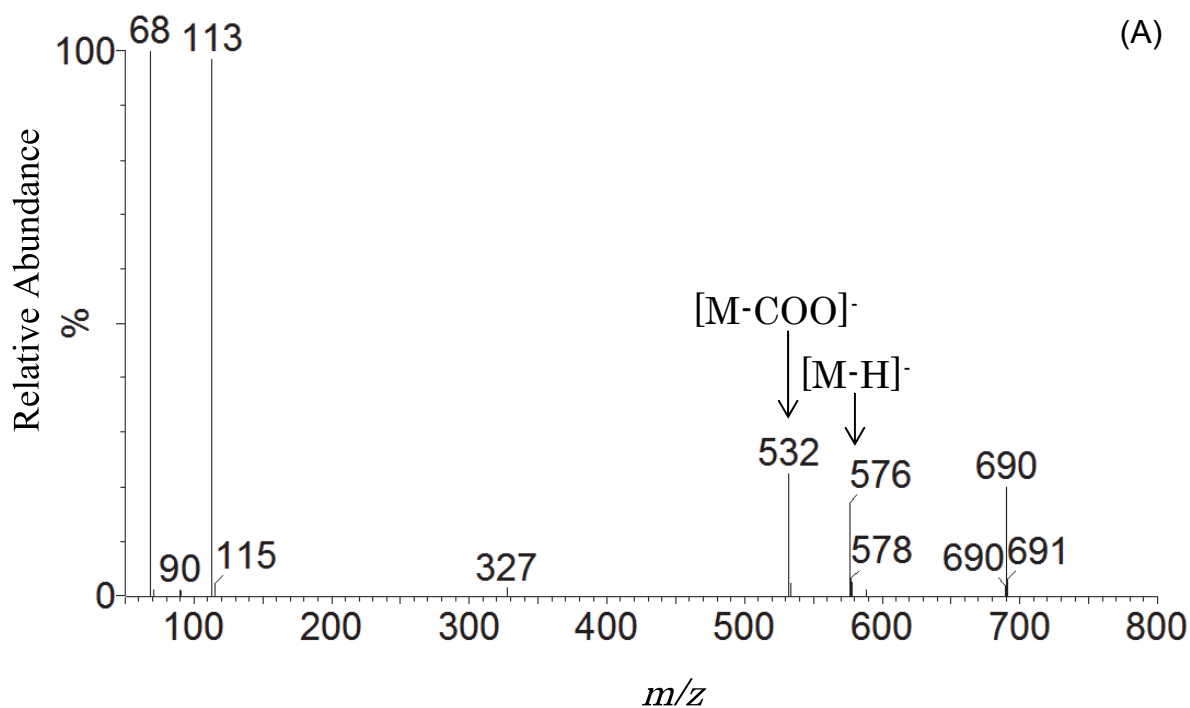


Figure 4. Mass spectrum of (A) malonylglucoside and (B) demalonylated glucoside of **2**.

2.2.2 Metabolism of Mandestrobin in Water Milfoil

In this section, the behavior of mandestrobin in water milfoil was investigated for comparison to the wheat metabolism described in section 2.2.1. Since majority of the radioactive components found in the wheat forage and hay (grown 14 days after the spray treatment of the fungicide) retained the ester bond between the two aromatic rings and no specific metabolites for the phenyl label were identified, only the [Bz-¹⁴C] label of mandestrobin is considered sufficient for understanding the profile in the water milfoil exposure.

In this study, the same chemicals and analytical methods applied in the wheat metabolism study of mandestrobin were employed, unless otherwise noted. The same abbreviations used in the wheat study for mandestrobin and its degradates are transcribed.

MATERIALS AND METHODS

Chemicals

The radiolabeled material [Bz-¹⁴C] **1** was applied in this study. An additional reference standard applied was: 2-[2-(2-hydroxy-3,6-dimethylbenzyl)phenyl]-2-methoxy-*N*-methylacetamide (**12**), prepared in our laboratory according to the previous report (Adachi et al. 2018). The chemical structures of reference standards applied in this study are shown in Table 1.

Chromatography

The Reversed-phase HPLC analysis of the test substance and its degradates was conducted using a LC-20A module (Shimadzu Ltd., Kyoto, Japan) equipped with a SUMIPAX ODS A-212 column. The two dimensional (2-D) TLC was conducted using chloroform/methanol = 9/1 (v/v/v) and ethyl acetate/methanol/acetic acid = 18/2/1 (v/v/v) as the first and second eluents, respectively. The typical HPLC retention times and TLC R_f values of each reference compound were described in the previous wheat metabolism study, and the ones of metabolite **12** were as follows: HPLC with ODS column, 40.3 min; TLC with chloroform/methanol eluent, R_f = 0.63, with ethyl acetate/methanol/acetic acid eluent, R_f = 0.62.

Plant Material and Treatment

Water milfoil (*Myriophyllum elatinoides*) plants purchased from Aqua Rise Co. were used in the experiment. The acclimatization and its growth conditions were the same as the metofluthrin study of water milfoil.

The ^{14}C material dissolved in acetonitrile was mixed with the non-radiolabeled **1** to the isotopic ratio $^{12}\text{C}:^{14}\text{C} = 100:80$ as the dose solution. Then, the solution was injected to a 800 mL of the AAP medium in a glass beaker to prepare 0.5 ppm of **1** as the exposure concentration (3.34 MBq), to ensure sufficient detection of the radioactivity. To the exposure water, 10 water milfoil plants (length 11.2 ± 1.0 cm, roots 2–5 cm) were immersed and incubated in the climate chamber.

Sampling, Extraction and Analysis

Aliquot of the exposure water was sequentially sampled till 14 days and directly analyzed by LSC and HPLC. At Day 14, the plants were sampled and extracted with the similar manner as the metofluthrin metabolism study of water milfoil.

Identification of Metabolites

The identity of the metabolites was confirmed by HPLC and TLC co-chromatography with the non-radiolabeled reference standards. In order to clarify the presence of sugar-conjugated metabolites, approximately each 200,000 dpm of the exposure water and the plant extract was dried using evaporator, re-dissolved in 5 mL of 10 mM sodium acetate buffer (pH 5.0) and 3 mg of β -glucosidase was added to the solution, then incubated at 37°C for 7 days.

Estimation of Chemical Property

n-octanol/water Partition coefficient (K_{ow}) of the degradates were predicted using EPISuite from the U.S. EPA (version 4.11) (EPA 2017).

RESULTS AND DISCUSSIONS

^{14}C Distribution

The ^{14}C amount and constituents in the exposure water during 14 days and in the

plant at day 14 are given in Tables 1 and 2, respectively. The radioactivity applied in the exposure water decreased to 85.4%AR immediately after 0.5 day and gradually thereafter to 79.7%AR after 14 days. Majority of the radioactive constituents in the exposure water was **1** (56.4–85.4%AR), and the detected degradates were **5**, **6**, **12** and other minors (maximum 3.6, 4.8, 9.7 and 5.2 %AR at Day 14). The un-recovered radioactivity was probably caused by the volatilization of **1** and its degradates as observed in the previous photolysis (Adachi et al. 2018) and the wheat metabolism (Ando et al. 2018) studies of mandestrobin. The degradate **12** (rearranged product) was shown to be the photodegradation product in aqueous solution (Adachi et al. 2018), while **5** (carboxylated product at the 5-methyl moiety on the benzene ring) and **6** (demethylated product) were known to be generated by photolysis on soil, as well as by incubation in soil under dark condition which likely involved metabolism by habiting microorganisms (EFSA 2015). Hence, both photochemical and microbial (or periphyton-mediated) reactions were considered as the factors for the production of these degradates. Incidentally, **12** was not detected as major photoproduct either on the wheat surface (Ando et al. 2018; EFSA 2015) or soil (EFSA 2015), while the production in aqueous solution was significant (Adachi et al. 2018; EFSA 2015). This implies the restricted molecular dynamics of **1** in the solid state on the surfaces compared to the solution state, so the rearrangement in the latter condition likely proceeded.

With respect of the water milfoil, 6.9%AR was accumulated and the extractable and unextractable radioactivities accounted for 6.4 and 0.5 %AR (93.2 and 6.8%TRR), respectively. In the plant extract, the unchanged **1** was the prominent radioactive chemical, 66.0%TRR (4.6%AR). The degradates detected were **2**, **4**, **5**, **6**, **12** and other minor products which amounted to 2.2 (0.2), 1.7 (0.1), 3.1 (0.2), 6.0 (0.4), 9.0 (0.6) and 5.2%TRR (0.4%AR), respectively. The distribution ratio of **1**, **5**, **6** and **12** in the plant was somewhat similar to the one in the exposure medium, and this may suggest some portions of each product in the plant derived from the water medium. Particularly, **12** detected in the plant at certain amount should dominantly be originated from the photoreaction in the exposure water followed by uptake, and this may be attributed to the highest log K_{ow} 3.30 among all the degradates (**5**, log K_{ow} 2.88; **6**, log K_{ow} 3.11) which is considered most favorable for accumulation, taking into account the empirical observations that accumulation by water milfoil positively elevates with the increase of

lipophilicity of the exposure chemical (Gobas et al. 1991; Carvalho et al. 2007). Regarding the contribution of plant metabolism, all the detected metabolites, except for **12**, were generated by the wheat metabolism (Ando et al. 2018), probably *via* phase I reactions, *i.e.*, hydroxylation, oxidation and ether cleavage, thus, supported the similar metabolic ability for water milfoil. At least, capacity for hydroxylating **1** to produce **2** and **4**, which were not detected in the exposure water, by water milfoil was confirmed in this study, whereas, the hydroxylate **3** observed in wheat was not detected and indicated possible difference in the enzyme species involved in phase I metabolism between these plants.

Metabolite Characterization

In order to examine the sugar-conjugated metabolites, glucosidase hydrolysis was conducted for the plant extract. Some of the minor components categorized to ‘others’ released mono-hydroxylates **2** and **4**, indicating the presence of their saccharide conjugates, however, the conjugates were not definitively distinguished from other minor components and the structures were not further characterized due to their small amount. In the wheat metabolism study, the mono-glucose conjugates of **2** and **4** were characterized to exhibit HPLC retention times at around 19 and 23 min, respectively (Ando et al. 2018). Because the ‘minors’ detected in the water milfoil contained components at these retention times, it was assumed that water milfoil conjugated **2** and **4**, indicating the occurrence of phase II conjugation.

From the results, behavior of mandestrobin in water milfoil is proposed in Figure 1.

Tables

Table 1: The chemical structures of reference standards.

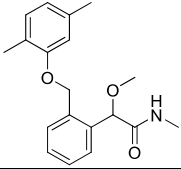
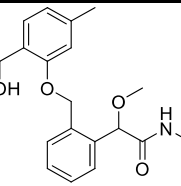
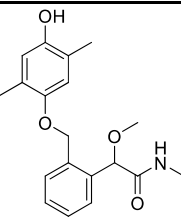
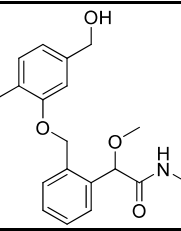
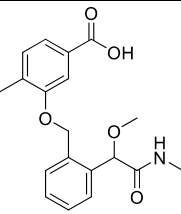
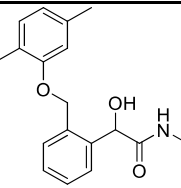
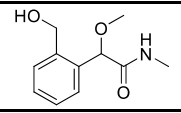
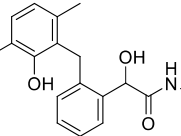
Designation	Chemical structure
1	
2	
3	
4	
5	
6	
7	
12	

Table 2: ¹⁴C distribution in the exposure water.

%AR					
	Days after exposure				
	0	0.5	2	7	14
1	100.0	85.4	80.5	66.2	56.4
5	ND	ND	0.7	1.7	3.6
6	ND	ND	1.2	3.5	4.8
12	ND	ND	2.0	4.5	9.7
Others*	ND	ND	1.2	4.9	5.2
Total	100.0	85.4	84.7	80.6	79.7

ND: not detected.

*: the sum of multiple components, each <1.2%.

Table 3: ¹⁴C distribution in the water milfoil at 14 day after the exposure.

%AR and %TRR		
	AR	TRR
Extract	6.4	93.2
1	4.6	66.0
2	0.2	2.2
4	0.1	1.7
5	0.2	3.1
6	0.4	6.0
12	0.6	9.0
Others*	0.5	5.2
Unextractables	0.5	6.8
Total	6.9	100.0

ND: not detected.

*: The sum of multiple components, each <0.1%AR/<1.3%TRR. Some of the components were chromatographically characterized as glucose conjugates of **2** and **4**.

Figures:

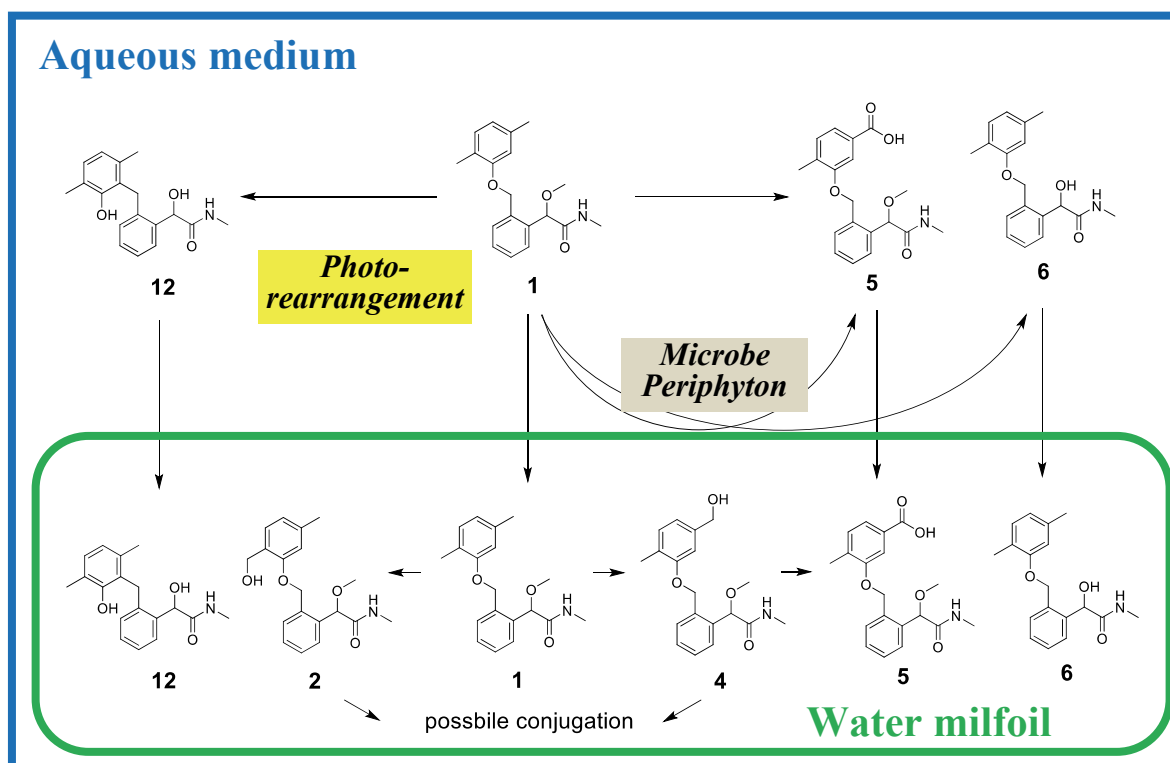


Figure 1. Proposed metabolic pathway of mandestrobin in water milfoil.

2.2.3. Fate Comparison Between Wheat and Water Milfoil

At below, the major differences revealed from the two mandestrobin studies are summarized:

1. Mandestrobin underwent photo-transformation in the aqueous medium to give the rearranged product at the certain level. In addition, the carboxylated and demethylated degradates were generated by abiotic/biotic reactions. These products were not detected in the wheat surface.
2. Mandestrobin was the major exposure source accumulated in both plants, while water milfoil was exposed to the additional degradates, and especially, taken up the rearranged product as the unique plant residue.
3. Although many metabolic reactions were considered identical, the metabolite distribution in each plant showed difference. Importantly, one hydroxylated metabolite was missing in water milfoil, indicated the involvement of dissimilar enzymatic systems in the metabolism between the plants.

In contrast to metofluthrin, hydrolytically stable mandestrobin did not receive hydrolysis, but instead, both biotic and abiotic reactions proceeded in the water medium concomitantly to be accumulated into water milfoil and affected the overall behavior.

2.3. Conclusion

From the four studies described in chapter 2, the importance of biotic and abiotic reactions at external plant was experimentally demonstrated, which critically influenced the overall behavior of each pesticide on the terrestrial plant and water milfoil. The following three conclusions are given.

1. Terrestrial and water milfoil could be exposed to different chemical species generated *in situ* from the pesticide by abiotic and biotic reactions at each growing condition of the plant, and the level of their contribution depends on the chemical nature of the pesticide.
2. Production ratio at external plant and chemical properties of the degradates, hydrophobicity or water solubility as major ones, are likely responsible for the accumulation level in plants.
3. Variety of metabolic reactions in water milfoil may be somewhat limited and can be covered by the knowledge from terrestrial plants. However, in the overall, there would be a large difference in the metabolite distribution/quantity between terrestrial plants and water milfoil.

3. Development of Experimental Design to Investigate Uptake, Translocation and Metabolism of Chemicals by Water Milfoil

In the exposure experiment of pesticides for water milfoil, to experimentally elucidate individual behavior of the uptake, translocation and metabolism after shoot and root exposures, it was necessary to adopt a study design which enables to separately expose shoot and root to the test chemical. There are a few exposure design that could be referred. For instance, Hinman et al. (1992) applied the exposure system separating shoot and root regions by agar-coated Teflon boundary placed in the exposure system (Fig. A).

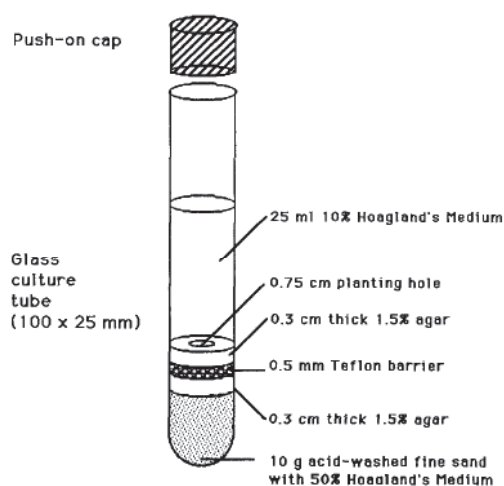


Figure A: Exposure system applied by Hinman et al. (1982).

They found that root uptake of sediment-spiked atrazine was fast as leached to the uptake steady state by 1 day, while chlordane was continuously taken up through 30 days and resulted in higher accumulation in water milfoil. For both accumulated chemicals, significant portions were detected in shoot and the authors concluded this attributes to the high acropetal translocation from root to shoot. However, since the Teflon had a hole for planting water milfoil, dispersion of the pesticides from sediment to upper water column during exposure (cross contamination), causing shoot uptake, may not be neglected. Besides, test chemicals may interact with Teflon and agar at the sediment phase and the experimental setting is complicated and difficult. Other experimental

design is the hydroponic system which had been applied by many researchers. As representative, Briggs et al. (1982) applied the system to investigate root uptake by terrestrial plants and found bell-shaped curve showing optimum log K_{ow} at 1–3. Carvalho et al. (2007) also used hydroponic design for water milfoil and reported the similar relation, though the uptake duration was short as less than 2 days. Hydroponic system is easy to be applied and provides clear, useful information for root uptake. However, such system cannot be applied for water milfoil due to rapid shoot dryness as critical limitation in conducting long term cultivation necessary to investigate the metabolic fate of pesticides in the plant.

Incidentally, Fritioff et al. (2007) introduced a unique design to elucidate the uptake and translocation behaviors of cadmium in water milfoil (Figure B).

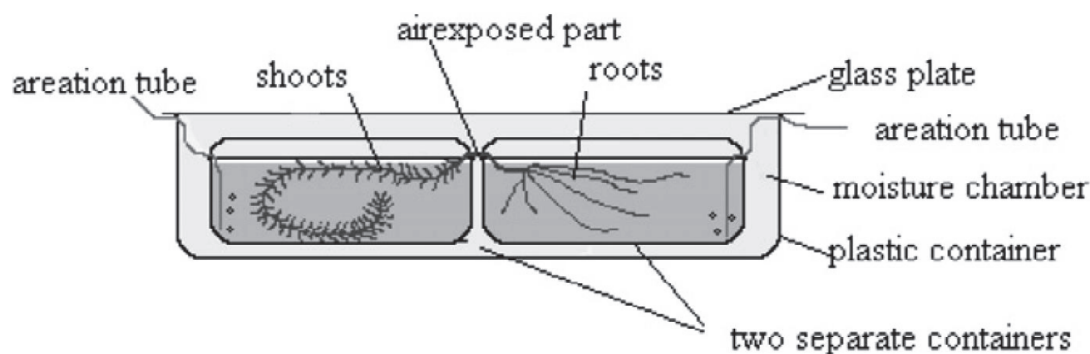


Figure B: Sequestered chamber designed by Fritioff et al. (2007).

Using the system, they successfully showed that both shoot and root enable to uptake and accumulate cadmium followed by transportation from root to shoot and *vice versa*, without any visible damage and growth inhibition.

We judged their system is convenient and fully matches to our purpose, namely, to clarify each uptake/translocation/metabolism behavior after shoot and root exposure. In this chapter, the above exposure system was modified and applied to separately examine the shoot exposure *via* water medium and roots exposure *via* sediment using 3-phenoxybenzoic acid as a model test compound, and confirmed the validity of the system.

Materials and Methods

Chemicals

3-Phenoxybenzoic acid (**I**) uniformly labeled with ^{14}C at the phenoxyphenyl ring (specific radioactivity 4.37 GBq/mmol, radiochemical purity 100% by HPLC) was synthesized in our laboratory (Yoshitake et al. 1981). Non-radiolabeled **I**, 3-phenoxybenzaldehyde (**II**) and 3-phenoxybenzyl alcohol (**III**) were purchased from Sigma-Aldrich Co. 3-(2'-hydroxyphenoxy)benzoic acid (**IV**), 3-(4'-hydroxyphenoxy)benzoic acid (**V**), 3-(2'-hydroxyphenoxy)-benzyl alcohol (**VI**), and 3-(4'-hydroxyphenoxy)benzyl alcohol (**VII**) were synthesized in our laboratory according to the reported method (Miyamoto et al. 1974). The chemical purity of each standard was determined to be >95% by HPLC. All reagents and solvents used in this experiment were of analytical grade.

Chromatography

A reversed-phase HPLC system to analyze **I** and its metabolites consisted of a Hitachi LC module (model L-7000) equipped with a SUMIPAX ODS A-212 column (5 μm , 6-mm i.d. \times 15 cm, Sumika Chemical Analysis Service, Ltd.). The following gradient system operated at a flow rate of 1 mL/min; 0 min, %A (acetonitrile containing 0.1% formic acid)/%B (0.1% formic acid)/%C (methanol), 5/85/10; 0–10 min, 30/60/10 at 10 min, linear; 10–30 min, 45/45/10 at 30 min, linear; 30–35 min, 75/15/10 at 35 min, linear; 35–40 min, 75/15/10, isocratic (HPLC method A). The typical retention times (min) were 33.5 (**I**), 37.5 (**II**), 29.9 (**III**), 23.2 (**IV**), 21.9 (**V**), 20.6 (**VI**), and 19.0 (**VII**). The radioactivity in a column effluent was monitored with a Flow Scintillation Analyzer Radiomatic 500TR (Perkin Elemer, Co.) radiodetector equipped with a 500 mL liquid cell using Ultima-Flo AP[®] (Perkin Elemer, Co.) as a scintillator.

Spectroscopy and Radioanalysis

One-dimensional NMR spectra (^1H - and ^{13}C -) were measured in methanol- d_4 with 0.03% TMS using a Varian Mercury 400 (Varian Technologies Ltd.) spectrometer at 400 MHz. LC–ESI–MS analysis was conducted using a Waters Tandem Quadruple TQD

spectrometer equipped with a Waters Separation Module Acquity UPLC (Ultra Performance Liquid Chromatograph) and a Waters Acquity Photodiode Array Detector (HPLC method A). The following parameters were used: source temperature, 130°C; desolvation temperature, 400°C; capillary voltage 3.2 kV; cone voltage, 10–40 V; collision energy, 10–20 V. Radioactivity in water, sediment extract, and rinsate/extract of the plant was determined by LSC with a Packard Model 2900TR spectrometer after mixing each aliquot with 10 mL of Perkin Elmer Emulsifier Scintillator Plus[®]. The shoot and roots of the plant were sampled at 0.5–5 day, and the bound residue of each portion was individually combusted using a Perkin Elmer Model 307 sample oxidizer. The ¹⁴CO₂ produced was absorbed into 9 mL of Perkin Elmer Carb[®]-CO₂ absorber and mixed with 15 mL of Perkin Elmer Permafluor[®] scintillator. The radioactivity therein was quantified by LSC. The efficiency of combustion was determined to be greater than 96.5%.

Plant Material and Treatment

Water milfoils (*Myriophyllum elatinoides*) were purchased from Aqua Rise Co. (Osaka). Approximately 1.5 cm of their root tips was planted in commercial sediment (Aqua Soil, Aqua Design Amano Co., Ltd.) in an aquarium filled with tap water and acclimatized for at least 10 days in a greenhouse at 20 ± 2°C under natural sunlight to induce root development. The plants were then transplanted to a beaker containing the AAP (American Academy of Pediatrics) water medium at pH 7.0 ± 0.5 and an OECD synthetic sediment (OECD 2004) to grow for 3 days at 20 ± 2°C in a climate chamber LH-220S (NK Systems Ltd.) under white fluorescent lightning (120 μE·m⁻²·s⁻¹⁰, 16 h per day). The exposure experiments were conducted using a glass vessel partitioned with a welded grass board that included shoot and roots chambers as shown in Figure 1.

The shoot and roots chambers were individually filled with 120 mL of the AAP medium and 35 g of OECD sediment moistened with 20 mL of the AAP medium, each of which was autoclaved at 1.5 kg cm⁻² and 120°C for 20 min. The rooted plant with no flower (length: 16.5–18.3 cm; fresh body weight: 0.34–0.51 g) was immersed in 500 mL of 0.5% sodium hypochlorite with sonication under reduced pressure for 1 min and thoroughly washed with 1 L of sterilized water. The acetonitrile solution (25–50 μL)

of $^{14}\text{C-I}$ isotopically diluted with non-radiolabeled material **I** was applied to the AAP medium in the shoot chamber (water treatment) or to the sediment in the root chamber followed by uniform mixing (sediment treatment). The total radioactivity applied in each chamber was 0.167 MBq, adjusting the isotopic dilution ratio for each treatment to establish an exposure concentration of 3.28 ppm, based on the total weight of water medium and sediment plus medium for water and sediment treatments, respectively. The root tip of the sterilized plant was then buried into the sediment and the shoot portion was immersed in the AAP medium. The sequestered glass chamber was covered with a polyethylene wrap and incubated at $20 \pm 2^\circ\text{C}$ in the climate chamber (16 h light per day). Each exposure was conducted in triplicate.

Analytical Procedures

The sampling was conducted at 0.5, 1, 3, 5, 7 and 14 days after the ^{14}C treatment. The rinsate of the plant with 50 mL of a fresh medium was combined with the test medium in the shoot chamber. After measuring its wet weight and length, the plant was further rinsed with 50 mL of acetonitrile (surface rinse). The autoradiogram of some of the plants attached to a BAS-III's Fuji Imaging Plate (Fuji Photo Film Co., Ltd.) overnight was measured by a Bio-Imaging Analyzer Typhoon (GE Healthcare). The plant was separated into shoot and roots, and the radioactivity in each portion sampled at 0.5–48 hours was measured by combustion analysis. Each plant portion sampled at 7 and 14 days was extracted with 20 mL of methanol using a homogenizer AM-8 (Nissei Ltd.) at 10,000 rpm and 0°C for 10 min. The homogenate was vacuum filtered and the plant residue was further extracted in the same manner once with methanol and another with methanol/1M HCl (100/1, v/v). The sediment and medium (pore water) in the roots chamber were separated by vacuum filtration. The sediment was washed once with 100 mL of a fresh medium, combined with the pore water and radioassayed. The ^{14}C -treated sediment was extracted with 30 mL of acetone for 10 min by mechanical shaking with a Taiyo SR-IIw recipro-shaker (Taiyo Chemical Industry Co., Ltd.). The residue after vacuum filtration was successively extracted twice with 30 mL of acetone and once with 30 mL of acetone/1 M HCl (100/1, v/v) in the same manner.

Radioactivity in the sediment caused by the water treatment was determined by

combustion analysis, and no further extraction was conducted due to the insignificant amount of ^{14}C that remained. Each aliquot of the rinsate, extract and medium was analyzed with LSC and HPLC co-chromatography with authentic standards, and the extracted residues were subjected to combustion analysis.

RESULTS

No growth inhibition of the plants was confirmed in the sequestered glass chambers after comparing the length (1.1 – 1.8 cm) and fresh weight (0.7 – 0.11 g) with those grown in the control acclimation aquarium during a 14-day incubation. The total recovery of ^{14}C in each treatment was greater than 95%AR throughout the test period, indicating the insignificant ^{14}C loss by volatilization or adsorption to the test vessel. The extremely low radioactivity ($\leq 0.03\%$ AR) detected from the untreated chamber showed no cross contamination from the ^{14}C -treated chamber.

In the water treatment, approximately 80%AR remained in the medium, and no ^{14}C was detected in the sediment chamber (Table 1). All the ^{14}C remaining in the medium was unaltered **I**. The radioactivity in the medium was rapidly incorporated into the shoot and likely reached the uptake plateau after 0.5 days, while no ^{14}C was recovered by the surface rinse of plants. The total ^{14}C in the shoot ranged 15.85 – 17.37%AR, whereas the amount in the roots was much lower as 0.06 – 1.13%AR during 7 days. The slight distribution of the radioactivity in the roots was also confirmed by autoradiograms (data not shown). The identified metabolites in the shoot were **I**, **III** and **VIII** (monoglucose conjugate of **I**), with each amounting to 17.81 – 35.06, 3.05 – 6.95 and 50.40 – 57.13% of the total radioactive residue (%TRR) in plants, respectively, after 7 and 14 days (Table 3). In the roots, **I** and **V** were detected at 1.78 – 2.60 and 2.28 – 3.22%TRR, respectively. The total ^{14}C bound in the plant was 4.59 – 9.10%TRR.

Chemical identities of **I**, **III** and **V** were confirmed not only by HPLC co-chromatography with the corresponding authentic standards but also by LC–ESI–MS analyses ($[\text{M}-\text{H}]^-$ m/z at: 213, **I**; 119, **III**; 229, **V**). The detailed spectroscopic analyses by LC–ESI–MS/MS and NMR were conducted for **VIII** isolated from the shoot extract of 14-day samples using the HPLC method A. The MS analysis in the negative ion mode showed the molecular ions of **VIII** at m/z 421 $[\text{M}+\text{HCOO}]^-$ and 375 $[\text{M}-\text{H}]^-$. The

MS/MS fragmentation of these ions gave consecutive daughters corresponding to [M-glucose-H]⁻ and [glucose-H]⁻ at *m/z* 213 and 163, respectively, which suggested the chemical structure as the monoglucoside form. The structure of **VIII** was further confirmed by ¹H- and ¹³C-NMR analyses, which resulted in the assignment of the typical proton/carbon signals of glucose and **I** as follows; ¹H-NMR (methanol-*d*₄); δ = 7.01 – 7.84 ppm (m, 9H, aromatics), 5.70 ppm (m, 1H, anomeric) and 3.34 – 3.83 ppm (m, 5H, glucose); ¹³C-NMR; δ = 131.1, 131.0, 125.5, 125.0, 124.7, 120.4 and 120.1 ppm (s, aromatics), 96.3 ppm (s, anomeric), 78.8, 77.9, 73.8, 70.8 and 62.1 ppm (s, glucose).

In case of the sediment treatment, approximately 80%AR remained as unaltered **I** in the root chamber, most of which was distributed in the interstitial medium water of the sediment, *i.e.*, pore water (Table 2). The radioactivity applied in the sediment was gradually taken up by the plant, which reached its maximum 8.08%AR after 14 days. The radiocarbon in the plant rinsate was below the detection limit. The majority of ¹⁴C was located in the roots (6.37%AR), while 1.71%AR was translocated to the shoot portion 14 days after treatment. The ¹⁴C distribution in the plant was confirmed by the autoradiogram (data not shown). **I**, **III**, and **V** were detected as major metabolites in the roots, each amounting to 7.96 – 40.06, 7.67 – 26.09 and 14.68 – 32.40%TRR, respectively. **I**, **III**, and **VIII** in the shoot were 2.95 – 8.55, 1.99 – 5.13 and 9.40 – 17.06%TRR, respectively, after 7 and 14 days (Table 3). The total bound residues were 5.90 – 8.03%TRR.

From the results, the metabolic pathway of **1** in water milfoil is proposed in Figure 2.

DISCUSSIONS

During the water treatment, the fast uptake of **I** from the exposure medium by the shoot of water milfoil was observed as its equilibrium was established within 0.5 days. This is similar to the uptake profile reported for duckweed (Fujisawa et al. 2006). This observed rapid accumulation most likely derived from the character of surface structure of the macrophyte. Macrophyte cuticular membranes are generally thin (0.05 – 0.10 μ m) (Denny 1980; Jeffree 2006), and their tissues contain little hydrophobic components, *e.g.*, lignin contents are <10% on a dry weight basis (Gobas et al. 1991). It is reported

that the isolated cuticular wax of a fully submerged macrophyte, shining pondweed (*Potamogeton lucens*), is more permeable to water by a factor of 1000 than those of terrestrial plants (Schönherr 1976), and that the amount of dissociated organic acids, 2,4-D and benzoic acid penetrated through the isolated layer of cuticle wax was proportional to the permeation of water molecule (Schreiber 2002).¹³ Furthermore, the pores existing in the plant cuticle membrane of submerged plants swelled in water likely promote the uptake of water-dissolved chemicals, similarly as elucidated for terrestrial plants (Schönherr 2006; Schreiber 2002). In fact, it has been clarified that ionic solutes traverse membranes through water-filled pores therein, e.g., stoma, glandular trichome, and so on (Schönherr 2006). After absorption, **I** was expected to effectively undergo distant transportation from the shoot to roots *via* a phloem route because weak acids are known to facilitate their retention in the symplast due to ion-trapping (Bromilow et al. 1990; Briggs et al. 1982). However, the amount of radioactivity translocated from the shoot to roots was very low, less than 1.13%AR, which suggested that the phloem mobility of **I** is not high.

With respect of the sediment treatment, most of the accumulated radioactivity remained in the roots. Briggs et al. (1982) and Carvalho et al. (2007) have individually reported that the amount of transpiration-dependent translocation from roots to shoot versus $\log P$ (partition coefficient) plot showed Gaussian curve with a maximum $\log P$ value of c.a., 1.8 in barley and hydroponic milfoil having emergent leaves. These indicate that chemicals possessing much lower or higher values far from $\log P$ 1.8 are unsuitable for root uptake followed by acropetal translocation. In addition to the bell-shape, they also showed the positive relation that accumulation of chemicals in root increase with the elevation of $\log P$, and suggested that highly lipophilic compounds may not be translocated to shoot due to irreversible adhesion in root. For the ionic compound **I**, whose dissociation constant (pK_a) and $\log P$ are 3.95 and 3.91, respectively (Fujisawa et al. 2006), it mostly exist as dissociated anion at around neutral pH condition. Hence, $\log D$ (distribution coefficient) value instead of $\log P$ is reasonable to be applied. By using the following equation (Waterbeemd and Testa 1987), the $\log D$ of **I** is calculated to be 0.9, which is the similar level observed for many benzoic acid derivatives (Rocher et al. 2009).

$$\text{Equation : } \log D = \log P - \log [1 + 10^{(\text{pH} - \text{p}K_a)}]$$

The calculated value expresses moderate root uptake, and although the transpiration stream may diminishes in complete submergence, it was considered that **I** was taken up and translocated in water milfoil.

With respect of the metabolites, three major products **III**, **V** and **VIII** were detected in *M. elatinoides*, which have similarly identified as major metabolites of various synthetic pyrethroids such as permethrin, deltamethrin and phenothrin in terrestrial plants (Leahey 1985). In duckweed, it is reported that **I** was conjugated with malonyl-glucose and malonic acid (Fujisawa et al. 2006). These results clearly show that typical metabolic reactions, *i.e.* oxidation, reduction, and conjugation, also proceed in the macrophyte by corresponding enzymes, as summarized by Katagi (2010). Lamoureux and Rusness et al. (1986) reported that glucose conjugation is known as a general detoxification process for xenobiotic metabolism in the plant kingdom, and aromatic moieties of xenobiotics are easily conjugated with sugars *via* the linkage with amino, hydroxyl, and carboxy groups. Incidentally, **VIII** was only observed in the shoot, while **V** was dominant in the roots irrespective of the different exposure routes. This may be due to the difference of enzyme distribution within the plant (Shimabukuro and Walsh 1979).

CONCLUSION

In conclusion, in the water treatment, **I** was mainly taken up by the shoot of water milfoil, while the translocation to roots was not significant. With regard to the sediment treatment, while root uptake was slow and moderate, the ¹⁴C acropetal transportation to shoot occurred at the certain level. The metabolic reactions observed in the water milfoil were the reduction, hydroxylation and conjugation to produce **III**, **V**, and **VIII**, respectively, which are the common processes known in terrestrial plants. Importantly, the hydroxylation and conjugation products were the unique metabolites at root and shoot, respectively. From these results, we confirmed the usefulness of the developed study design, which enabled to separately exposure shoot *via* water and root *via* sediment, respectively, to investigate the uptake/translocation/metabolism of chemicals after each exposure.

Tables:

Table 1. ¹⁴C distribution in the test system (water treatment).

	%AR*					
	Days after exposure					
	0.5	1	3	5	7	14
Shoot/leaves chamber	83.04 (2.41)	81.87 (2.37)	81.97 (2.64)	80.16 (2.87)	79.30 (3.31)	80.51 (3.81)
Medium	83.04 (2.41)	81.87 (2.37)	81.97 (2.64)	80.16 (2.87)	79.30 (3.31)	80.51 (3.81)
Root chamber	N.D.	N.D.	N.D.	N.D.	N.D.	N.D.
Plant (whole)	15.91 (2.83)	16.51 (1.95)	16.43 (2.11)	17.57 (3.37)	17.19 (3.67)	17.98 (4.10)
Shoot/Leaves	15.85 (2.81)	16.35 (1.96)	16.27 (1.99)	17.37 (3.19)	16.06 (3.77)	17.12 (4.11)
Roots	0.06 (0.02)	0.16 (0.07)	0.16 (0.06)	0.20 (0.09)	1.13 (0.25)	0.86 (0.30)
Total	98.95 (2.04)	98.38 (2.35)	98.4 (2.59)	97.73 (2.91)	96.49 (3.45)	98.49 (3.44)

N.D.: Not detected.

*: Average values ($n = 3$). Standard deviations are given in parentheses.

Table 2. ¹⁴C distribution in the test system (sediment treatment).

	%AR*					
	Days after exposure					
	0.5	1	3	5	7	14
Shoot/leaves chamber	N.D.	N.D.	<0.01 (<0.01)	<0.01 (<0.01)	0.01 (<0.01)	N.D.
Medium	N.D.	N.D.	N.D.	0.01 (<0.01)	0.01 (<0.01)	N.D.
Root chamber	95.68 (2.41)	97.64 (3.00)	96.55 (3.12)	93.49 (2.98)	88.07 (3.55)	87.20 (3.70)
Pore water	92.55 (2.61)	91.39 (3.18)	91.31 (3.37)	87.41 (3.24)	78.56 (3.46)	80.62 (3.48)
Sediment	3.13 (0.49)	6.25 (1.33)	5.24 (1.10)	6.08 (1.99)	9.51 (1.85)	6.58 (1.78)
Plant (whole)	0.33 (0.15)	0.47 (0.16)	0.67 (0.22)	2.15 (0.41)	7.46 (1.63)	8.08 (1.95)
Shoot/Leaves	0.08 (0.01)	0.11 (0.03)	0.13 (0.06)	0.60 (0.10)	2.32 (0.52)	1.71 (0.44)
Roots	0.25 (0.10)	0.36 (0.15)	0.54 (0.19)	1.55 (0.33)	5.14 (1.19)	6.37 (2.03)
Total	96.01 (2.70)	98.11 (3.19)	97.25 (3.25)	95.65 (3.54)	95.54 (3.91)	95.28 (4.03)

N.D.: Not detected.

*: Average values ($n = 3$). Standard deviations are given in parentheses.

Table 3. Metabolite distribution in the plant after 7 and 14 days incubation.

	%TRR			
	Water treatment		Sediment treatment	
	Days after exposure			
	7	14	7	14
Surface rinse	ND	ND	ND	ND
Shoot/leaves	93.43	95.22	31.1	21.16
Extract	89.59	86.84	30.83	20.78
I	35.06	17.81	2.95	8.55
III	3.05	6.95	5.13	1.99
VIII	50.4	57.13	17.06	9.40
others	1.08	4.95	5.69	0.85
Bound residue	3.84	8.38	0.27	0.38
Roots	6.57	4.78	68.9	78.84
Extract	5.82	4.06	63.27	71.19
I	2.60	1.78	40.06	7.96
III	N.D.	N.D.	7.67	26.09
V	3.22	2.28	14.68	32.40
others	N.D.	N.D.	0.86	N.D.
Bound residue	0.75	0.72	5.63	7.65
Total	100.00	100.00	100.00	100.00

ND: Not detected.

Figures:

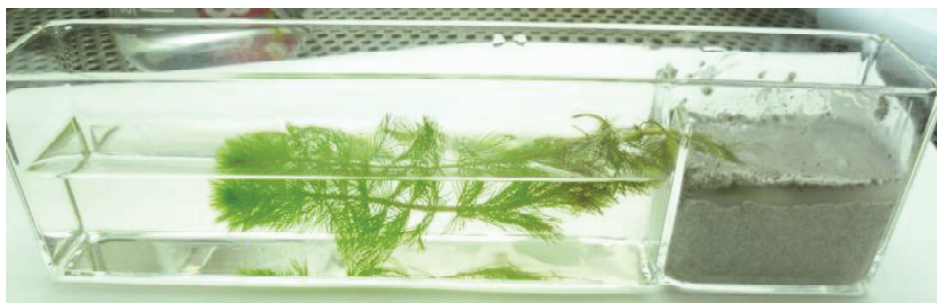
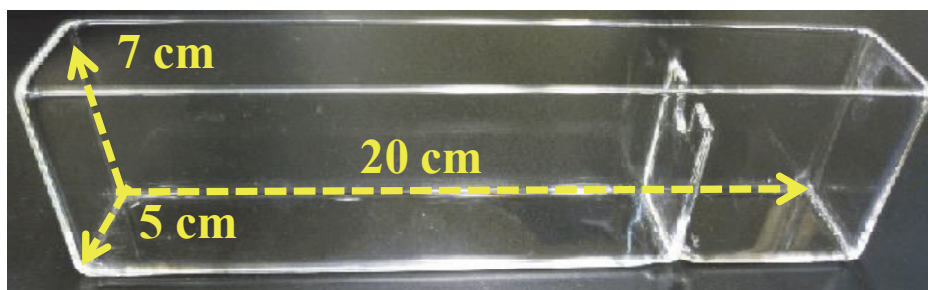
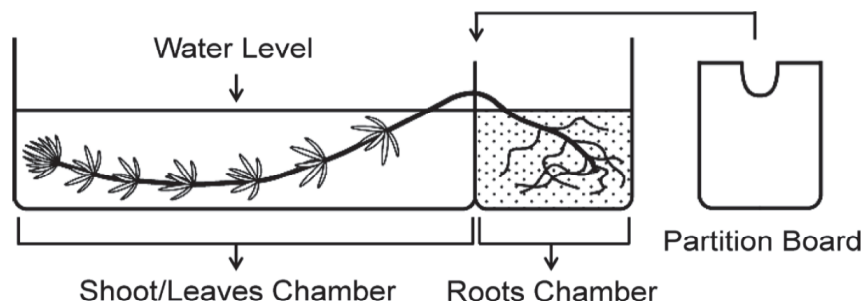


Figure 1: Exposure chamber developed for separate exposure of shoot and root.

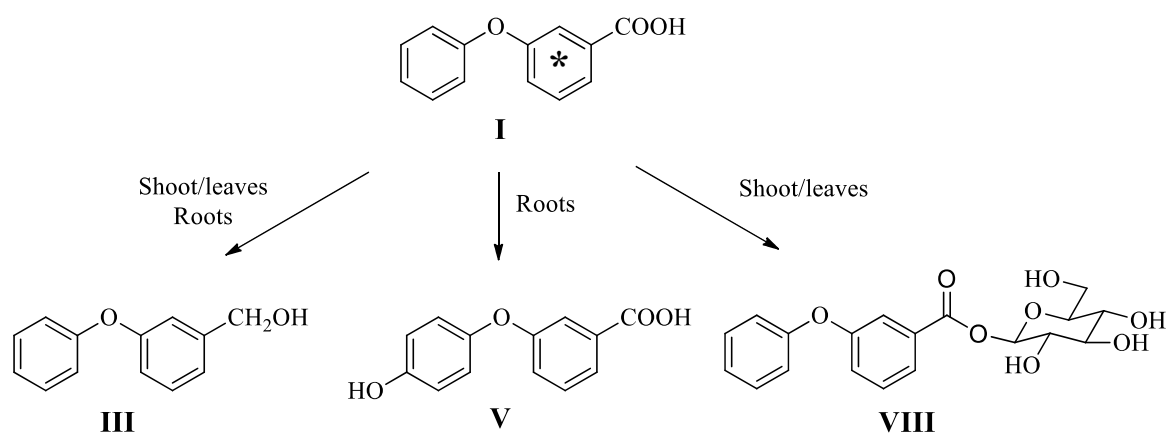


Figure 2: Proposed metabolic pathway of **I** in water milfoil. The radiolabeled position is shown by asterisk

4. Uptake, Translocation, and Metabolism of Phenols by Water Milfoil: Kinetic Analysis and Correlation With Physicochemical Properties

In this chapter, we set the object to compare various physicochemical parameters of the test chemicals with the kinetics of uptake and metabolism by water milfoil to gain basic relations to understand each behavior.

In the experiment, using the newly developed exposure system, water milfoil was exposed to five simple phenols and clarified individual uptake *via* shoot and root, followed by translocation and metabolism. The kinetics of uptake and observed metabolic reactions in water milfoil were estimated, and compared with various physicochemical parameters of the phenols by regression analysis and obtained correlations between them

Materials and Methods

Chemicals

The ^{14}C compounds uniformly radiolabeled at the phenyl ring were used in the study (Figure 1); phenol (**1**), 4-nitrophenol (**2**) were purchased from American Radiolabeled Chemicals, Inc.; 4-cyanophenol (**3**), 4-hydroxybenzamide (**4**) and 4-hydroxybenzoic acid (**5**) were prepared in our laboratory according to the reported methods (Yoshitake et al. 1979; Saito and Kawabata 2005; Chen et al. 2007). The specific activities were 2.96 (**1**), 2.85 (**2**) and 4.37 GBq/mmol (**3** – **5**). Each ^{14}C compound had the radiochemical purity exceeding 98% as purified by reversed-phase HPLC prior to the use. Non-radiolabeled **1**–**5** with the chemical purity >95% were purchased from Sigma-Aldrich Co. All the reagents and solvents used in this experiment were of analytical grade.

Chromatography

A reversed-phase HPLC system to analyze the test phenols and their metabolites consisted of a Hitachi LC module (model L-7000) equipped with a SUMIPAX ODS A-212 column (5 μm , 6mm i.d.×15 cm, Sumika Chemical Analysis Service, Ltd.). The

following gradient system was employed to analyze each phenol and its metabolites at a flow rate of 1 mL/min.; 0.1% formic acid (solvent A) and acetonitrile (solvent B): 0 min, %A/%B (v/v), 100/0; 40 min, 10/90; 40.1 min, 100/0; 45 min, 100/0. The typical retention times of the corresponding phenols were 18.6 (1), 22.1 (2), 19.8 (3), 6.7 (4) and 12.9 (5) min. The radioactivity in the column effluent was counted with a Flow Scintillation Analyzer Radiomatic 150TR (Perkin Elemer, Co.) radiodetector equipped with a 500 μ L liquid cell using Ultima-Flo AP[®] (Perkin Elemer, Co.) as a liquid scintillator. The LOD for the radioactivity in HPLC analysis was 30 dpm. TLC was carried out using pre-coated silica gel 60F254 thin-layer chromatoplates (20 \times 20 cm, 0.25 mm thickness; E. Merck) for the purification of the glucose conjugates of each tested phenol. The TLC solvent used for development was butanol/acetic acid/water, 4/1/1 (v/v/v). The autoradiogram was prepared by exposing the TLC plates to BAS-III's Fuji imaging plates (Fuji Photo Film Co., Ltd.) for several hours, and the corresponding radioactive spot transcribed onto the imaging plate was detected by a Bio-Imaging Analyzer Typhoon (GE Healthcare).

Spectroscopy

One (¹H) and two (¹H-¹H COSY) dimensional NMR spectra of the sugar conjugates of 2, 4 and 5 were measured in methanol-*d*₄ with 0.03% TMS using a Varian Mercury 400 spectrometer (Varian Technologies Ltd.) at 400 MHz. LC-ESI-MS/MS analysis was conducted for the phenols and their metabolites using a Waters Tandem Quadruple TQD spectrometer equipped with a Waters Separation Module Acquity UPLC (Ultra Performance Liquid Chromatograph) and a Waters Acquity photodiode array detector. The following parameters were used for the typical analysis: source temperature 150°C; desolvation temperature 450°C; capillary voltage 3.2 kV; cone voltage 10 – 40 V; collision energy 5 – 20 V.

Radioanalysis

Water medium and extracts of sediment and plant were determined by LSC with a Packard Model 2900TR spectrometer after mixing each aliquot with 10 mL of Perkin Elmer Emulsifier Scintillator Plus[®]. The LOD for LSC analysis was 30 dpm. The post

extracted bound residues in plant and sediment were combusted using a Perkin Elmer Model 307 sample oxidizer. The $^{14}\text{CO}_2$ produced by the procedure was trapped into 9 mL of Perkin Elmer Carb[®]-CO₂ absorber and mixed with 15 mL of Perkin Elmer Permafluor[®] scintillator. The radioactivity therein was quantified by LSC. The efficiency of the combustion was determined to be greater than 94.4%.

Plant Material and Treatment

M. elatinoides purchased from Shimizu Laboratory Suppliers. Co. Ltd. was used in the experiments as previous chapter (Ando et al. 2012, chapter 3). After 10 days of root development in an aquarium filled with the AAP water medium and OECD synthetic bottom sediment, the plant was sterilized using 0.5% sodium hypochlorite with sonication under reduced pressure for 1 min, washed using sterilized water and subjected to the exposure experiment. The glass test vessel used for this study had the glass partition board which completely separates shoot and root chambers as shown in Figure 1 in chapter 3. The growth stage of the plants was as follows: shoot length, 17.1–18.8 cm; root length, 4.2–5.2 cm; root number, 7–11; fresh body weight, 0.41–0.49 g. The shoot and root chambers were individually filled with 120 mL of the water medium and medium-moistened sediment (20 mL and 35 g), respectively. The medium and sediment were adjusted to pH 7.0 ± 0.1 and autoclaved (1.5 kg cm^{-2} , 120°C , 20 min) before use. A 20 to 55 μL of the methanol solution containing each ^{14}C -phenol isotopically diluted with the corresponding non-radiolabeled compound was either spiked into the medium in the shoot chamber (water treatment) or the bottom sediment in the root chamber (sediment treatment) and homogeneously mixed to prepare exposure concentration of 0.1 ppm (0.083 MBq). Approximately 2 cm of the root node was buried into the sediment in the root chamber and the shoot was gently placed to be immersed under the water in the shoot chamber (Figure 1). To prevent ^{14}C cross contamination *via* vaporization/deposition between the chambers, an AAP-moistened cotton was settled on the partition board and each chamber was covered with a polyethylene wrap. Then, the glass vessel was incubated in a climate chamber LH-220S (NK Systems Ltd.) at $20 \pm 2^\circ\text{C}$ under fluorescence light (8,000 lux, 16 h per day) up to 96 hours. Each exposure was conducted in triplicate.

Analytical Procedures

The sampling was conducted sequentially after 1, 3, 6, 12, 24, 48 and 96 hours of each exposure. The plant sampled from the exposure chamber was surface-washed using 50 mL of a fresh water medium and the rinsate was combined with the water medium recovered from the corresponding chamber. After measuring its length and wet weight, the plant was further rinsed with 50 mL of acetonitrile (surface rinse). Then, the plant was divided into shoot and root portions, and the total radioactivity in each portion was measured by the combustion analysis, except for the shoots of the water treatment. The corresponding shoot portion was extracted with 20 mL of methanol using a homogenizer AM-8 (Nissei Ltd.) at 10,000 rpm and 0°C for 10 min. The homogenate was vacuum filtered and the plant residue was further extracted twice in the same manner. The sediment and water medium (pore water) in the root chamber were separated by vacuum filtration. The sediment was washed once with 100 mL of a fresh water medium, combined with the pore water and radioassayed. The ¹⁴C-treated sediment was further extracted with 30 mL of methanol by 10 min of mechanical shaking with a Taiyo SR-IIw recipro-shaker (Taiyo Chemical Industry Co., Ltd.). The soil residue after vacuum filtration was successively extracted twice in the same manner. Each aliquot of the surface rinses, extracts and water media was analyzed with LSC and HPLC co-chromatography with authentic standards. The plant/sediment extracted residues and ¹⁴C-unexposed sediment were subjected to the combustion analysis.

Identification of Major Metabolites

The major metabolites were isolated/purified by TLC from the plant samples and subjected to LC-MS and NMR analyses.

Kinetic Analysis

In order to understand the behavior of the phenols in *M. elatinoides*, kinetic analysis was employed for the samples of water treatment system using Model-Maker program (version 4, ModelKinetix). The simulation was carried out by a compartment model shown in Figure 2. Based on the kinetic parameters of **1–5**, the relative rate constants on the uptake and metabolism of each phenol derivative were calculated and their

logarithm values were subjected to regression analysis with various physicochemical parameters of the phenols using Microsoft Excel 2010. Physicochemical parameters applied for the analysis are listed in Table 1. Since the phase II conjugation reactions of chemicals are considered to be affected by nucleophilicity of the substrates (Cupid et al. 1999), the energy level of the highest occupied molecular orbital (E_{HOMO} , eV) with its distribution was calculated by SCIGRESS MO Compact program (version 1, standard, Fujitsu Ltd.) as a potential index to examine the correlation with the transformation rate constant to produce glucoside conjugate of phenols. The molecular geometry optimization of each phenol was implemented by MNDO-PM 3 Hamiltonian with the dielectric constant of $\epsilon = 78.4$, assuming the water environment, and calculated with a criterion introduced by inputting the PRECISE command. The calculation of each phenol was conducted for the neutral and ionized form at phenoxy oxygen abbreviated as $E_{HOMO(OH)}$ and $E_{HOMO(O^-)}$, respectively. The classical Hammett's constants (σ and σ^-) at the reaction center, i.e. phenolic oxygen, were also examined for the reactivity of phenols.¹⁹ The fraction of undissociated form of each phenol in the medium at pH 7 was calculated from its acid dissociation constant (K_a) by applying Henderson-Hasselbalch equation as follows; $f_{neutral} = [K_a \cdot 10^{-7} + 1]^{-1}$. Logarithm of the distribution constant ($\log D$) which indicates the hydrophobicity of chemicals adjusted with the dissociation effect was obtained from $\log K_{ow}$ and pK_a values according to the method of Van der Waterbeemd and Testa (1987).

RESULTS

Validity Confirmation of the Test System

During the 96-hour uptake period, no growth inhibition was observed for the plants exposed to any phenols compared with those acclimated in the control aquarium: increase in length, 0.4–1.1 cm; fresh body weight, 0.04–0.09 g. Cross contamination of the applied ^{14}C between the shoot and root chambers was considered negligible as extremely little radioactivity ($\leq 0.1\%AR$) was detected from the ^{14}C -untreated chambers throughout the study. The inner wall of the test vessel was thoroughly washed with methanol after each sampling and the recovered ^{14}C in the rinsate was below the LOD (<30 dpm), which clarified negligible loss of ^{14}C by adhesion onto the vessel.

¹⁴C Distribution in the Water Treatment System

The ¹⁴C distribution in the water treatment system after 96 hours is summarized in Table 2. The total ¹⁴C recovery for **2–5** ranged 93.7–97.2%AR with less recovery for **1** (81.3%AR). Large amount of the applied radioactivity remained in the water layer for **2–4** (>80.9%AR), while lower amount was observed for **1** (55.8%AR) and **5** (54.5%AR). From the HPLC analysis, the radioactive component in exposure water was clarified to be the unaltered parent only for all the test materials. The amount of ¹⁴C taken up from water *via* shoot with the incubation period is shown in Figure 3. The ¹⁴C uptake by the shoot after 96 hours reached 4.2–25.5%AR for **1–4**, and 41.7%AR for **5**. No detectable radioactivity was recovered from the plant surface wash. For most of the tested phenols, shoot uptake gradually approached to its steady state toward the end of exposure. Majority of the ¹⁴C taken up remained in the shoot and a minor radioactivity was detected from the root which amounted to 0.4% (**1**), ≤0.1% (**2–4**) and 0.9%AR (**5**). These results suggest that the basipetal ¹⁴C translocation from shoot to root is a minor process.

¹⁴C Distribution in the Sediment Treatment System

The ¹⁴C distribution in the test system at 96-hour exposure is summarized in Table 3. The total ¹⁴C recovery ranged from 91.7 to 98.2%AR. The radioactivity in the sediment is shown as the sum of ¹⁴C recovered in the methanol extract and unextractable bound residue, in which the latter amounted to be less than 3.5%AR. For all the phenols, most of the applied ¹⁴C remained in the root chamber (≥89.1%AR) and the radioactivity detected from the untreated water in the shoot chamber was insignificant (≤0.1%AR). In the root chamber, the amount of ¹⁴C in water/sediment after 96 hours was 47.0/42.1 (**1**), 34.4/61.0 (**2**), 42.2/51.8 (**3**), 85.9/11.5 (**4**) and 84.3%AR/6.5%AR (**5**). For both water and sediment fractions in the root chamber, the unchanged phenols were the only radioactive constituent confirmed by the HPLC analysis. Root uptake behavior of ¹⁴C from the sediment is shown in Figure 4. The ¹⁴C taken up after 96 hours reached 0.8–2.4%AR for **1–4** and 6.6%AR for **5**. No radioactivity was recovered by the plant surface rinse. In comparison with the water treatment, the ¹⁴C uptake from sediment *via* root was much lower and slower. The radioactivity translocated from root to shoot after

96 hours was extremely low for **1–4** ($\leq 0.1\%$ AR), which suggested the acropetal ^{14}C translocation from root to shoot is a minor process. On the other hand, **5** showed the highest potential of translocation as the radioactivity detected in the shoot was 1.5% AR. However, the metabolic profiles in root and shoot were not clarified due to their insufficient ^{14}C to be characterized.

Distribution of Metabolites in the Exposed Shoot

The metabolite distribution in the shoot portion of milfoil at 96-hour exposure is summarized in Table 4, as representative. In the shoot, $84.4 - 97.5\%$ TRR was extractable and $2.5 - 6.3\%$ TRR remained as unextractable bound fraction. In the extracts, the unchanged phenols were quantified to be $14.0 - 20.5\%$ TRR for **1–4**, while the was only 6.0% TRR for **5**, respectively. The glycoside conjugate of each phenol was the main metabolite which amounted to 72.9 (**6**), 78.8 (**7**), 83.4 (**8**), 63.5 (**9**) and 88.0% TRR (**10**), respectively, after 96 hours. For identification, metabolites **6–10** were analyzed by LC-MS. The MS analysis of each metabolite gave molecular-related ions which were identical to the mass number of mono-glucose conjugate of the corresponding phenol. Furthermore, the MS/MS analysis of $[\text{M}+\text{H}]^+$ or $[\text{M}-\text{H}]^-$ gave mass fragments suggesting the structure as follows: **6**, m/z 279 $[\text{M}+\text{Na}]^+$, 257 $[\text{M}+\text{H}]^+$, 95 $[\text{1}+\text{H}; \text{M}-\text{sugar}+\text{H}]^+$; **7**, m/z 324 $[\text{M}+\text{Na}]^+$, 302 $[\text{M}+\text{H}]^+$, 140 $[\text{2}+\text{H}; \text{M}-\text{sugar}+\text{H}]^+$; **8**, m/z 322 $[\text{M}+\text{Na}]^+$, 300 $[\text{M}+\text{H}]^+$, 138 $[\text{3}+\text{H}; \text{M}-\text{sugar}+\text{H}]^+$; **9**, m/z 304 $[\text{M}+\text{Na}]^+$, 282 $[\text{M}+\text{H}]^+$, 120 $[\text{4}+\text{H}; \text{M}-\text{sugar}+\text{H}]^+$; **10**, m/z 299 $[\text{M}-\text{H}]^-$, 255 $[\text{M}-\text{CO}_2-\text{H}]^-$, 137 $[\text{5}-\text{H}; \text{M}-\text{sugar}-\text{H}]^-$. With regard to metabolite **10**, the fragment ion m/z 255 was detected in the negative ion mode. Because this ion is considered to be produced by decarboxylation by the mass fragmentation similarly to **5**, **10** was supposed to have a free carboxylic acid group and *O*-glycosidic bond at the phenoxy oxygen. After the tentative identification by LC-MS, the conjugates **7**, **8** and **10** were subjected to NMR analyses. The chemical shifts of protons were assigned as follows: **7**, $\delta = 8.36$ ppm (2H, d, $J = 9.21$ Hz, aromatics), 7.34, (2H, d, $J = 9.21$ Hz, aromatics), 5.16 ppm (1H, d, $J = 8.01$ Hz, anomeric) and 3.60–4.01 ppm (5H, m, glucose); **8**, $\delta = 7.80$ ppm (2H, d, $J = 8.81$ Hz, aromatics), 7.27 (2H, d, $J = 8.81$ Hz, aromatics), 5.14 ppm (1H, d, $J = 7.61$ Hz, anomeric)

and 3.52–3.98 ppm (5H, m, glucose); **10**, $\delta = 7.87$ ppm (2H, d, $J = 8.61$ Hz, aromatics), 7.16 (2H, d, $J = 8.61$ Hz, aromatics), 5.02 ppm (1H, d, $J = 6.81$ Hz, anomeric) and 3.52–3.98 ppm (5H, m, glucose). The correlation between the anomeric and the vicinal protons was distinguishable by ^1H - ^1H COSY NMR technique for each conjugate, which strongly indicated the glucoside structure.

Kinetic Analysis

The kinetic analysis was conducted for each phenol exposed in the water treatment. The graph simulated ^{14}C -dissipation curves to estimate shoot uptake and metabolic rate constants for **5** is given in Figure 5, as representative. The optimization of the rate constants was done with a good correlation ($r^2 > 0.97$, $P < 0.05$) for all phenols. The relative rate constants of **2–5** with respect to **1** are summarized in Table 5. The relative rate constants for the production of “Others” and “Bound” were not obtained because these metabolic processes were very insignificant to be compared with those of the most predominant process “Glucose conjugation”. Successively, the correlation between the physicochemical parameters and the logarithm of the relative rate constants are examined by the regression analysis, as listed in Table 6. The highest correlation for shoot uptake, $\log [k_{1(i)}/k_{1(1)}]$, was observed for $\log K_{ow}$ as 0.656 (standard deviation: 0.325) followed by f_{neutral} (standard deviation: 0.328), while the other indexes showed a lower correlation ($< |0.323|$). With respect to the transformation rate to produce glucose conjugate, $\log [k_{2(i)}/k_{2(1)}]$, better correlations were obtained for the electrochemical parameters σ , σ^- and $E_{\text{HOMO(OH)}}$ as their absolute values exceeded 0.807 with the standard deviation of less than 0.036. The kinetic simulation for the sediment treatment resulted in poor fitting ($r^2 < 0.50$), so that no comparison with the parameters was attempted.

DISCUSSIONS

In some test systems, the total ^{14}C recovery gradually decreased over the period of incubation. The loss of radioactivity was prominent for **1** probably due to the vaporization from the test vessel considering its high vapor pressure at ambient temperature (0.35 mm Hg at 25°C) (ASTDR 1998).

In the water treatment, the ^{14}C uptake/accumulation to the plant decreased in the

order of **5**, **1**, **2**, **3** and **4**. With regard to the regression analysis between the relative rate constants and physicochemical parameters, $\log K_{ow}$ index showed the strongest correlation with the shoot uptake rate constants (k_l). Similarly to the case in many living organisms, this tendency complies with the result that uptake of water-dissolved chemicals through macrophyte surface closely correlates with their lipophilicity. For example, Gobas et al. (1991) investigated the uptake of non-ionizable pesticides from water by *M. spicatum* under submergence, and they observed the linear positive correlation between the accumulation factors and $\log K_{ow}$ values. The second-highest, negative correlation observed for $f_{neutral}$, expressing the rate of the ionized molecules, may support the importance of $\log K_{ow}$ index for accumulation of chemicals. The same relationship was also reported on macrophytes by Carvalho et al. (2007) but without the linearity at the lower range of $\log K_{ow}$, approximately below one, which exhibits the minimum uptake potential. Meanwhile, we also compared shoot uptake rate constant and $\log D$, reflecting the actual lipophilicity of an ionizable chemical under dissociation. For example, better positive correlation for $\log D$ than $\log K_{ow}$ was reported for the accumulation of ionized chemicals by fish which is believed to be dominated by interaction with gill (Franco and Trapp 2009). However, we obtained a poor correlation, especially because highly dissociated carboxylic acid derivative **5** ($f_{neutral} = 0.004$ at pH 7) exhibited outstanding accumulation in spite of its lowest $\log D$ value. In general, the ionized chemicals are considered unlikely to bioaccumulate in the leaf/shoot portion of plants because lipophilic materials such as epicuticular wax on the plant surface prevent the penetration of ionized compounds. However, Zhang *et al.* have clarified that many carboxylic compounds intensively dissociate in natural water bodies are largely taken up by macrophytes, irrespective of their extremely low lipophilicity expressed by $\log D$ (less than zero) (Zhang et al. 2014). In addition, 3-phenoxybenzoic acid (PBacid) which intensively dissociates in water at pH 7 as indicated by $f_{neutral} = 0.001$ was largely taken up by *M. elatinoides* (Ando et al. 2012). This trend may be explained from the reasons that ions could receive electric attraction/repulsion from electrically charged cell membranes, formation of molecular complex with cations and, as the most crucial process for weak acids, retention of anions at inner cells (ion trap theory) followed by metabolism which generally increase the solubility of xenobiotics to enhance the trapping (Rendal et al. 2011).

For the metabolic reaction, glucose conjugation was observed as major pathway. The conjugation followed by storage into vacuoles is the generally accepted detoxification process in terrestrial plants. This is probably the same case for macrophytes, since glucosidation is observed for many aquatic plants. For example, Day and Saunders reported glucose conjugation of halogenated phenols by duckweed, which is one of the major macrophytes (Day and Saunders 2004). In our kinetic analysis of the transformation rate constants to glucose conjugate (k_2), high correlations were found for Hammett constant (σ and σ^-) and $E_{HOMO(OH)}$. These results imply that the electronic distribution at the phenoxy group and/or phenol structure as a whole is important for glucose conjugation at the enzyme active site. Moreover, since the index σ^- also correlated with glucosidation, the inductive effect of electron withdrawing substituent on the phenyl ring, such as deprotonation and polarization enhancements, was considered to associate with the conjugation. The key mechanism for glucosidation by glucosyl transferases is generally expressed by the following steps (Modolo et al. 2009): (1) interaction of histidine at the binding acceptor domain of the enzyme with the hydroxyl group of the sugar-accepting substance to induce deprotonation, (2) nucleophilic attack by the deprotonated acceptor to the C1 anomeric carbon of the donor sugar. Hence, the nucleophilicity expressed by the index such as σ , σ^- or $E_{HOMO(OH)}$ likely showed good correlation to k_2 . Incidentally, for exhaustive reaction analysis or estimation, more detailed procedures such as molecular orbital calculation approach to estimate the energy gap between HOMO and LUMO (unoccupied molecular orbital) of the nucleophile and electron acceptor as well as their transition states, are assumed to be important for the bond formation. Furthermore, the conformation rearrangement during interaction with the binding domain followed by HOMO re-distribution of the nucleophile at the active site should be taken into account within the specific enzyme to precisely simulate the reaction (Siegel et al 2010). For such approach, extensive information, e.g., definitive three-dimensional structure of the target enzyme, detailed reaction path, appropriate calculation methodology, and etc., is required, and further studies are necessary.

With regard to reaction site for glucosidation, **5** possesses both phenoxy and carboxyl groups while the phenoxy group was judged as the predominant place in *M. elatinoides*. The HOMO coefficients at the carboxylic and phenoxy oxygen were

calculated as -0.372 and 0.047, respectively, while the LUMO constant at the anomeric carbon of glucose was -0.241. Deducing from the estimated electronic distribution, the carboxyl group is more likely to be involved in conjugation, but only this may not exclusively explain the selectivity of enzymatic glucosidation. The glucosidation of hydroxybenzoic acids including **5** by glucosyl transferases is known to proceed at hydroxyl or carboxyl group to give glucose ether or ester conjugate, respectively, depending on the substrate and the character of the enzymes (Lim et al. 2002). Additionally, there are bi-functional glucosyl transferases which are possible to catalyze either etherification or esterification, and the selectivity is known to be controlled by the reaction pH. For example, the glucosyl transferase in grape can selectively produce the ether glucoside of resveratrol at basic condition (pH >7) while the ester one at acidic pH (Hall and Luca 2007). Because etherifying glucosidation of 3-phenoxybenzoic acid is previously confirmed (Ando et al. 2012), *M. elatinooides* is considered to have both types of glucosyl transferases and/or bi-functional one.

In the sediment treatment, the ^{14}C uptake/accumulation to plant decreased in the order of **5**, **1**, **2**, **3** and **4**, which was the same trend observed with the water treatment. However, the total amount of radioactivity detected in the plant was much less than that in the water treatment. To estimate the uptake/transport of organic compounds from root to shoot, the TSCF, the concentration ratio of the compound in xylem (transpiration stream) and the solution adjacent to the roots, is commonly applied for terrestrial plants. Briggs et al. (1982) have reported bell-shaped Gaussian curves for plotting TSCF versus $\log K_{ow}$ with the non-ionizable compounds, which imply significant root uptake and translocation occur for the compound having an intermediate lipophilicity, $\log K_{ow}$ around 1–3, and the maximum uptake is expected at the vertex 1.8. The similar uptake trend was observed for water milfoils with emergent leaves incubated hydroponically (Carvalho et al. 2007). On the other hand, Dettenmaier *et al.* have proposed the sigmoidal relationship and suggested that the highly soluble/non-ionizable compound with a very low $\log K_{ow}$ has a highest uptake potential while that with a high $\log K_{ow}$ are low (Dettenmaier et al. 2009). Based on the Briggs's theory, the amount of radioactivity in the shoot was considered to decrease in the order of **2**, **3**, **5**, **1** and **4**, but the obtained results were not as expected. One of the reasons for this discrepancy may be explained

by the low applicability of the TSCF concept to submerged macrophytes, since their transpiration stream diminishes under submergence. Dettenmaier's theory seems to better elucidate our results, but further accumulation of basic data and knowledge would be necessary to understand precise root uptake profiles of organic chemicals, especially for ionizables, for submerged-rooted macrophytes.

CONCLUSION

In conclusion, the shoot uptake of phenols by *M. elatinoides* was faster and larger than the root uptake. The carboxylic acid derivative **5** showed the highest accumulation for both shoot and root treatment which indicated some specific potential for the weak acids to be effectively taken up by aquatic plants. Similarly to the terrestrial plants, the major metabolic pathway was the formation of glucose conjugate, which considered as the major detoxification strategy. The kinetic analysis showed relatively high correlation between shoot uptake rate constant and $\log K_{ow}$, while factors other than hydrophobicity are considered necessary to be taken into account for better correlation. The good correlation was observed between the transformation rate constant (glucose conjugation) and Hammett constants or $E_{HOMO(OH)}$ parameter.

Tables:

Table 1: Physicochemical properties of the phenol derivatives.

Phenol	pK_a^a	f_{neutral}^b	$\log K_{ow}^c$	$\log D^d$	σ^e	σ^-^e	$E_{HOMO(OH)}$	$E_{HOMO(O^-)}$
1	9.99	0.999	1.47	1.47	0	0	-8.95	-7.31
2	7.15	0.586	1.91	1.68	0.78	1.27	-9.51	-8.27
3	7.77	0.855	1.60	1.53	0.66	1.00	-9.16	-9.90
4	8.18	0.938	0.33	0.30	0.36	0.61	-9.18	-7.60
5	4.58, 9.23	0.004	1.58	-0.83	0.45	0.77	-9.28	-4.49

a: Calculated from ref (Sugii et al. 1986)

b: $f_{\text{neutral}} = [K_a/10^7 + 1]^{-1}$

c: Calculated from refs (Breyer et al. 1991; Cronin and Schultz 2001)

d: $\log D$ values at pH 7.0, calculated using $\log K_{ow}$ and pK_a according to ref (Van der Waterbeemd and Testa 1987)

e: Calculated from ref (Hansch and Leo 1979)

Table 2: ^{14}C distribution in the water treatment system after 96 hours.

	%AR ^a				
	1	2	3	4	5
Shoot chamber					
Water medium	55.8 (4.5)	82.9 (7.5)	80.9 (7.9)	92.1 (8.5)	54.5 (5.5)
Root chamber	ND	ND	ND	ND	ND
Plant (whole)	25.5 (2.2)	14.3 (1.3)	12.8 (1.2)	4.2 (0.5)	41.7 (4.2)
Shoot	25.1 (1.9)	14.3 (1.3)	12.8 (1.2)	4.2 (0.5)	40.8 (3.9)
Roots	0.4 (0.1)	ND	ND	ND	0.9 (0.1)
Total	81.3 (5.2)	97.2 (2.9)	93.7 (2.6)	96.3 (1.8)	96.2 (2.1)

ND: Not detected.

a: Average values ($n = 3$). Standard deviations are given in parentheses.

Table 3: ¹⁴C distribution in the sediment treatment system after 96 hours.

	%AR ^a				
	1	2	3	4	5
Shoot chamber					
Water medium	ND	ND	ND	ND	ND
Root chamber					
Pore water	47.0 (3.1)	34.4 (3.9)	42.2 (4.6)	85.9 (7.8)	84.3 (8.2)
Sediment	42.1 (3.9)	61.0 (5.1)	51.8 (5.3)	11.5 (1.3)	6.5 (0.6)
Plant (whole)	2.4 (0.2)	1.3 (0.1)	1.2 (0.1)	0.8 (0.1)	6.6 (0.7)
Shoot	ND	ND	ND	ND	1.5 (0.1)
Roots	2.4 (0.2)	1.3 (0.1)	1.2 (0.1)	0.7 (0.1)	5.1 (0.6)
Total	91.7 (3.3)	96.7 (2.9)	95.2 (3.0)	98.2 (3.5)	97.4 (2.3)

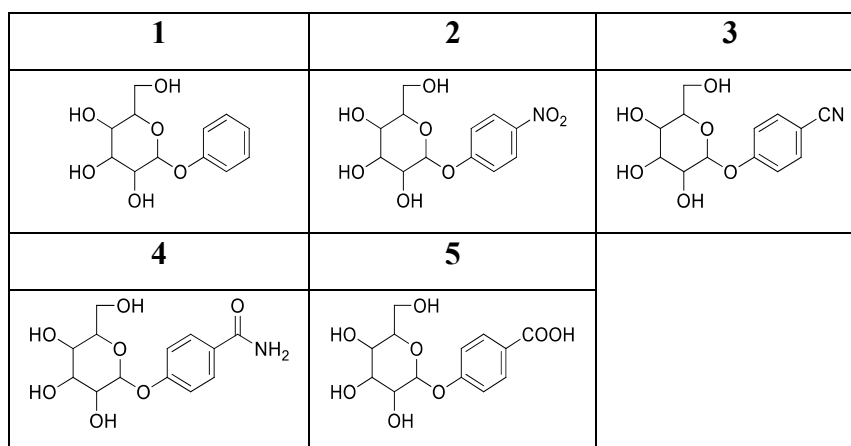
ND.: Not detected

a: Average values ($n = 3$). Standard deviations are given in parentheses.

Table 4: ¹⁴C metabolites in shoot exposed for 96 hours in the water treatment system.

	%TRR				
	1	2	3	4	5
Extractable					
Phenols	20.5	17.9	14	19.4	6.0
Glucose conjugate*	72.9	78.8	83.4	63.5	88
Others**	0.8	0.6	0.1	10.8	2.9
Bound	5.8	2.7	2.5	6.3	3.1
Total	100.0	100.0	100.0	100.0	100.0

*: The structure of each glucose conjugate are given below.



** : Minor degradates amounted less than 5%TRR and/or polar degradates un-retained by the HPLC column.

Table 5: Kinetic analysis of 1–5 in water milfoil (water exposure).

	1	2	3	4	5
Rate constant (hrs⁻¹)					
k_1 (uptake)	5.651×10^{-3}	2.332×10^{-3}	2.818×10^{-3}	9.063×10^{-4}	8.424×10^{-3}
k_2 (conjugation)	3.185×10^{-2}	4.359×10^{-2}	4.044×10^{-2}	4.193×10^{-2}	3.851×10^{-2}
k_3 (others)	6.389×10^{-3}	9.574×10^{-4}	6.346×10^{-3}	1.815×10^{-2}	3.323×10^{-3}
k_4 (bound)	8.284×10^{-3}	2.067×10^{-3}	1.064×10^{-2}	1.741×10^{-2}	3.489×10^{-3}
r^2	0.997	0.989	0.990	0.978	0.989
P	3.210×10^{-3}	1.866×10^{-2}	3.731×10^{-4}	4.209×10^{-2}	2.677×10^{-6}
Relative rate constant					
$\log [k_{1(i)}/k_{1(1)}]$	0	-0.384	-0.302	-0.795	0.173
$\log [k_{2(i)}/k_{2(1)}]$	0	0.136	0.104	0.119	0.083

Table 6: Correlation between logarithm values of the relative rate constant and parameters of the phenols.

	pK_a	f_{neutral}	$\log K_{ow}$	$\log D$	σ	σ^-	$E_{HOMO(OH)}$	$E_{HOMO(O^-)}$
$\log [k_{1(i)}/k_{1(1)}]$	-0.323	-0.564	0.656	-0.159	-0.263	-0.261	0.178	0.546
$\log [k_{2(i)}/k_{2(1)}]$	-0.467	-0.208	-0.100	-0.033	0.872	0.890	-0.807	-0.265

Figures:

Phenol	R
1	H
2	NO ₂
3	CN
4	CONH ₂
5	COOH

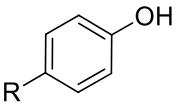


Figure1: Test materials.

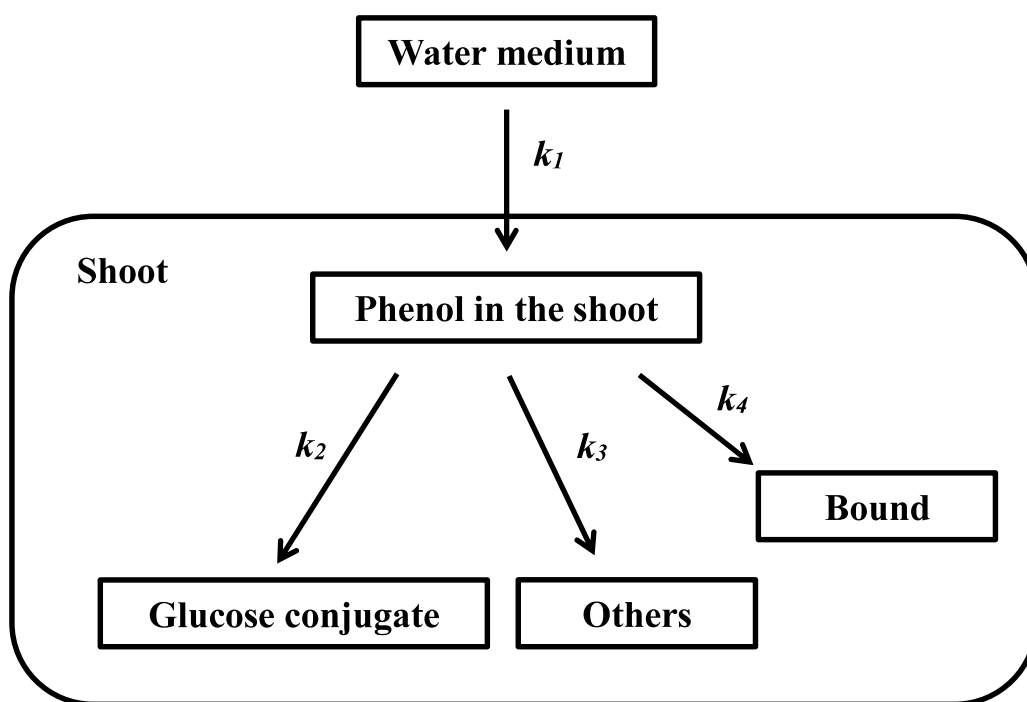


Figure 2: Compartment model employed for the kinetic analysis

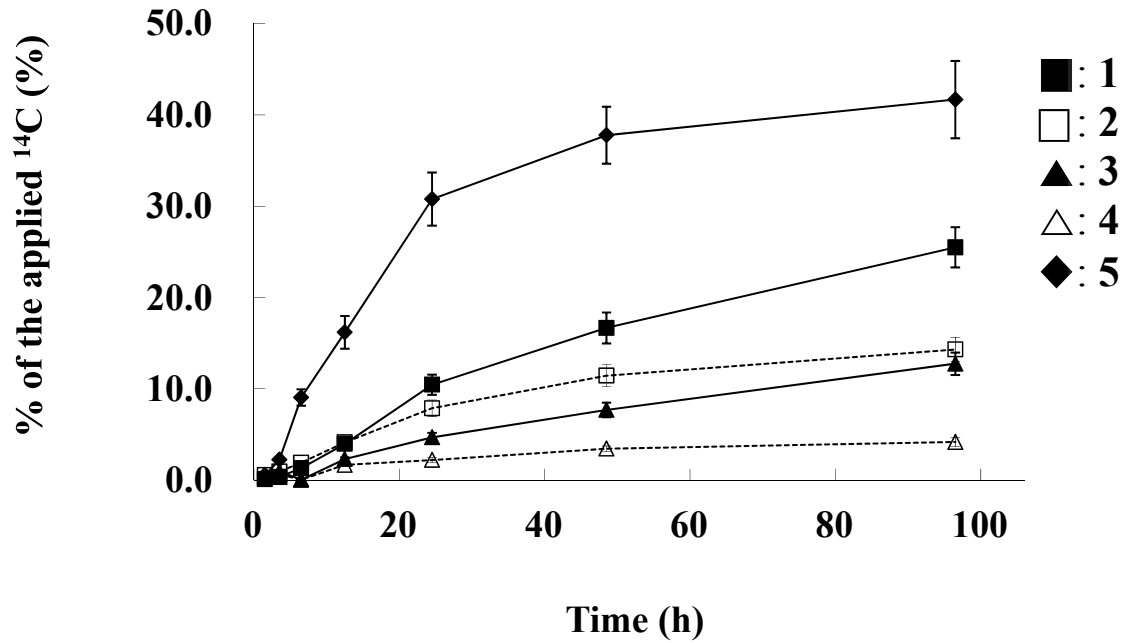


Figure 3: Accumulated ^{14}C by *M. elatinoides* in the water treatment system. The error bars represent mean standard deviation ($n = 3$; $p < 0.05$).

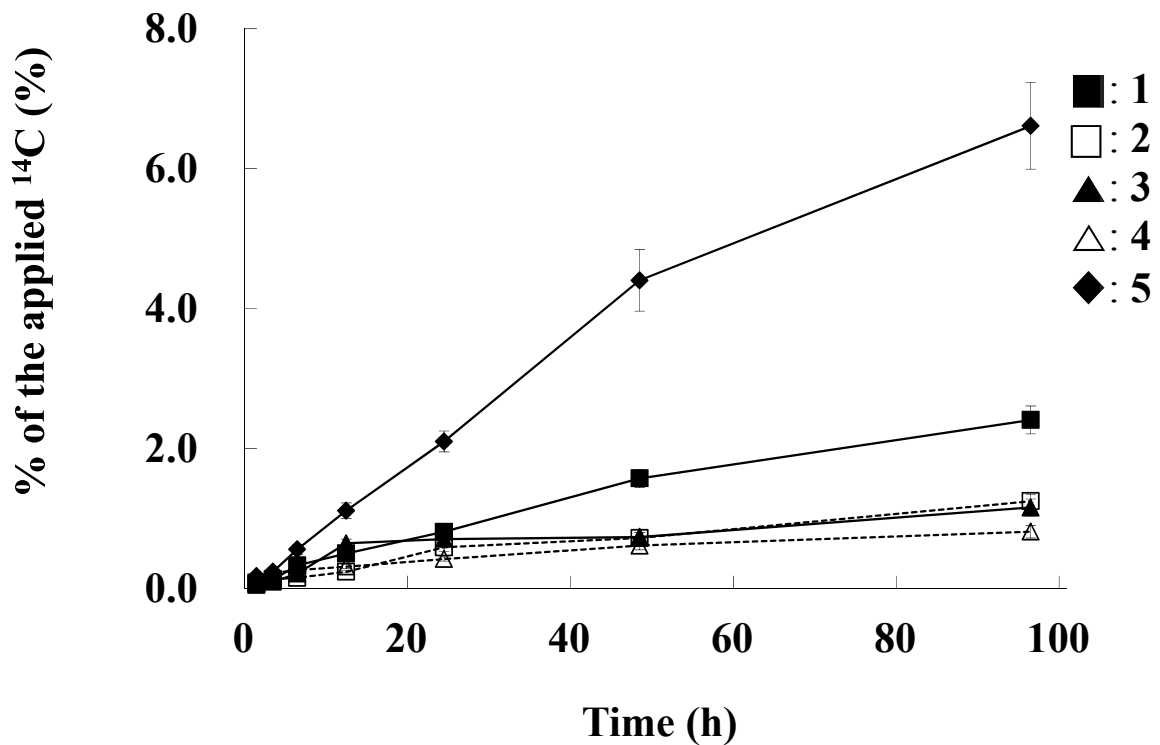


Figure 4: Accumulated ^{14}C by *M. elatinoides* in the sediment treatment system. The error bars represent mean standard deviation ($n = 3$; $p < 0.05$).

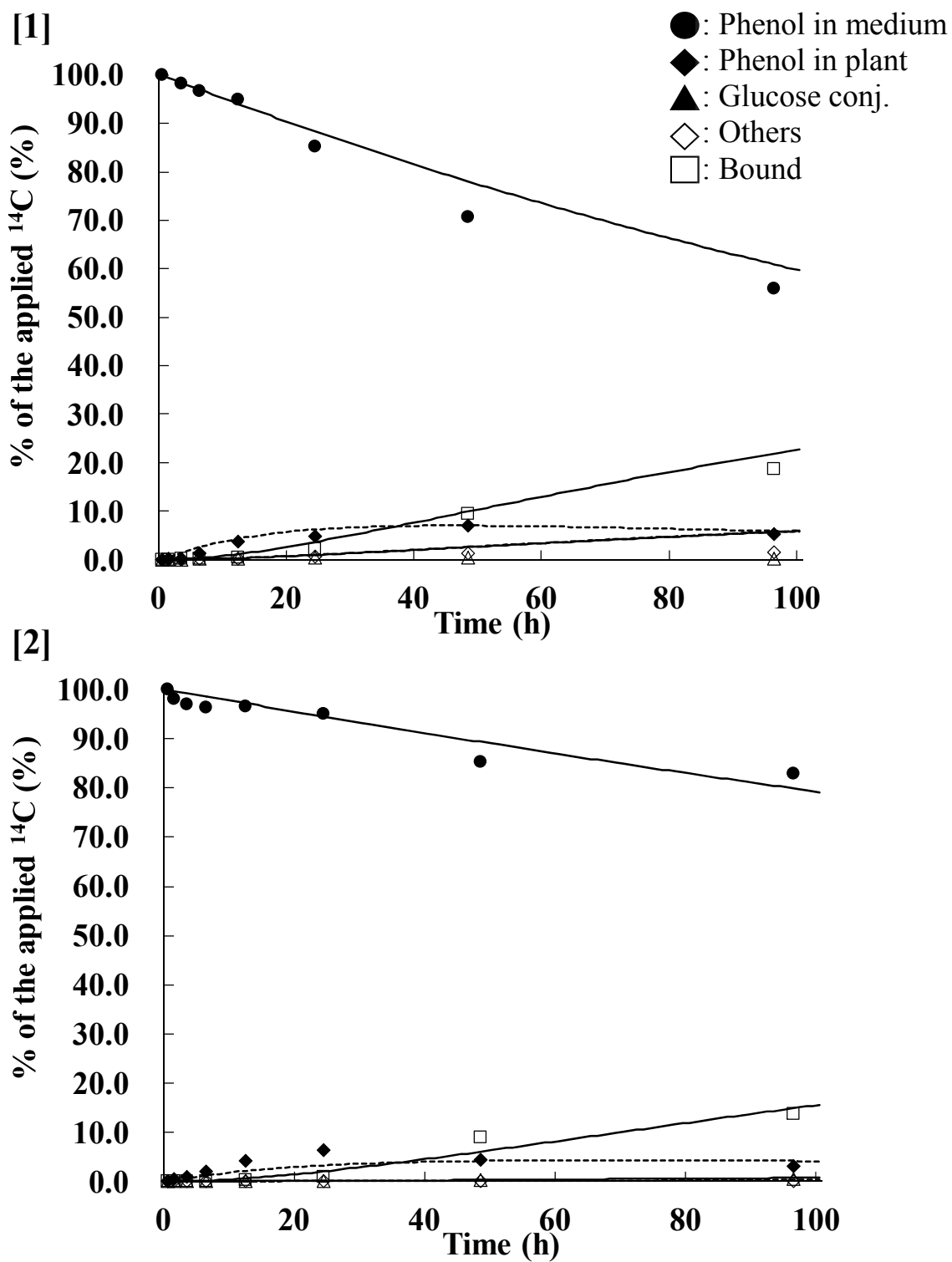


Figure 5: Simulated Uptake and metabolism curve of phenols by *M. elatinoides*.
Top: 1, Bottom: 2

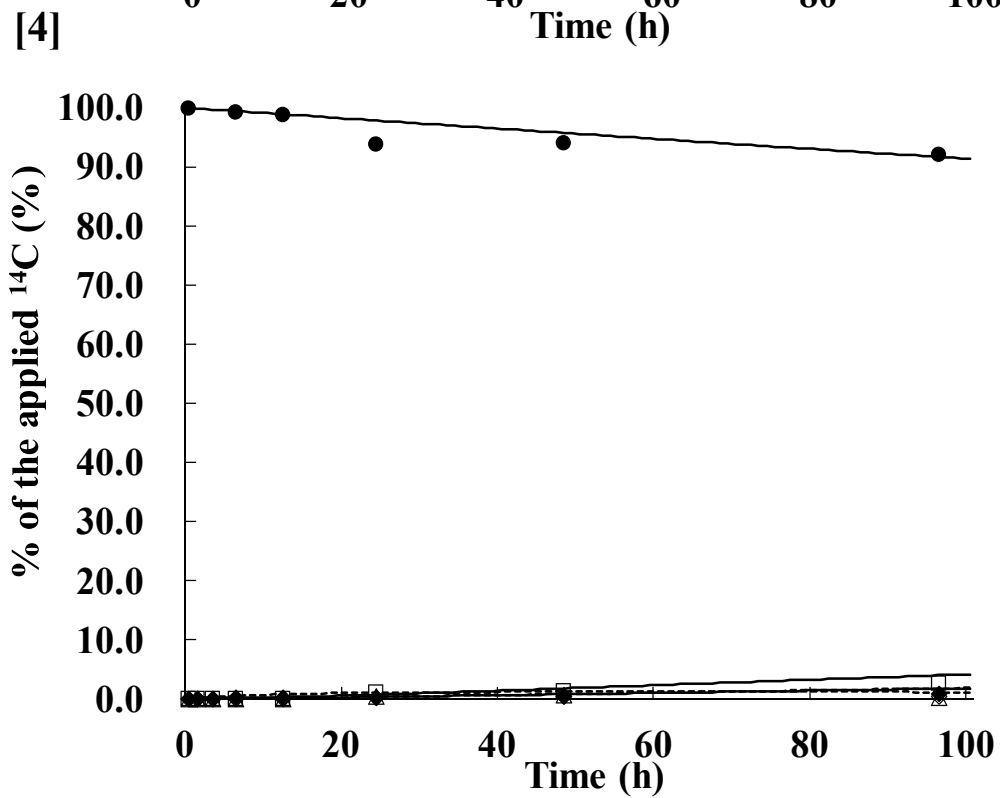
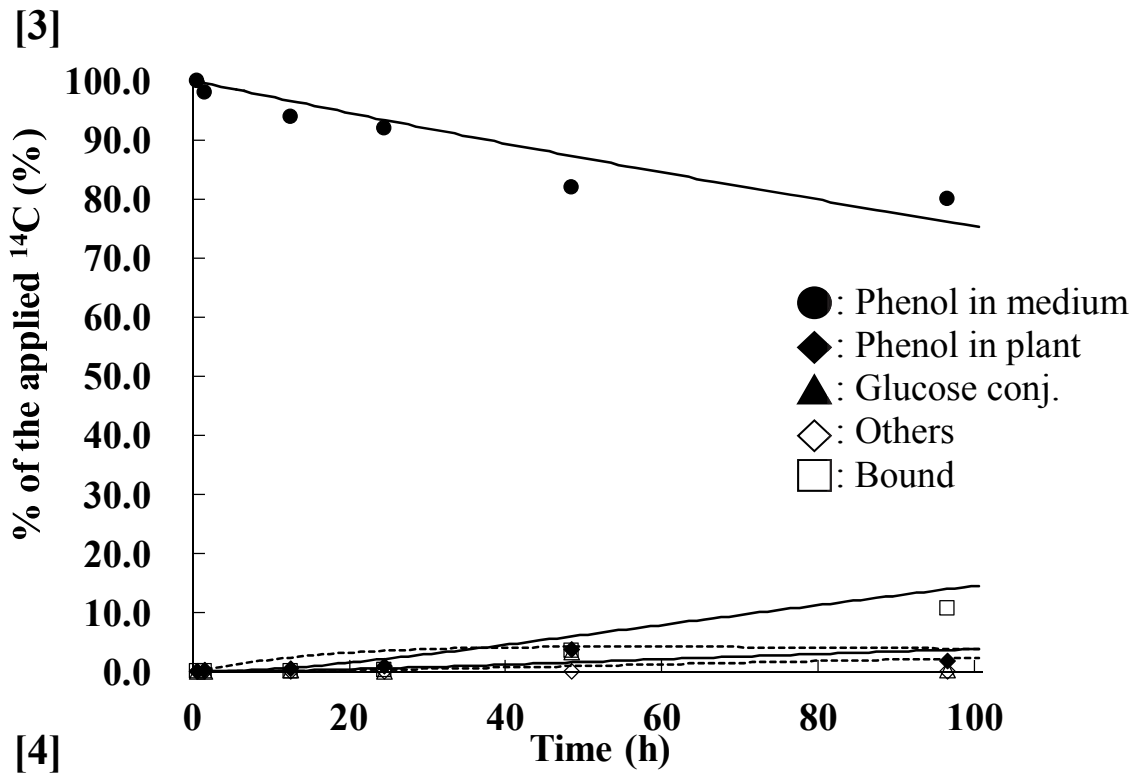


Figure 5 (continue): Simulated Uptake and metabolism curve of phenols by *M. elatinoides*. Top: 3, Bottom: 4

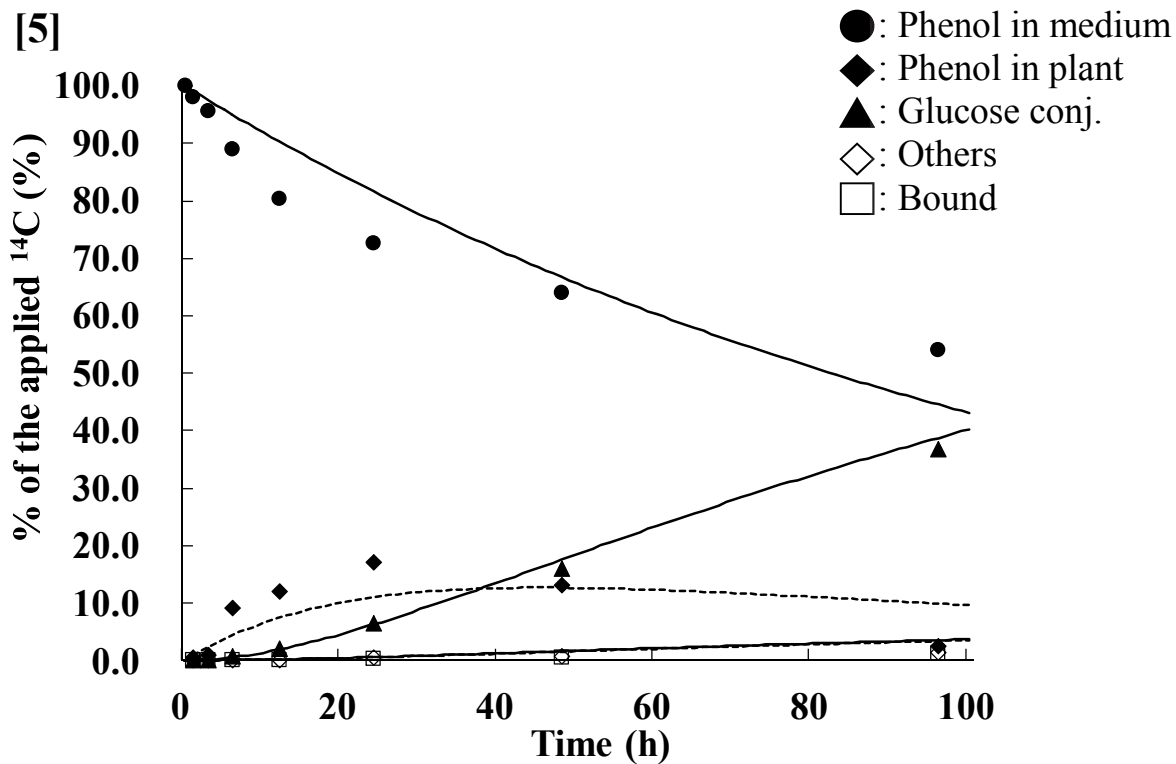


Figure 5 (continue): Simulated Uptake and metabolism curve of phenols by *M. elatinoides*. 5

5. Fate of Flumioxazin in Aquatic Plants, Two Algae, Duckweed and Water Milfoil

Through previous chapters, we have established the study design and obtained basic information of uptake/translocation/metabolism of chemicals by water milfoil, while the behavior of a pesticide for other aquatic species, which is our major object, has not been examined. As next step, we examined the fate of a herbicide in aquatic plants to gain practical information for the risk assessment.

Flumioxazin (**1**), 2-[7-fluoro-3,4-dihydro-3-oxo-4-(2-propynyl)-2*H*-1,4-benzoxazin-6-yl]-4,5,6,7-tetrahydro-1*H*-isoindole-1,3-(2*H*)-dione, is the herbicide to control annual broad-leaved weeds by inhibiting protoporphyrinogen oxidase which involves in the common tetrapyrrole biosynthetic pathways of chlorophylls and cytochrome (Theodoridis et al. 2000).¹ Excluding direct water application to control aquatic plants, **1** has a potential to enter environmental water bodies by unintended paths. The adverse effects of **1** to inhibit the growth of aquatic plants are reported in several literatures. For instance, Geoffroy et al. (2004) reported the retarding magnitude of cell divisions for *Scenedesmus obliquus* and *Lemna sp.* under exposure of **1** in the aqueous culture medium. A variety of macrophytes are also known to be affected by **1**, causing them to leak biochemical electrolytes from injured cells (Glomsli and Netherland 2013).

While toxicological researches for living organisms are typical approaches for the risk assessment of chemicals, it is also important to know the metabolic behaviors of the chemicals within test species as a basic knowledge for more robust hazard characterization. The metabolic fate of **1** in administered rats has been extensively studied (Tomigahara et al. 1999). The major metabolic reactions observed were: cleavage of imide linkage followed by ring opening of benzoxazine and maleimide structures, hydroxylation, sulfonation at cyclohexane and/or maleimide, and acetylation at free aniline moiety. The metabolic profile in terrestrial plants with soil application partially resembled those in rats, but differed as it mostly consisted of hydrolytic products, i.e. opening of the maleimide ring, which can be generated by aqueous hydrolysis at mild conditions, pH 5-9 (FAMIC 2019). As the hydrolysis could proceed in natural aquatic

environments, aquatic plants can be exposed not only to **1** but also to its hydrolysates, then the latter may accumulate, receive metabolic transformation and become major residues in aquatic plants. However, the fate of **1**-derived chemicals in aquatic plants is unknown.

In this study, we investigated the uptake followed by metabolism of **1** by a series of aquatic plants: two algae (*Pseudokirchneriella subcapitata* and *Synechococcus* sp.), duckweed (*Lemna* sp.) and water milfoil (*Myriophyllum elatinoides*), which were precisely selected with the aim of covering a wide variety of aquatic flora. The water milfoil was individually exposed to the test substance from shoot and roots to clarify shoot uptake *via* water medium and root uptake *via* sediments, respectively, using the sequestered chamber which have been developed previously (Ando et al. 2012, 2015).

MATERIALS AND METHODS

Chemicals

Two kinds of ^{14}C radiolabeled **1** were prepared in our laboratory as described previously (Shibata et al. 2011). The compound radiolabeled at two carbonyl carbons of the tetrahydrophthaloyl moiety, abbreviated as [THP- ^{14}C]**1**, had a specific radioactivity of 12.6 MBq/mg, and the another was uniformly radiolabeled at the phenyl ring, [PH- ^{14}C]**1**, 13.2 MBq/mg. Each ^{14}C compound was purified using reversed-phase HPL prior to use and the radiochemical purity exceeded 99.7%. Non-radiolabeled authentic standards of **1** and its degradates, *N*-[7-fluoro-3-oxo-4-(2-propynyl)-2*H*-1,4-benzoxazin-6-yl]-3,4,5,6-tetrahydrophthalamic acid (**2**), *N*-(2-propenyl)-4-[4-carboxy-3-fluoro-2-(2-carboxy-1-cyclohexene carbonylamino)-2-butenylidene]azetidione (**3**), 3,4,5,6-tetrahydrophthalic acid (**4**), 6-amino-7-fluoro-4-(2-propynyl)-2*H*-1,4-benzoxazin-3(4*H*)-one (**5**) and 1-hydroxy-1,2-cyclohexenedicarboxylic acid (**6**) were prepared in our laboratory (Shibata et al. 2011). Chemical structure and physicochemical parameters of each compound are shown in Table 1. The chemical purity of each standard was >90%. All the reagents and solvents applied in this experiment were in an analytical grade. The enzyme β -glucosidase (almond) was purchased from Wako Pure Chemical Industries, Ltd. All other chemicals were of a reagent grade and obtained from commercial suppliers.

Chromatography

A reversed-phase HPLC system to analyze the test substance and its degradates consisted of a Shimadzu LC module (LC-20A series) equipped with a SUMIPAX ODS A-212 column (5 μm , 6 mm i.d. \times 15 cm, Sumika Chemical Analysis Service, Ltd.). The following gradient system was employed at a flow rate of 1 mL/min; 0.1% formic acid (Solvent A) and acetonitrile (Solvent B): 0 min, %A/%B (v/v), 95/5; 40 min, 10/90. The typical retention times of **1** and other synthetic standards were 35.2 (**1**), 28.2 (**2**), 25.3(**3**), 20.8 (**4**), 26.3 (**5**) and 18.7 (**6**) min. The radioactivity in the column effluent was counted using a Flow Scintillation Analyzer Radiomatic 150TR (Perkin Elmer, Co.) radiodetector equipped with a 500 μL liquid cell using Ultima-Flo AP[®] (Perkin Elmer, Co.) as a liquid scintillator.

Radioanalysis

The water medium, sediment and plant extracts was determined by LSC with a Packard Model 2900TR spectrometer after mixing each aliquot with 10 mL of Perkin Elmer Emulsifier Scintillator Plus[®]. The post extracted bound residues of plant and sediment were combusted using a Perkin Elmer Model 307 sample oxidizer. The ¹⁴CO₂ produced by the procedure was trapped into 9 mL of Perkin Elmer Carb[®]-CO₂ absorber and mixed with 15 mL of Perkin Elmer Permafluor[®] scintillator. The radioactivity therein was quantified by LSC. The efficiency of combustion was determined to be greater than 92.7%.

Mass Spectroscopy

LC-ESI-HRMS or HRMS/MS analyses of the metabolites/degradates were conducted using a Q-Exactive Focus (Thermo Fisher Scientific Inc.) mass spectrometer equipped with the same HPLC instruments/radiodetector and HPLC gradient system described in the chromatography section. The analytical parameters at mass module controlled by the Xcalibur software (version 2.2) are shown below: sweep gas flow 10, source temp., 100°C, desolvation temp., 350°C, capillary voltage 3.5 kV, cone voltage 10-40 eV. MS/MS analysis was implemented with stepped collision energies at 10, 15 and 20 eV. The HPLC column eluent was diverted into 4:1 and introduced to the mass spectrometer and radiodetector, respectively.

Plant Materials and Maintenance

Two algae, *Pseudokirchneriella subcapitata* (strain No. NIES-35) and *Synechococcus* sp. (NIES-937), were provided from National Institute for Environmental Studies, Ibaraki, Japan. Duckweed (*Lemna* sp.) was obtained from a paddy field located at the Kasai experimental farm of Sumitomo Chemical Co., Ltd. Water milfoil (*M. elatinoides*) was purchased from Shimizu Laboratory Suppliers. Co. Ltd. Each alga was aseptically grown in a flask containing AAP water medium with continuous agitation on orbital shaker (at 100 rpm) placed in a climate chamber LH-220S (NK Systems Ltd.) at $20 \pm 1^\circ\text{C}$ under fluorescence light (8,000 lux, 16 h per day). The algae were periodically inoculated into fresh media to keep cells at their logarithmic growth phase. The cell density of each alga in the pre-culture was monitored by measuring optical density at 680 nm using a Shimadzu UV-2550 spectrometer in a quartz cuvette (1 cm path length), the absorbance which is known to correlate with algal cell density (Kasai et al. 1993). At least 10 days before the exposure experiments, *Lemna* sp. was pre-cultivated in an aquarium filled with AAP water, while *M. elatinoides* was grown in a chamber filled with AAP water with its root apex buried in the OECD synthetic bottom sediment, in the climate chamber with the same temperature and lighting condition to algae. The AAP water and OECD sediment were adjusted to pH 7.0 ± 0.5 and autoclaved at 1.5 kg cm^{-2} and 120°C for 20 min before use.

Plant Exposure

Prior to transfer of each plant to the exposure flask or beaker, 50 – 80 μL of acetonitrile solution dissolving ^{14}C -1 was added to the test vessel containing AAP water and thoroughly mixed to prepare the exposure concentration of 0.020 ppb (water exposure systems). The concentration was chosen taking into account PEC_{sw} (PEC at surface water) of the EU ponds, 0.009 to 0.045 ppb, estimated using FOCUS_{sw} program (step 3) (EFSA 2014). The value of the ponds was referred as representative habitat applicable to all test aquatic plants. To each 200-mL Erlenmeyer flask containing 120 mL of the AAP water dissolving ^{14}C compound, an aliquot of each alga cell suspension was transferred and adjusted to an approximate final optical density of 0.005 at 680 nm, c.a. 10^6 cells/mL (Kasai et al. 1993). *Lemna* sp. was immersed in 0.5% sodium hypochlorite

with sonication under reduced pressure for 1 min to sterilize microbes on plant surface, and thoroughly washed with autoclaved water. Healthy plants owing 3 to 5 fronds without any visible damage were collected and the total fresh weight of 0.33–0.35 g (approximately 10 specimens) was transferred to a 200-mL beaker containing 120 mL of the ^{14}C -applied AAP water. For *M. elatinooides*, two exposure types were applied, namely, water and sediment exposure systems using the sequestered vessel having shoot and root chambers developed previously. The shoot and root containers were filled with 120 mL of the AAP water and AAP-moistened OECD sediment (20 mL of the AAP medium and 35 g of the sediment), respectively, where either one of the containers received ^{14}C -1, i.e., water or sediment exposure. The test concentration for water exposure was 0.020 ppb. For sediment exposure, since PEC_{sed} (PEC at sediment) of the EU ponds ranged 0.019 to 0.166 ppb (μg per dry sediment), the concentration was conveniently set to 0.031 ppb (dry sediment basis), which is equivalent to 0.020 ppb on wet sediment basis, for simple comparison with the water exposure system. After *M. elatinooides* was sterilized in the same manner as *Lemna sp.*, a selected plant (shoot length, 15.5–17.3 cm; root length, 1.8–4.3 cm; root number, 4–8; fresh weight, 0.39–0.48 g) was transplanted to the chamber to initiate exposure. All the exposure vessels were capped with silicon plug or covered with a polyethylene wrap and incubated in the climate chamber under the same condition as pre-incubation, and were conducted in triplicate. As a control experiment, the AAP water and AAP-moistened OECD sediment without ^{14}C application were incubated under the same condition.

Analytical Procedures

Samples were sequentially analyzed at 6, 12, 24, 72, 120, 168, 240 and 336 h after the incubation. All the test systems were separated into plant, water and sediment to be analyzed individually. The suspension containing each alga was centrifuged at $3000 \times g$ for 15 min at room temperature followed by decantation to remove supernatant exposure water, and the remained algal pellet was washed using 10 mL of fresh water medium. The cell mixture was re-centrifuged in the same manner, supernatant was mixed with the exposure water and wet weight of the cell pellet was measured. *Lemna sp.* and *M. elatinooides* were collected by paper filtration. Plants were surface-washed using 20 mL

of fresh water medium and the rinsate was combined with the exposure water. After gently blotting adhered water using tissue paper, wet weight of *Lemna sp.* and *M. elatinoides* was measured. The length of *M. elatinoides* was measured and separated into shoot and root portions. Each plant and shoot/root portion incubated for 6–120 h was combusted to directly determine the radioactivity. For all the plants incubated for 168 h, extraction with 20 mL of acetonitrile/water (4/1, v/v) was conducted using a homogenizer AM-8 (Nissei Ltd.) at 10,000 rpm and 0°C for 10 min. The homogenate was vacuum filtered and the plant residue was further extracted once in the same manner. For the sediment exposure system adapted to *M. elatinoides*, the ¹⁴C-treated sediment in the root chamber was vacuum-filtered and separated into sediment and pore water fractions. The sediment fraction was washed once with 50 mL of fresh water medium and the filtrate was combined with the pore water. Then, the sediment was extracted with 30 mL of acetone by 10 min of mechanical shaking with a Taiyo SR-IIw reciprocator (Taiyo Chemical Industry Co., Ltd.). The residue after vacuum filtration was re-extracted in the same manner. Each aliquot of the water, pore water and extract fractions was analyzed with LSC and HPLC co-chromatography with authentic standards. The extracted bound residue of plant and sediment, and ¹⁴C-unexposed sediment were subjected to the combustion analysis.

Metabolite Characterization

As the surrogate sample to collect sufficient amounts of label-specific unknown metabolites detected in plants, approximately fifty water milfoils was exposed to either [THP-¹⁴C]**4** or [Phenyl-¹⁴C]**5** at 500 ppb in a beaker containing 1 L of the water medium. The radiolabeled **4** and **5** were prepared by hydrolyzing corresponding [¹⁴C]**1** in 0.1 M HCl at 80°C for 3 to 5 h followed by HPLC isolation (each radiochemical purity 100%). After 14 days of the exposure, plants were sampled, extracted and analyzed as described in the analytical section. The unknown metabolites were subjected to LC-MS analysis for structural characterization. In order to clarify sugar-conjugated metabolites, approximately 100,000 dpm of the extract was dried, re-dissolved in 1 mL of 10 mM sodium acetate buffer (pH 5.0) and 3 mg of β-glucosidase was added to the solution. The mixture was incubated in a BR-180LF BioShaker (TAITEC Co. Ltd., Japan) at 37°C

and 100 rpm. After 7 days, an aliquot of the reaction mixture was analyzed by HPLC. In addition, methyl derivatization was performed for the metabolites detected for [THP-¹⁴C]**4** application. The dried extract containing *ca.* 100,000 dpm was dissolved in 3 mL of methanol, then 500 μL of trimethylsilyldiazomethane (0.1% in *n*-hexane, Tokyo Chemical Industry Co., Ltd.) was added dropwise at room temperature and left-stand for 4 h for the derivatization.

RESULTS

Plant Growth and Test Validity

The fresh weight of each plant specimen exposed to [¹⁴C]**1** for 14 days was as follows: 0.23–0.29 g, 0.19–0.23 g, 0.47–0.53 g and 0.45–0.51 g for *P. subcapitata* and *Synechococcus* sp., *Lemna* sp. and *M. elatinoides*, respectively. No obvious visual damages were observed and the growth rates of each plant were similar to the corresponding control (without exposure), except for algae showed growth retardation as their wet weights after 14-days of the exposure ranged 17 to 42% of the control. To investigate ¹⁴C adhesion onto the test vessels, inner walls of all vessels were thoroughly washed using acetonitrile after removing the plant, water and sediment. The recovered ¹⁴C in each rinsate was below LOD (<30 dpm). For the sequestered exposure chamber applied for *M. elatinoides*, no radioactivity was detected from either side of the ¹⁴C-untreated chambers, indicated the ¹⁴C cross contamination between the shoot and root chambers did not occur.

¹⁴C Distribution in the Water Exposure Systems

The time course of the ¹⁴C distribution in the water exposure system with *M. elatinoides*, as representative, is depicted in Figure 1. A 98.8 to 99.7%AR was recovered from both [THP-¹⁴C] and [PH-¹⁴C] treated systems. The [¹⁴C]**1** applied to the water medium rapidly dissipated and the amount of **2** in the water reached the maximum 82.0%AR after 3 days. Along with the incubation period, continuous increase of **4** (45.2%AR) and **5** (27.5%AR) was observed after 14 days for [THP-¹⁴C] and [PH-¹⁴C] treated water, respectively. For both radiolabels, **3** was detected as a minor product not exceeding 1.0%AR. Other degradates were detected at the total maximum of 1.2 (day-

10) and 17.1%AR (day-14) for THP and PH labels, respectively, but none of each exceeded 5.0%AR as a single component. The radioactivity was gradually taken up from the water and accumulated by *M. elatinoides* up to 3.5–4.7%AR. Such time-dependent ^{14}C distribution was very similar for all the water exposure systems with other aquatic plants, as well as the control system without plant (results not shown). The ^{14}C product distribution in each water exposure system after 14 days is summarized in Table 2. The total ^{14}C recovery from test systems ranged 95.1–99.8%AR. Most of the radioactivity remained in each water medium ($\geq 91.6\%$ AR), while the residual amount of **1** therein was low as $\leq 3.2\%$ AR. In all systems, major products detected in the water were **2** (40.2–59.2%AR), **4** (45.2–54.2%AR, THP label), **5** (18.5–27.5%AR, PH label) and **3** as a minor component ($\leq 0.6\%$ AR, both labels). The other constituents in the water ranged 0.2–3.2 and 11.2–19.2%AR in total for THP and PH-labels, respectively, while each component was less than 2.0 and 4.3%AR, respectively. The ^{14}C -uptake behavior by each plant during exposure is shown in Figure 2. The ^{14}C -uptake was slightly faster or higher for PH label than THP label for all the species. The slope of each uptake curve gradually plateaued with the exposure period, in particular for THP label, approaching to the uptake steady-state. The %AR and ^{14}C -based concentration per plant wet weight (ppb) after 14 days were calculated to be: %AR (ppb), 2.0–3.0 (0.168–0.358), 2.1–4.0 (0.216–0.575), 1.9–3.5 (0.097–0.158) and 3.5–4.7 (0.187–0.221) for *P. subcapitata* and *Synechococcus* sp., *Lemna* sp. and *M. elatinoides*, respectively. For the radioactive constituents in plants, **1** was minor as $\leq 0.1\%$ AR for both radiolabels. The major ones for [THP- ^{14}C] treatment were **2** and **4** which amounted to 0.3–0.7 and 0.7–1.5%AR, respectively. The photo-unique degradate **3** was less than the LOD. As metabolites, **6** and its glucose conjugate, which were characterized by LC-MS analysis, were detected as maximum 0.3 and 0.6%AR, respectively. All the other ^{14}C components were less than 0.3%AR ($< 0.2\%$ AR as single constituent) and the plant bound residue was below 0.3%AR. In the PH label, **2** and **5** accounted to 0.3–0.9 and 0.5–0.7%AR, respectively, while **3** was not detected. Three conjugates of **5**, malonic acid (**5-MA**), lactic acid (**5-LA**) and acetyl conjugates (**5-Ac**), assigned by LC-MS, amounted to the maximum values of 0.3, 0.2 and 0.3%AR in water milfoil,

respectively, while the distribution of these metabolites was dependent on test plants. Other radioactive components ranged from 1.2 to 1.9%AR (<0.3%AR as a single constituent) and %AR in the bound residue was 0.4–0.7%AR.

¹⁴C Distribution in the Sediment Exposure Systems

Root uptake from the ¹⁴C-treated sediment was additionally investigated for *M. elatinooides* using the sequestered chamber. The time course ¹⁴C distribution in the test system is summarized in Table 3. The recovery of the radioactivity throughout the incubation ranged 96.6 – 99.6%AR. For both radiolabeled compounds, the radioactivity applied to the sediment container gradually distributed from the pore water to the sediment particles along with the incubation period. After 14 days, radioactivity at the sediment particles amounted to 41.3 and 61.4%AR for THP and PH labels, respectively. For THP label in the 14-day exposure, the amount of **1** in the pore water gradually decreased to 4.5%AR, while that in the sediment showed a maximum (20.1%AR) after 1 day and decreased thereafter to 3.4%AR. The hydrolysate **2** in the pore water rose up to 42.0%AR after 3 days followed by a decrease finally to 15.1%AR, while that in the sediments showed increase tendency (13.4–14.6%AR, after 7–14 days). A significant amount of **4** was detected in the pore water (max. 35.6%AR), but it was minor in the sediments (≤4.6%AR). The photoproduct **3** and other components were negligible as ≤0.4%AR. The sediment bound residue consistently increased and reached 19.7%AR. In the PH label system, distribution pattern of **1** and **2** between the pore water and sediment showed similar trend to the one observed for THP label system. Dissimilar to THP-specific **4**, **5** almost evenly distributed to the pore water and sediments resulted in 8.2 and 6.8%AR, respectively, at the end of exposure. Likewise, other minor ¹⁴C components (each ≤3.2%AR) at each fraction similarly distributed as 12.1 and 10.4%AR in the pore water and sediments after 14 days, respectively. **3** was transiently detected in the pore water (≤0.2%AR) at all sampling points. The radioactivity in the bound residue increased during the exposure and finally reached 24.2%AR. In respect of *M. elatinooides* for both radiolabels, extremely low radioactivity not exceeding 0.9%AR was accumulated by root uptake, and no detectable ¹⁴C was transported to the shoot portion.

Metabolite Characterization in Plants

To characterize ^{14}C metabolites detected in the aquatic plants of the water exposure systems, the additional surrogate *M. elatinoides* exposed to [THP- ^{14}C]4 and [PH- ^{14}C]5 was further analyzed. In brief, the surrogate plants did not receive any visible damages and accumulated 26.8 and 39.1%AR for radiolabeled 4 and 5, respectively. The HPLC analyses of these metabolites revealed that 4 and 5 were the most prominent radioactive component which accounted to 14.8 and 15.5%AR, respectively, while other major components generated were chromatographically identical to the metabolites originally detected in the corresponding [^{14}C]1 exposed plants, hence, the common metabolites in the surrogate extracts were further analyzed to obtain their structural information. By LC-MS analyses, mass spectra of single metabolite from [THP- ^{14}C]4 and four metabolites from [PH- ^{14}C]5 exposure were obtained successfully. To distinguish their mass spectra from the ones derived from massive plant matrices, the intrinsic radioisotopic pattern of each radiolabel was visually searched as targeted mass profile, since each pattern should be conserved for the corresponding metabolites, unless any ^{14}C elimination occurred. The pattern of each radiolabel was confirmed to be: [THP- ^{14}C]4, $^{14}\text{C}_2/^{14}\text{C}_1 = 100/10$ (% relative abundance); [PH- ^{14}C]5, $^{14}\text{C}_0/^{14}\text{C}_5/^{14}\text{C}_6 = 100/21/22$. For the THP-labeled metabolite eluted at 17.0 min by the formic acid HPLC system, amounted to 0.6%AR and 4.1%AR in the corresponding water milfoils exposed to [THP- ^{14}C]1 and [THP- ^{14}C]4, respectively, the mass spectrum was only able to be obtained after methyl derivatization combined with the modified HPLC eluent replacing formic acid to 10 mM ammonium acetate (identical gradient). The methyl derivative eluted at the retention time of 18.8 min by the modified eluent, and its molecular related ion of di- ^{14}C radioisotope was successfully obtained at m/z 386.1769 [$\text{M}+\text{NH}_4$] $^+$ ($^{14}\text{C}_2\text{C}_{13}\text{H}_{28}\text{NO}_{10}^-$: -0.742 ppm), which was accompanied by the mono-isotope at m/z 384.1739 [$\text{M}+\text{NH}_4$] $^+$ ($^{14}\text{C}\text{C}_{14}\text{H}_{28}\text{NO}_{10}^-$: -0.246 ppm). Successively, the following mass fragments were obtained by MS/MS analysis: radioisotopic fragments; m/z 207.0977 ($^{14}\text{C}_2\text{C}_7\text{H}_{15}\text{O}_4^+$: -0.164 ppm), 205.0945 ($^{14}\text{C}_1\text{C}_8\text{H}_{15}\text{O}_4^+$: -0.351 ppm), 189.0872 ($^{14}\text{C}_2\text{C}_7\text{H}_{13}\text{O}_4^+$: +0.312 ppm), 187.0838 ($^{14}\text{C}_1\text{C}_8\text{H}_{13}\text{O}_4^+$: -0.200 ppm), 161.0925 ($^{14}\text{C}_2\text{C}_6\text{H}_{13}\text{O}_3^+$: +0.839 ppm), 159.0891 ($^{14}\text{C}_1\text{C}_7\text{H}_{13}\text{O}_3^+$: -0.143 ppm), non-radioisotopic fragment; 180.0865 ($\text{C}_6\text{H}_{14}\text{O}_5\text{N}^+$: -0.106 ppm). From each candidate chemical formula, the metabolite was considered as the

mono-methylated glucose ester of **6** and the position of glucose esterification was tentatively proposed at the less sterically hindered carboxylic acid (Figure 3). Regarding the PH-radiolabeled metabolite detected at 21.8 min, the negative ion at m/z 305.0581 $[M-H]^-$ ($C_{14}H_{10}FN_2O_5^-$; +4.307 ppm) clustered by $^{14}C_5$ and $^{14}C_6$ isotopes at m/z 315.0745 $[M-H]^-$ ($^{14}C_5C_9H_{10}FN_2O_5^-$, +4.805 ppm) and 317.0776 $[M-H]^-$ ($^{14}C_6C_8H_{10}FN_2O_5^-$; +4.011 ppm), which amounted to 0.3%AR and 6.2%AR in *M. elatinoidea* for the $[PH-^{14}C]1$ and $[PH-^{14}C]5$ applications, respectively. Concurrently to the molecular related mass, ions at m/z 219.0570 ($C_{11}H_8FN_2O_2^-$; +2.592 ppm), 229.0734 ($^{14}C_5C_6H_8FN_2O_2^-$, +3.090 ppm) and 231.0767 ($^{14}C_6C_5H_8FN_2O_2^-$; +3.530 ppm) were detected as characteristic fragments, which corresponded to $[PH-^{14}C]5$ (Figure 4). From these information, the metabolite was assigned as *N*-malonic acid conjugate of **5** (**5-MA**, Figure 4). The metabolite accounted to 0.2%AR and 4.5%AR for $[PH-^{14}C]1$ and $[PH-^{14}C]5$ exposures, which eluted at 19.5min, showed m/z 307.0738 $[M-H]^-$ ($C_{14}H_{12}FN_2O_5^-$, +4.279 ppm), 317.0898 $[M-H]^-$ ($^{14}C_5C_9H_{12}FN_2O_5^-$, +3.765 ppm) and 319.0933 $[M-H]^-$ ($^{14}C_6C_8H_{12}FN_2O_5^-$, +4.519 ppm), and the corresponding fragments at m/z 263.0838 ($C_{13}H_{12}FN_2O_3^-$, +4.041 ppm), 273.1001 ($^{14}C_5C_8H_{12}FN_2O_3^-$, +4.515 ppm) and 275.1035 ($^{14}C_6C_7H_{12}FN_2O_3^-$, +4.802 ppm). The fragments indicated decarboxylation and the metabolite was characterized as *N*-lactic acid conjugate of **5** (**5-LA**), taking into account the proposed chemical formula (Figure 5). Additionally, in the positive ion mode, the metabolite detected at 19.9 min gave its molecular related cations at m/z 263.0824 $[M+H]^+$ ($C_{13}H_{12}FN_2O_3^+$, -1.205 ppm), 273.0985 $[M+H]^+$ ($^{14}C_5C_8H_{12}FN_2O_3^+$, -1.307 ppm), and 275.1018 $[M+H]^+$ ($^{14}C_6C_7H_{12}FN_2O_3^+$, -1.087 ppm), which amounted to 0.3%AR and 4.8%AR for $[PH-^{14}C]1$ and $[PH-^{14}C]5$ exposures, respectively. From the candidate chemical formula, the metabolite was proposed as *N*-acetyl **5** (**5-Ac**, Figure 6). Mass spectra of other minor metabolites were not able to be characterized due to their extremely low amounts with poor signal to noise ratios or low ionizabilities. As additional characterization, each surrogate extract was subjected to enzymatic hydrolysis using β -glucosidase to verify the presence of sugar-related conjugates. Several minor metabolites not exceeding 1.4%AR as a single component, which correspond to <0.1%AR metabolites in $[^{14}C]1$ extract, shifted to their aglycones on the HPLC chromatogram. The results indicated the presence of possible sugar

conjugates, but they did not match any of the reference standards. LC-MS analysis was attempted for the aglycones, but failed to obtain their spectroscopic information, except for **6**. The metabolic pathway of **1** in aquatic plants is proposed in Figure 7.

DISCUSSIONS

1 is susceptible to hydrolysis even under mild aqueous condition at pH 5–9 *via* opening of the maleimide ring followed by the amide bond cleavage, showing the degradation half-life shorter than 24 h (Katagi 2003; Kwon et al. 2004). Consistent to the previous results, **1** applied in our water or sediment systems showed rapid decomposition from at the beginning of each exposure to give **2**, **4** and **5** as main degradates. Under such circumstances, all the test plants gradually accumulated the radioactivity applied to either water-layer or bottom-sediment, but each accumulation was very limited as not exceeding 4.7 and 0.9%AR throughout the exposure. The results indicated low accumulation potentials of **1** and its major hydrolysates by aquatic plants under the exposure concentration of 0.020 ppb simulating the realistic aqueous environment. To estimate bioaccumulation potential, there is a general opinion that the lipophilicity of the target chemical is an effective indicator. For instance, Carvalho et al. (2007) showed a linear positive correlation between the bioaccumulation level by aquatic plants and K_{ow} values of the water-exposed chemicals. The log K_{ow} , or log D of **1** and the hydrolysates **2**, **3**, **4** and **5**, which may be useful as practical parameter for ionic compounds, were estimated to be 2.55, -1.75, -4.63, -3.15 and 1.19 (Table 1), respectively, indicating lower accumulation potentials of all degradates than the parent molecule. Based on the parameter, **5**, a PH label-specific compound, may have the highest accumulation potential among the hydrolysates since its lipophilicity is the highest. This is likely true since the accumulated ^{14}C by plant in each water exposure system was somewhat higher for PH label compared with THP label, supported by the evidence that relatively high amount of **5** and varieties of its conjugates were detected in plant extracts. On the other hand, **4**, having much lower lipophilicity that is unlikely to bioaccumulate, and its secondary metabolites were detected in plant extracts at certain ratios. This discrepancy can be explained by introducing the ion trap theory that can uniquely acts on weak acid compounds (Rendal et al. 2011). As their ionization can

preferably proceed in slightly alkaline inner plant (e.g., pH~7.8 at algal cytoplasm) (Kusel et al. 1990) than the outside aquatic phase, once they entered in plants, the acids can be trapped by accelerated ionization which physically hampers permeation through lipophilic biomembranes, and further be metabolized. Such scheme can be applied not only to **4**, which was successively metabolized to **6** and **6**-glucose conjugate at inner plant, but also to **2**. From these aspects, it was conceived that **2** and both **4** and **5** contributed to ^{14}C bioaccumulation by aquatic plants in water exposure systems, though their concentrations in plants were limited.

Unlike the water exposure, water milfoil showed equivalent levels of root uptake between THP and PH labels, suggested no preferential uptake could be expected for label-specific degradates. Dettenmaier et al. (2009) examined TSCF, which reflect root uptake ability, of water soluble chemicals. They found the reverse sigmoid relationship between TSCF and K_{ow} to propose that polar, highly water soluble compounds with lower $\log K_{ow}$ possess high potentials to be taken up by root, which become the maximum plateau at $\log K_{ow}$ below approximately 2. The degradates **4** and **5** likely ranged within such polar chemicals having high potentials, and combined with each production ratio and distribution between the pore water and sediment particles, it is considered that they overall came out to reveal small difference in the amount taken up by water milfoil.

In the test plants, since the un-changed **1** was hardly detected, it is likely that the compound could not compete with rapid hydrolysis before taken up by plants under the test conditions or it received immediate metabolism in plants. The ^{14}C components mainly consisted of the hydrolysates **4** and **5**, but also included multiple components, some of which were characterized by LC-MS analysis, and this indicates the ability of the aquatic plants to metabolize herbicide-derived molecules or even **1**. The key enzymes playing important role in herbicide detoxification known at gene levels for terrestrial plants are: CYP, GSH S-transferase, glucosyltransferase, ABC/drug transporter, and etc. (Xu et al. 2015; Duhoux et al. 2015). In the detoxification of organic compounds in algae and macrophytes, phase I metabolic reactions by CYP or its isozymes such as EROD and ECOD have been reported (Torres et al. 2008; Thies et al. 1996; Pflugmacher and Steinberg 1997). Similarly, phase II reactions against xenobiotics to generate glucose and GSH conjugates are known in aquatic plants (Pflugmacher and Steinberg 1997; Pflugmacher et al. 1999, 2000; Pflugmacher and Sandermann 1998a).

Thus, it is likely that aquatic plants have similar detoxification capacity to terrestrial plants. In our study, phase I hydroxylation to produce **6** and phase II glucose and *N*-malonic acid, -lactic acid and -acetyl conjugations were characterized. In addition to glucose and GSH conjugations, direct *N*-conjugations with organic acids are well known in terrestrial plants such as; *O*- and *N*-malonyl conjugations are catalyzed by malonyltransferases in selective manners which are specific on substrates or dependent on plant species (Winkler and Sandermann 1989; Lao et al. 2003; Sandermann et al. 1991); *N*-acetylation can be occurred on, e.g., several neonicotinoids in spinach seedlings (Ford and Casida 2008), while such reactions are likely assisted by the function of symbiotic microbes (Rodrigues et al. 2006); conjugations with lactic acid, alanine and acetic acid are known as detoxification processes for a variety of triazole derivatives, which is one of the most prominent groups known for such conjugation reactions in pesticide metabolism (FAO 2019).³⁴ Likewise to terrestrial plants, similar conjugation reactions by aquatic plants have been reported. For example, duckweed can metabolize benzoic acid derivative by direct malonyl conjugation at the carboxyl group, though the reaction product was *O*-malonyl ester (Fujisawa et al. 2006). In the metabolism of propanil by *Lemna minor*, after the amide bond cleavage, *N*-acetylation proceeds at the aniline moiety with the contribution of acetyl-CoA (Mitsou et al. 2006). Thus, *N*-malonylation and acetylation found in our study are considered plausible. For *N*-lactic acid conjugation, as well as *N*-alanine and -acetic acid conjugations, has not been reported for aquatic plants as far as we know. Further studies are necessary to conclude if aquatic plants hold the same mechanism as terrestrial plants.

CONCLUSION

In conclusion, it is expected that **1** contaminated into the natural environment at the realistic concentration 0.020 ppb could immediately be hydrolyzed before reaching aquatic plants and become less bioavailable, unless it is directly and continuously flowed into their habitats. The degradates, which can be the alternative toxicants, will not intensively be taken up and accumulated by those species under such condition. Furthermore, if the herbicide and its hydrolysates are to be incorporated into aquatic plants, these chemicals will likely be metabolized to multiple minor products by inherent phase I and II detoxification mechanisms which were characterized as general reactions

known in terrestrial plants. Regarding the metabolic comparison between tested aquatic plants, reactions in the tested aquatic plants were considered similar, however, phase II conjugation patterns were different where macrophytes (water milfoil and duckweed) showed various conjugation manners.

Tables:

Table 1: Test chemicals and physicochemical parameters.

Designation	Structure	pKa ¹⁾	log <i>K_{ow}</i> or log <i>D</i> at pH 7 ¹⁾
1		-0.01	log <i>K_{ow}</i> = 2.55 ²⁾
2		0.63, 4.67	log <i>D</i> = -1.75
3		-2.14, 3.06	log <i>D</i> = -4.63
4		3.94	log <i>D</i> = -3.15
5		3.12	log <i>K_{ow}</i> = 1.19
6		-	-

▲: ¹⁴C-labeled position of [PH-¹⁴C]. *: ¹⁴C-labeled position of [THP-¹⁴C].

-: Not determined.

1): Estimated values using Advanced Chemistry Development (ACD/Labs) Software V11.02 (Advanced Chemistry Development, Inc.).

2): Experimental value from reference (EFSA 2014).

Table 2: ^{14}C distribution in the water exposure system after 14 days.

[THP- ^{14}C]	%AR ^a			
	<i>P. subcapitata</i>	<i>Synenocossus</i>	<i>Lemna sp.</i>	<i>M. elatinoides</i>
Water layer	97.1 (1.9)	97.7 (1.8)	97.3 (0.6)	95.3 (0.7)
1	0.1 (<0.1)	0.1 (<0.1)	3.2 (1.9)	1.0 (0.3)
2	44.5 (3.2)	43.2 (4.1)	40.2 (3.6)	48.2 (3.6)
3	0.2 (0.1)	ND	0.4 (0.2)	0.6 (0.3)
4	50.2 (3.5)	54.2 (4.8)	50.3 (3.5)	45.2 (4.2)
others*	2.1 (0.8)	0.2 (0.1)	3.2 (1.1)	0.3 (0.1)
Plant	2.0 (0.6)	2.1 (1.1)	1.9 (0.5)	3.5 (0.3)
1 ^b	0.1	ND	0.1	0.1
2 ^b	0.4	0.3	0.5	0.7
3 ^b	ND	ND	ND	ND
4 ^b	1.0	0.9	0.7	1.5
6 ^b	<0.1	0.2	0.1	0.3
6-Glc ^b	0.2	0.3	0.3	0.6
others**b	0.3	0.3	0.1	0.1
bound ^b	<0.1	0.1	0.1	0.2
Total	99.1 (1.7)	99.8 (1.9)	99.2 (0.6)	98.8 (0.9)

a: Average values ($n = 3$). Standard deviations are given in parentheses.

b: Triplicates samples were mixed before HPLC analysis. ND: Not detected

*: Multiple components (<2.0%AR, each) **: Multiple components (<0.2%AR, each)

[PH- ^{14}C]	%AR ^a			
	<i>P. subcapitata</i>	<i>Synenocossus</i>	<i>Lemna sp.</i>	<i>M. elatinoides</i>
Water layer	95.0 (1.9)	95.5 (2.6)	91.6 (0.8)	95.0 (1.0)
1	ND	ND	0.1 (<0.1)	0.1 (<0.1)
2	51.9 (3.4)	58.3 (4.0)	59.2 (3.6)	52.7 (3.6)
3	ND	ND	0.3 (0.2)	0.3 (0.2)
5	23.9 (4.1)	18.5 (3.3)	20.8 (3.7)	27.5 (3.5)
others*	19.2 (4.7)	18.7 (4.9)	11.2 (4.0)	14.5 (4.3)
Plant	3.0 (1.5)	4.0 (1.9)	3.5 (0.4)	4.7 (0.4)
1 ^b	ND	0.1	0.1	ND
2 ^b	0.3	0.7	0.9	0.9
3 ^b	ND	ND	ND	ND
5 ^b	0.6	0.7	0.5	0.7
5-MA ^b	0.1	ND	0.2	0.3
5-LA ^b	ND	ND	<0.1	0.2
5-Ac ^b	0.1	0.1	0.2	0.3
others**b	1.4	1.9	1.2	1.6
bound ^b	0.5	0.5	0.4	0.7
Total	98.0 (2.0)	99.5 (2.7)	95.1 (0.6)	99.7 (1.2)

a: Average values ($n = 3$). Standard deviations are given in parentheses.

b: Triplicates samples were mixed before HPLC analysis. ND: Not detected.

*: Multiple components (<4.3%AR, each). **: Multiple components (<0.3%AR, each).

Table 3: ¹⁴C distribution in the sediment exposure system during 14 days.

	[THP- ¹⁴ C]		%AR ^a					
	days after exposure							
	0	1	3	5	7	10	14	
Pore water	100.2 (0.3)	71.5 (1.1)	62.8 (2.2)	58.1 (2.7)	55.8 (3.5)	56.8 (3.2)	55.4 (3.7)	
1	100.2 (0.3)	29.2 (3.6)	10.3 (2.4)	8.7 (2.5)	7.5 (2.4)	6.3 (2.1)	4.5 (2.5)	
2	ND	39.0 (2.1)	42.0 (2.7)	30.3 (2.5)	25.4 (2.7)	20.1 (3.1)	15.1 (2.4)	
3	ND	0.1(<0.1)	0.3 (0.2)	0.4 (0.2)	0.1 (0.1)	ND	ND	
4	ND	3.2 (0.6)	10.2 (1.3)	18.5 (3.2)	22.3 (3.6)	30.1 (3.3)	35.6 (3.5)	
others*	ND	ND	ND	0.2 (0.1)	0.5 (0.2)	0.3 (0.1)	0.2 (0.1)	
Sediment	ND	25.8 (2.3)	34.8 (2.5)	38.9 (3.6)	41.3 (2.4)	39.6 (3.1)	41.3 (3.3)	
1	ND	20.1 (2.1)	19.3 (3.4)	11.0 (2.2)	8.0 (2.1)	4.3 (1.9)	3.4 (1.8)	
2	ND	1.4 (0.2)	6.3 (1.3)	8.4 (1.0)	14.1 (2.1)	14.6 (2.9)	13.4 (2.2)	
3	ND	ND	ND	ND	ND	ND	ND	
4	ND	ND	0.3 (0.2)	1.0 (0.3)	1.4 (0.4)	2.2 (0.4)	4.6 (0.7)	
others*	ND	ND	ND	0.2 (0.1)	0.1 (0.1)	0.3 (0.1)	0.2 (0.1)	
bound	ND	4.3 (0.3)	8.9 (1.4)	18.3 (3.3)	17.7 (4.1)	18.2 (4.2)	19.7 (3.9)	
<i>M. elatinoides</i>	ND	<0.1	0.2 (<0.1)	0.4 (0.1)	0.6 (0.2)	0.7 (0.2)	0.8 (0.3)	
Total	100.3 (0.23)	97.4 (0.5)	97.8 (1.3)	97.4 (1.6)	97.7 (1.2)	97.1 (1.4)	97.5 (2.7)	

a: Average values ($n = 3$). Standard deviations are given in parentheses.

ND: Not detected * : Multiple components (<0.3%AR, each)

	[PH- ¹⁴ C]		%AR ^a					
	Days after exposure							
	0	1	3	5	7	10	14	
Pore water	100.1 (0.3)	67.9 (1.8)	60.1 (3.3)	50.4 (2.6)	47.5 (4.1)	40.0 (2.9)	36.4 (3.5)	
1	100.1 (0.3)	31.6 (1.3)	11.3 (1.4)	8.3 (1.1)	7.6 (2.3)	3.2 (1.8)	2.1 (0.8)	
2	ND	34.6 (2.4)	42.4 (1.6)	31.2 (3.2)	26.6 (3.3)	19.9 (3.4)	14.0 (3.6)	
3	ND	ND	0.1 (0.1)	ND	0.1 (<0.1)	0.2 (0.1)	ND	
5	ND	0.2 (0.1)	2.1 (1.1)	5.5 (1.7)	6.5 (2.2)	7.4 (1.9)	8.2 (2.0)	
others*	ND	1.5 (0.8)	4.2 (1.2)	5.4 (1.3)	6.7 (1.6)	9.3 (2.1)	12.1 (3.4)	
Sediment	ND	30.7 (2.0)	37.7 (2.4)	46.3 (2.3)	51.7 (3.3)	55.3 (3.6)	61.4 (3.1)	
1	ND	16.6 (1.5)	13.3 (1.7)	9.7 (1.4)	7.9 (2.2)	5.7 (1.3)	6.6 (2.3)	
2	ND	2.3 (0.3)	7.8 (0.5)	12.1 (1.3)	13.7 (1.6)	15.7 (2.4)	11.3 (2.9)	
3	ND	ND	ND	ND	ND	ND	ND	
5	ND	2.3 (0.2)	3.1 (0.2)	3.8 (0.9)	5.9 (1.1)	6.0 (1.6)	6.8 (2.2)	
others*	ND	2.1 (0.9)	4.8 (1.5)	7.6 (2.4)	8.8 (3.1)	7.7 (3.8)	10.4 (2.1)	
bound	ND	8.3 (0.5)	10.2 (0.7)	14.8 (1.9)	15.0 (3.4)	21.3 (4.1)	24.2 (3.3)	
<i>M. elatinoides</i>	ND	0.1 (<0.1)	0.3 (0.1)	0.5 (0.2)	0.7 (0.2)	0.9 (0.3)	0.9 (0.2)	
Total	100.1 (0.3)	99.6 (0.8)	99.6 (1.1)	98.9 (2.5)	99.5 (1.4)	97.3 (1.8)	96.6 (2.6)	

a: Average values ($n = 3$). Standard deviations are given in parentheses.

ND: Not detected * : Multiple components (<3.2%AR, each)

Figures:

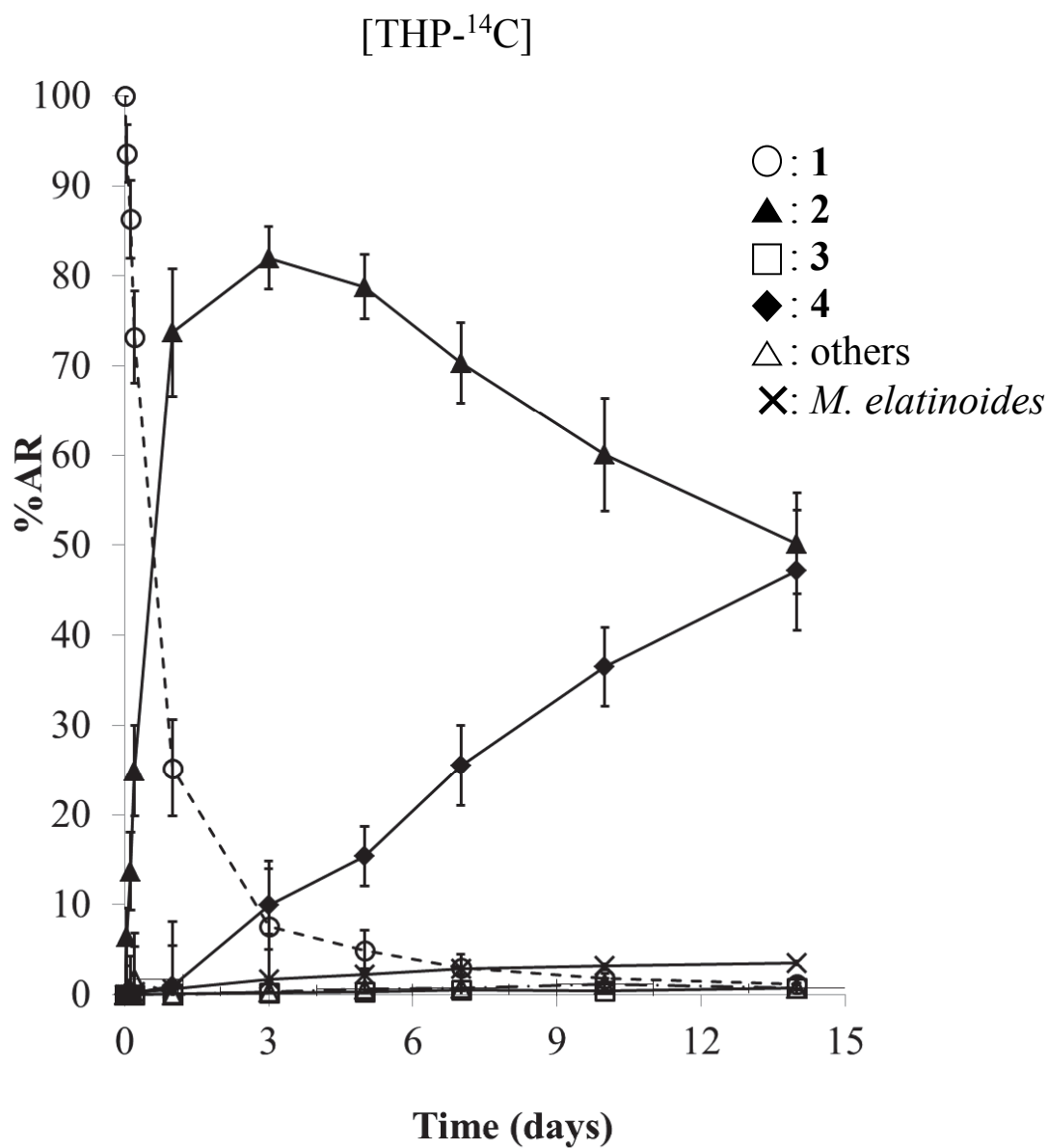


Figure 1: ¹⁴C distribution in the water exposure system with *M. elatinoides* (THP-label). The error bars represent standard deviation of triplicate samples ($n = 3$).

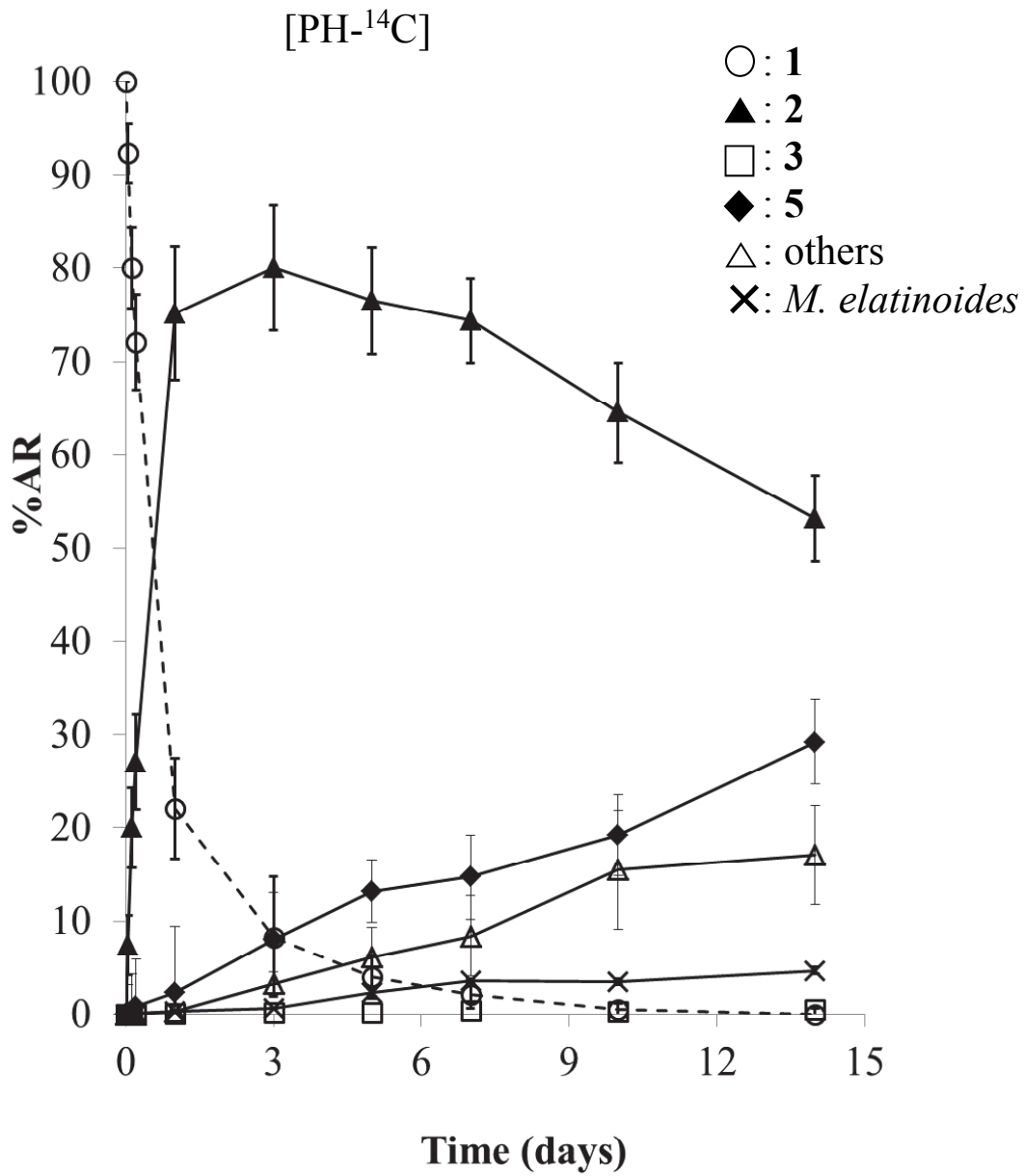


Figure 1 (continue): ¹⁴C distribution in the water exposure system *M. elatinoides* (PH-label). The error bars represent standard deviation of triplicate samples ($n = 3$).

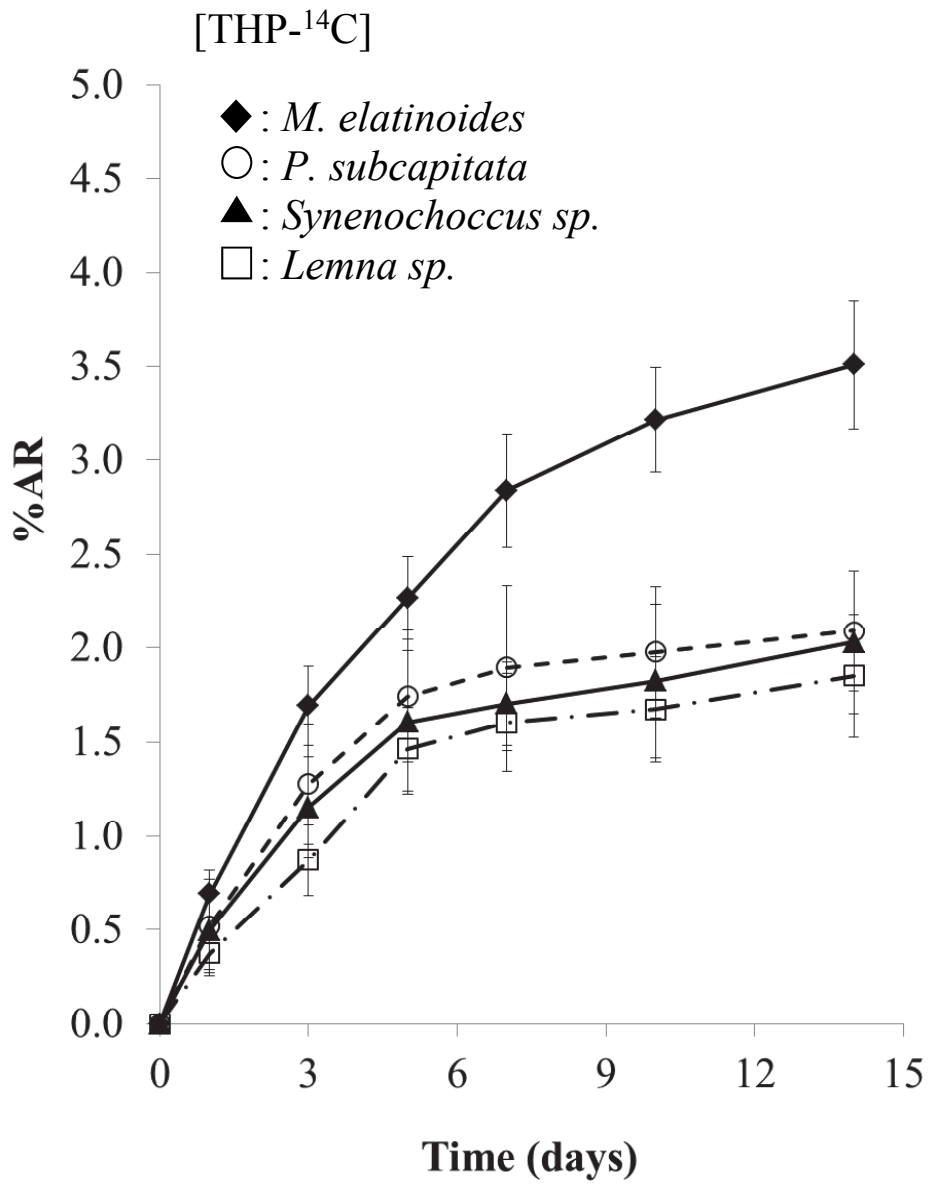


Figure 2: ¹⁴C accumulation by plants in the water exposure system (THP-label). The error bars represent standard deviation of triplicate samples ($n = 3$).

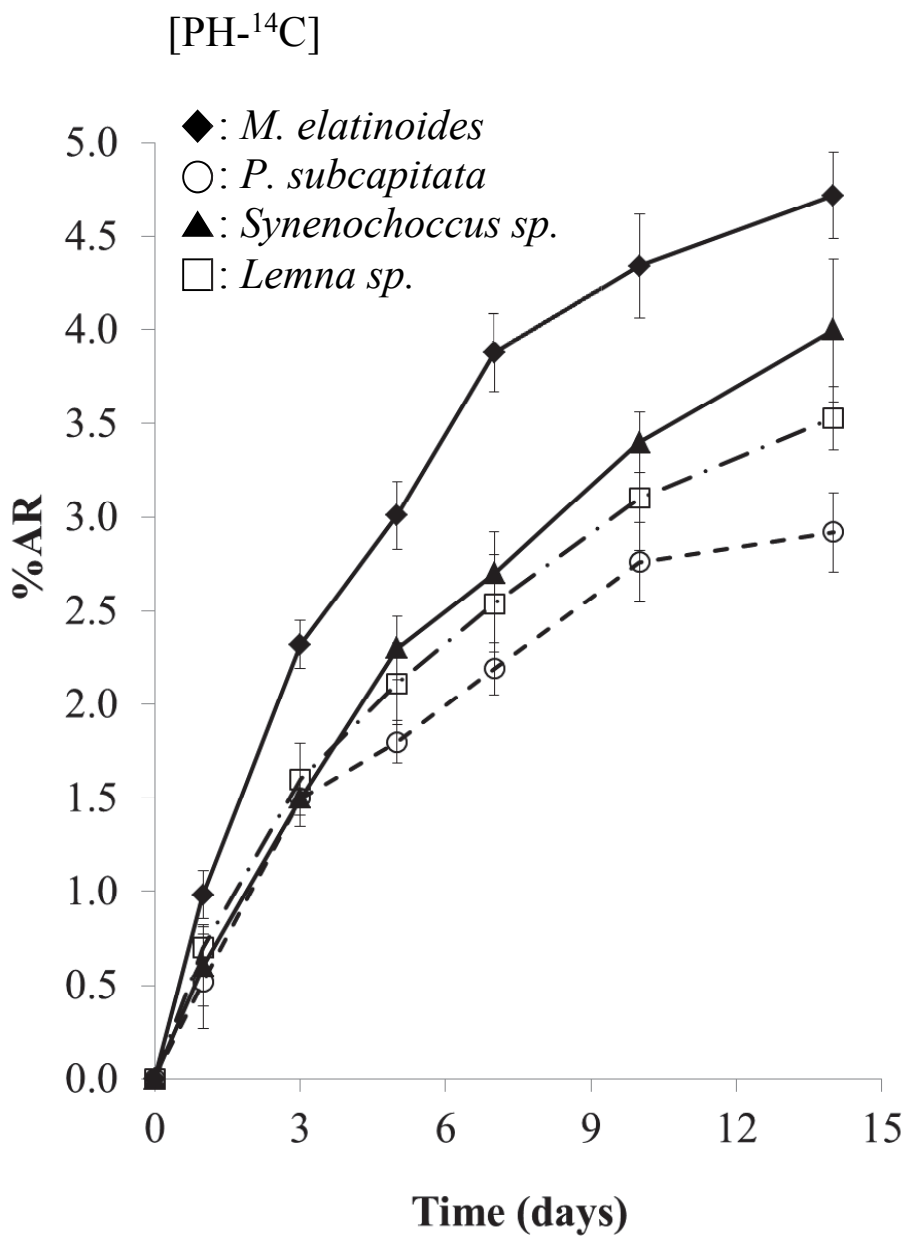


Figure 2 (continue): ¹⁴C accumulation by plants in the water exposure system (PH-label). The error bars represent standard deviation of triplicate samples ($n = 3$).

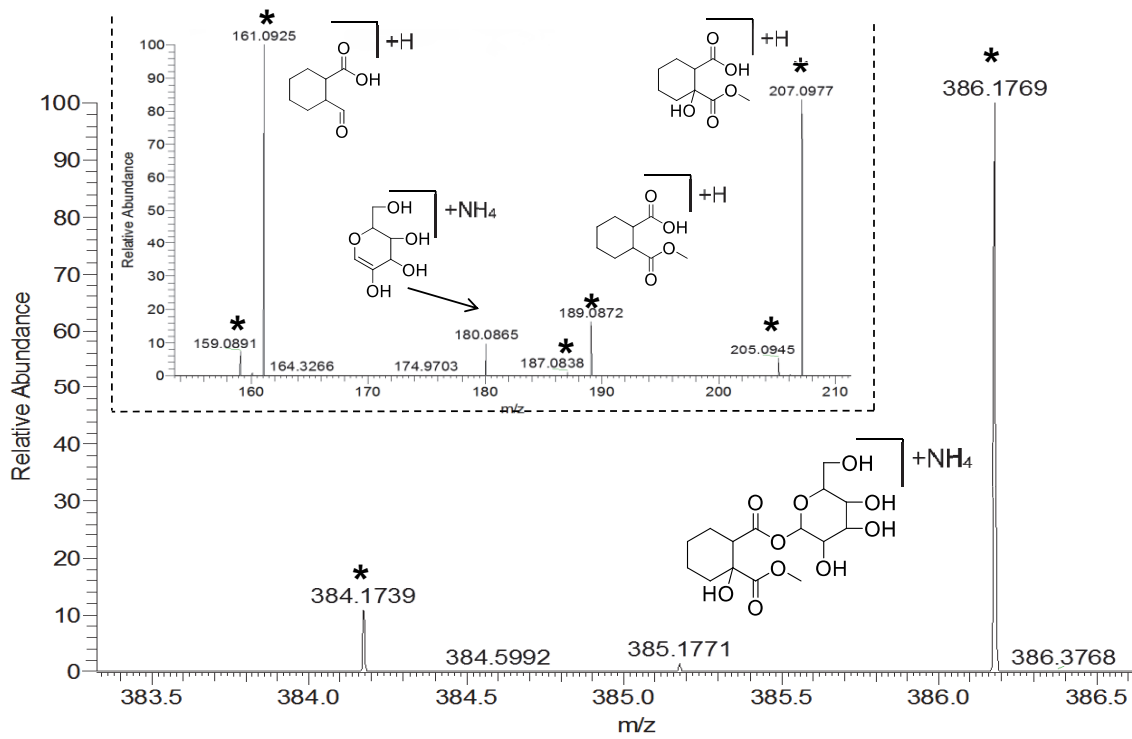


Figure 3: Mass spectrum of methylated 6-glucose. Asterisks show radioisotopic ions.

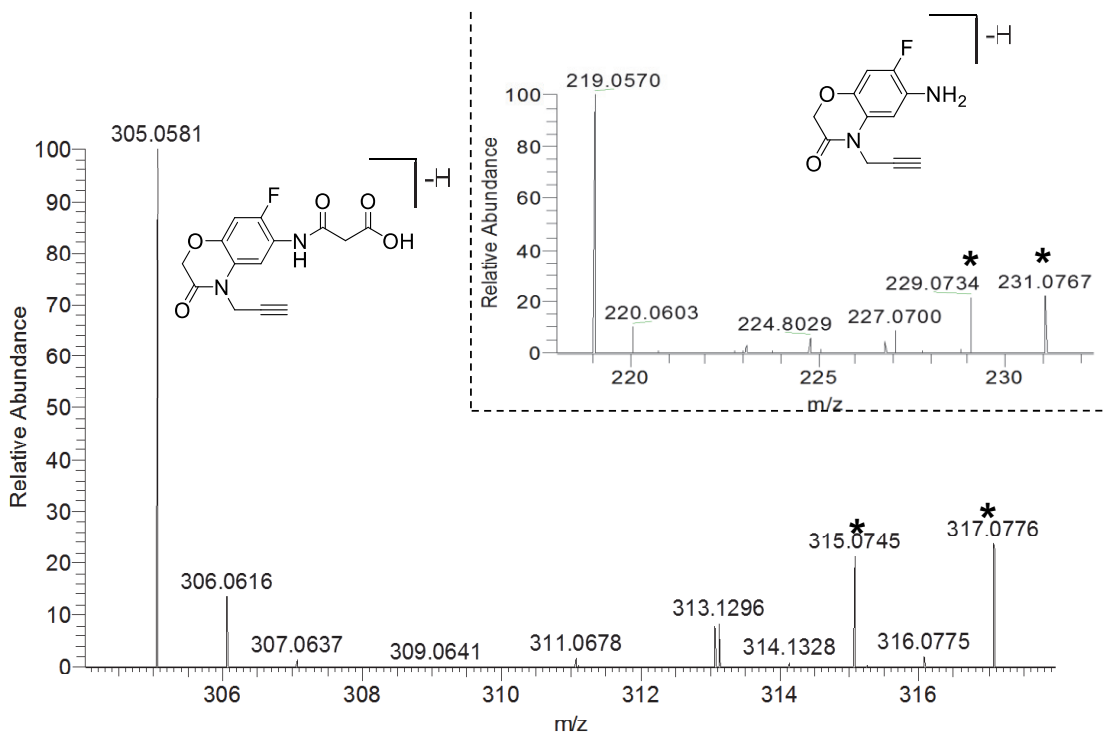


Figure 4: Mass spectrum of 5-malonic acid. Asterisks show radioisotopic ions.

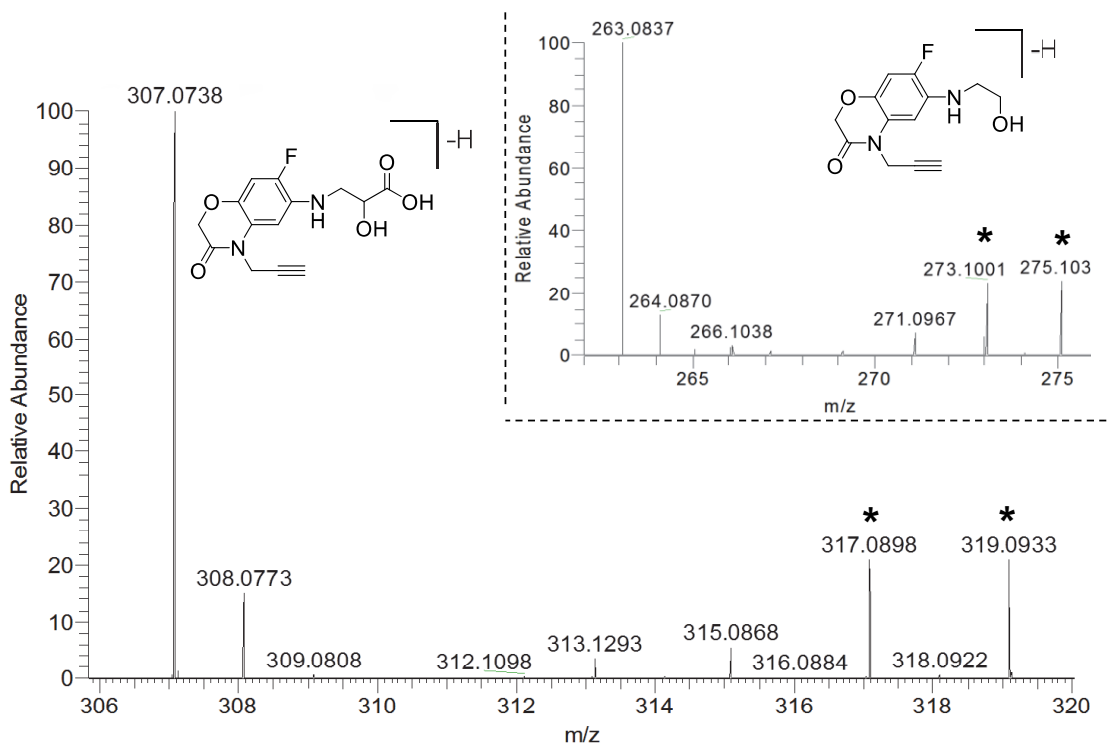


Figure 5: Mass spectrum of 5-lactic acid. Asterisks show radioisotopic ions.

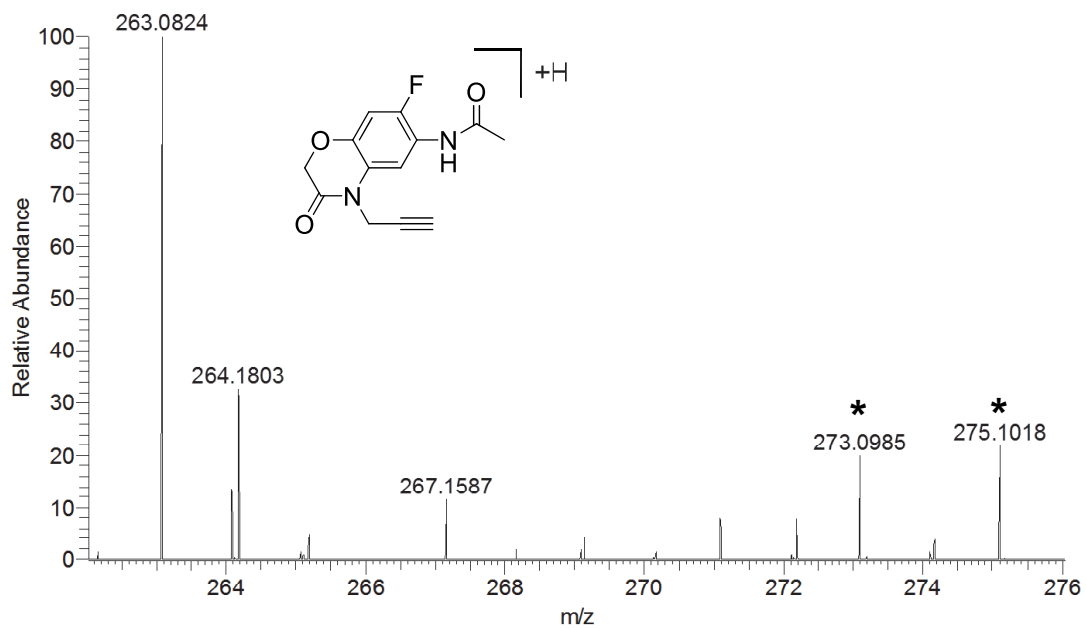


Figure 6: Mass spectrum of 5-acetylate. Asterisks show radioisotopic ions.

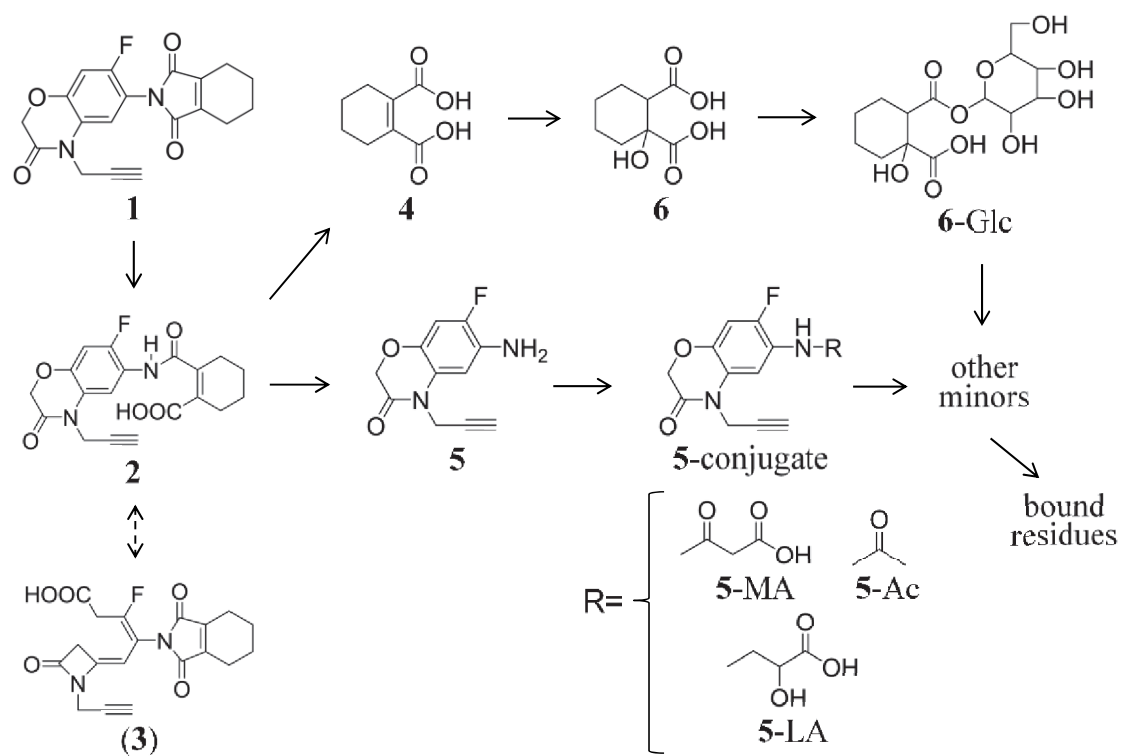


Figure 7: Proposed metabolic pathway of flumioxazin in aquatic plants.

6. Overall Summary, Discussion and Conclusion

Summary

In this thesis, we set the object to water milfoil which is one of the essential aquatic plant species as primary producer in the aquatic ecosystem that must be protected from potential adverse effects caused by pesticides. For robust hazard characterization, we examined to clarify the detailed behaviors of chemicals in water milfoil with the special focus on understanding the individual uptake, translocation and metabolism after selective shoot exposure *via* water medium and root exposure *via* sediment, respectively.

In chapter 1, the importance of pesticide risk assessments on water milfoil was described. Unlike suspending and floating aquatic plants, submerged, sediment-rooted macrophytes, water milfoil as representative, may be exposed to the pesticide not only *via* water column, but *via* sediment as an additional route. Hence, risk assessment on water milfoil is necessary to cover wider range of aquatic flora.

As fundamental knowledge, behaviors of chemicals in uptake followed by translocation and metabolism were briefly summarized for terrestrial and aquatic plants. From the literature review, it was considered that biotic and abiotic reactions at outer plant could largely affects the fate of pesticides prior to be taken up by plants, depending on the chemical structure of the pesticide. The uptake and translocation are likely the processes highly dominated, but not totally, by the physicochemical parameters such as hydrophobicity, water solubility and acidity, which may be applicable for water milfoil. However, due to the morphological difference and limited transpiration stream under submergence, a definitive conclusion of the relationship between physicochemical properties and uptake/translocation by water milfoil requires further studies. With respect of the metabolic reactions, aquatic plants likely possess phase I, II (and III) mechanisms which can widely be seen for terrestrial plants and considered mostly similar, however, since only a limited information is available for water milfoil, this is not conclusive.

In chapter 2, the behaviors of the insecticide metofluthrin, a synthetic pyrethroid for hygiene usages, and the fungicide mandestrobin, a strobilurin to control wide range of crop diseases, in cabbage/wheat and water milfoil were examined as model case comparison. Metofluthrin is known as photo-labile and hydrolytically unstable, and mandestrobin is resistant to aqueous hydrolysis, respectively. As results, metofluthrin received ozone oxidation on cabbage surface, while it underwent immediate hydrolysis in water medium, which gave large difference in the distribution of chemical species that exposed to each plant, and eventually, plants exhibited dissimilar metofluthrin-derived residues. Mandestrobin was relatively stable against hydrolysis but partially underwent photo-rearrangement in aqueous medium, and the product was successively accumulated by water milfoil as unique chemical species that was not observed in wheat. With respect of metabolism, reactions observed for both plants were typical, namely, phase I, II (and III) mechanisms, and considered mostly similar between the plants. However, for mandestrobin, wheat produced the additional hydroxylated metabolite which was not detected in water milfoil, and this indicated that the metabolic reactions on xenobiotics in terrestrial plants are somewhat more diverse than in water milfoil.

In chapter 3, the new exposure system which enables to selectively expose shoot and root was designed and validated using 3-phenoxybenzoic acid (**I**) as the model test compound. The occurrence of immediate shoot uptake of **I** from the water medium was confirmed, while basipetal translocation from shoot to root was an unlikely event. On the other hand, smaller and slower uptake was observed for root exposure than shoot exposure, however, acropetal translocation from root to shoot took place at certain level as 1/4 of the radioactivity taken up by root was translocated to shoot. The metabolites of **I** found in the shoot was mainly the glucose conjugate and the reduction product at the carboxylic acid functional group, while hydroxylation at the phenoxy moiety was observed as root-specific metabolite. The results clearly demonstrated the effectiveness of the developed exposure system for our objects, *viz*, to clarify each uptake, translocation, metabolism behavior after shoot and root exposure *via* water medium and *via* sediment, respectively.

In chapter 4, to understand basic relations, kinetics approach was implemented to

compare physicochemical parameters of the test compounds with the uptake and metabolism by water milfoil. Using the newly developed exposure system, the shoot or root of water milfoil was selectively exposed to five simple phenols, and clarified each uptake *via* shoot and root followed by translocation and metabolism. The shoot uptake occurred at certain level, whereas, only limited root uptake was confirmed, suggested insignificance of the latter path for simple phenols. The kinetics on uptake and glucose conjugation, the major metabolic reaction observed, were estimated and compared with various physicochemical properties of the phenols by regression analysis. A good correlation with the kinetics of shoot uptake was observed for $\log K_{ow}$, while $\log D$ and other indexes showed poor relations. A poor correlation for $\log D$ was mainly due to *p*-hydroxybenzoic acid, which showed the highest uptake contrary to its complete ionization and lowest hydrophobicity, indicated some particular mechanisms such as ‘ion-trap effect’ for the dissociated weak acids or ions. For the kinetics of glucose conjugation, electronic distribution at the phenoxy group (or as a whole structure), expressed by Hammett constant and HOMO, showed the highest relationship.

In chapter 5, the fate of the widely used herbicide flumioxazin in water milfoil was investigated exposed at the predicted environmental concentration in EU ponds. For comparison, two algae (*Pseudokirchneriella subcapitata* and *Synechococcus* sp.) and one floating macrophyte (*Lemna* sp.) were also exposed to the herbicide. Flumioxazin underwent immediate/intensive hydrolysis in both the water medium and sediment systems, and all aquatic plants likely accumulated the hydrolysates of the parent herbicide. Though water milfoil showed slightly higher accumulation among the plants, there were no significant quantitative difference on the uptake level. With respect to the metabolic reactions in plants, in addition to hydroxylation as typical phase I detoxification, various phase II conjugations were observed, *i.e.*, glucosidation, acetylation, lactic acid and malonic acid conjugations. All these conjugation patterns are known in terrestrial plants, thus, it was considered that aquatic plants possess similar phase II mechanisms to terrestrial plants. Among the test plants, the macrophytes (duckweed and water milfoil) produced all the mentioned conjugates, while algae did not show lactic acid or malonic acid conjugates, suggesting that there are some differences in phase II reactions among aquatic plants.

From the findings, we conclude the behaviors of pesticides as follows:

1. The biotic/abiotic reactions in the water column largely affect the fate of pesticides prior to be taken up by water milfoil.
2. Both shoot and root uptakes contribute to the accumulation of chemicals, while each degree differs. Although further systematic investigations are necessary, it is likely that hydrophobicity expressed by $\log K_{ow}$ is not a complete parameter to determine the uptake level of the substances, and especially, weak acids prone to show high potential for both shoot and root uptakes followed by translocations.
3. The basic metabolic/detoxification phase I reactions in water milfoil and other aquatic plants is mostly similar to the ones in terrestrial plants, while in some cases, terrestrial plants likely produce wider array of metabolites. Phase II reactions (and phase III) are considered identical, however, involving types could be different across the aquatic plants. In addition, in shoot and root of water milfoil, site-specific metabolite(s) can be generated.

Further studies using chemicals with wider pesticide classes and range of physicochemical properties would give us more systematic view for understanding each behavior.

Discussion

Understanding the distribution/quantity of pesticide and the metabolites (and degradates) in water milfoil is the first step for in-depth risk assessments on the species. Since the contribution of shoot and root uptakes of pesticides followed by metabolite generation to the overall accumulation can be clarified by the water milfoil study, further research focusing on the events at each exposure can be proceeded. For example, if the root uptake was extensive and specific metabolite(s) was detected in the plant, one can examine: the relation of root uptake degree of the pesticide and character of sediment, e.g., textures (clay/silt/sand or mud/gravel), organic matter content, pH, water content and etc.; the origin of the metabolite, e.g., whether it is generated in the sediment, rhizosphere,

or in roots (or in shoot following acropetal translocation). The extended studies help us to understand in which scenario the pesticide or degradates in the sediment would maximally be taken up, or the metabolite be generated in water milfoil, and which experimentally quantitated values should be applied in the “worst-case” risk assessments. With respect of the risk assessments of other aquatic plants in fresh water ecosystem, since water milfoil alone does not reflect all the plants, the species difference in sensitivity as well as metabolic difference should be taken into account, as indicated by the flumioxazin study (chapter 5) demonstrated the different metabolite distribution/species among water milfoil, duckweed and algae. Hence, it is better to clarify the metabolic fate of pesticides in various aquatic plants for detailed risk evaluation to adequately cover wider aquatic vegetation. The similar point of view can further be extended to edible aquatic plants for human such as lotus root (*Renkon*), *Sagittaria trifolia* (*Kuwai*) and so on, and this is especially important to discuss the possibility of any specific, toxic, metabolite generation in the plants to cause adverse effect for human after ingestion. Incidentally, it is important to select realistic residue/accumulation levels of the pesticide/metabolites in water milfoil, otherwise the magnification could be over or underestimated. In the water milfoil study (and for other aquatic plants), thus, reasonable exposure concentration in aquatic environment such as PEC_{sw} and PEC_{sed} introduced in chapter 5, should be applied to mimic realistic aquatic environment as much as possible.

When toxic potential was considered, researchers can compare and relate the obtained each distribution/quantity of the pesticide and metabolites to the toxicity and specify implicating bioactive species. If the toxicity of the concerning metabolites are unknown, (quantitative) structure-activity relationship ([Q]SAR) based *in silico* hazard characterization can be done as preliminary approach, which has been greatly improving the accuracy in recent years and gaining much recognition as one of the important measures for decision making in conducting further toxicological examinations, especially in the mammalian risk assessments where excess vertebrate testing is prohibited from the aspect of animal welfare. In the ecotoxicological hazard prediction, likewise, there are active researches providing excellent models for aquatic plants, planktons, fish and etc., that can be adopted (Sanderson and Thomsen 2009; Cassani et al. 2013; Gramatica et al. 2014; Sangion and Gramatica 2016). When there were any

‘alert’ indicating a high toxicity potential, one should confirm it experimentally. Toxicity of the chemicals can be determined by conducting acute, chronic, reproduction/recovery tests and so on (OECD 2002, 2004, 2006, 2014; Reinert et al. 2002; USEPA, 2012), to set a toxicity threshold such as LC₅₀ (median lethal concentration) or NOEC (non-observed effect concentration). After these values are determined, the values are compared to the level of each pesticide and metabolites in water milfoil to judge if the risks for the plant are acceptable. In this step, each of the levels in plant can be estimated from the expected/simulated aquatic environmental concentration, as extrapolation of exposure concentration, and the distribution of pesticide/metabolites determined by the water milfoil study, then, be compared with the toxicities.

The distribution/quantity information from the water milfoil study can further be exploited to estimate biomagnification level to higher aquatic organisms *via* food-chain. Combining the predicted toxicities or definitive thresholds, risks on higher aquatic organisms, which can be exposed to the hazardous pesticide/metabolites by directly consuming water milfoil or *via* water column through leakage of the metabolites after the plant damage or death, can be estimated. To assess biomagnification, there are robust, widely recognized models for fish as representative aquatic organism which have been applied in the OECD guidance of bioaccumulation/biomagnification tests (Arnot and Gobas 2006; OECD 2016), and further advanced models are continuously developed (Arnot and Mackay 2018; Mackay et al. 2018). As exposure routes of the chemical to fish, the models employ both dietary and aqueous pathways and can be introduced by applying the concentration of the pesticide and metabolites in water milfoil, and leakage products if occurred, as conservative scenario. On the other hand, it is empirically proposed that only highly lipophilic, unready biodegradable compounds such as PCBs and HCHs tend to biomagnify (Arnot and Gobas 2006; OECD 2016; Mackay 2018; Mackay et al. 2018), hence, risk of less hydrophobic metabolites may generally not become critical issues. Incidentally, the biomagnification estimate can also be referred for considering human dietary exposure *via* consuming fresh water-derived groceries, particularly fish species (bluegill, trout, carp and etc.). In the current EU risk assessment for the fish consuming, farmed fish, which do not participate aquatic plant intake as fish feed, has been assumed (EU commission 2013b). However, if fish from the natural fresh water is the target and continuously consumed, then chronic exposure to human should

be considered. For other species for human risks, though not related to water milfoil, consumption of algae is considered. People seek more food sources since arable lands on earth are limited, and algae containing high protein have been expected as innovative food candidate (Becker 2007; Bleakley and Hayes 2017; Caporgno and Mathys 2018). The consumption of algae may currently be not popular, however, if the demand increases, the risk assessment on algae consumption should be necessary.

When the risks were evaluated unacceptable, then as further approach, definitive accumulation levels of pesticide and metabolites should be determined. For this purpose, one may conduct an outdoor semi-field study(s) like microcosm or mesocosm (Caquet et al. 2000; Møhlenberg et al. 2001; Srivanstava et al. 2004). The inclusive study design consists of a wider range of aquatic species (microorganisms, aquatic plants, planktons, benthic species and even fish), natural water containing dissolved organic matters, bottom sediment, the natural sunlight and so on, that closely reflects the natural aquatic ecosystem. In the microcosm/mesocosm study, the target pesticide and metabolites identified by the potential-finding exam such as our water milfoil study described in this thesis and/or equivalent metabolism studies, are analyzed/quantitated as analytes to find semi-realistic residue concentration in water milfoil (and other species) and compared to toxicity thresholds as definitive risk evaluation.

Conclusion

Our study design is useful to clarify each behavior of uptake, translocation and metabolism through different exposure paths, i.e., shoot *via* water column and root *via* sediment, respectively. The obtained fundamental results of distribution/quantity of the pesticide and metabolites gives us specific view for the importance of shoot and root uptakes, and necessity of performing further researches to understand each event, depending on the nature of the pesticides. The results can be used to deeply correlate with toxicity, to specify the potentially toxic metabolites as essential information for the starting point for further studies. In conclusion, the obtained results are novel, useful and important for the risk assessment of water milfoil.

7. References

- Adachi, T.; Suzuki, Y.; Fujisawa, T.; Katagi, T. Photodegradation of strobilurin fungicide mandestrobin in water. *J. Agric. Food Chem.* **2018**, *66*, 8514–8521.
- Agency for Toxic Substances and Disease Registry (ATSDR). *Toxicological Profile for Phenol (Update)*. Public Health Service, U.S. Department of Health and Human Services, Atlanta, GA, **1998**.
- Albuquerque, N. C. P.; Carrão, D. B.; Habenschus, M. D.; Oliveira, A. R. M. Metabolism studies of chiral pesticides. *J. Pharm. Biomed. Anal.* **2018**, *147*, 89–109.
- Ando, D.; Fujisawa T.; Katagi T. Uptake, translocation and metabolism of 3-phenoxybenzoic acid in the submerged rooted water milfoil (*Myriophyllum elatinoides*). *J. Pestic. Sci.* **2012**, *37*, 342–346.
- Ando, D.; Fujisawa T.; Katagi T. Uptake, translocation and metabolism of phenols by submerged rooted macrophyte, water milfoil (*Myriophyllum elatinoides*). *J. Agric. Food Chem.* **2015**, *63*, 5189–5195.
- Ando, D.; Fujisawa, T.; Katagi, T. Mandestrobin of the strobilurin fungicide mandestrobin in wheat. *J. Agric. Food Chem.* **2018**, *66*, 10154–10162.
- Ando, T.; Jacobsen, N. E.; Toia, R. F.; Casida, J. E. Epoxychrysanthemates: two-dimensional NMR analyses and stereochemical assignments. *J. Agric. Food Chem.* **1991**, *39*, 600–605.
- Ando, T.; Toia, R. F.; Casida, J. E. Epoxy and hydroxy derivatives of (*S*)-bioallethrin and pyrethrins I and II: synthesis and metabolism. *J. Agric. Food Chem.* **1991**, *39*, 606–611.
- Arnot, J. A.; Mackay, D. The influence of chemical degradation during dietary exposures to fish on biomagnification factors and bioaccumulation factors. *Environ. Sci.: Processes Impacts.* **2018**, *20*, 86–97.
- Arnot, J.A.; Gobas, F. A. P. C. A review of bioconcentration factor (BCF) and bioaccumulation factor (BAF) assessments for organic chemicals in aquatic organisms. *Environ. Rev.* **2006**, *14*, 257–297.
- Bailey, P. S.; Ferrell, T. M. Mechanism of ozonolysis. A more flexible stereochemical concept. *J. Am. Chem. Soc.* **1978**, *100*, 899–905.
- Baker, E. A. Chemistry and morphology of plant epicuticular waxes. In: Cutler, D. F.;

- Alvin, K. L.; Price, C. E. (eds) The plant cuticle, Academic Press, London, **1982**, pp 139–166.
- Baker, E. A.; Hayes, A.L.; Butler, R.C. Physicochemical properties of agrochemicals: their effects on foliar penetration. *Pestic. Sci.* **1992**, *34*, 167–182.
- Balba, H. Review of strobilurin fungicide chemicals. *J. Environ. Sci. Health Part B.* **2007**, *42*, 441–451.
- Barber, J. T.; Sharma, H. A.; Ensley, H. E.; Polito, M. A.; Thomas, D. A. Detoxification of phenol by the aquatic angiosperm, *Lemna gibba*. *Chemosphere.* **1995**, *31*, 3567–74.
- Bauld, N. L.; Thompson, J. A.; Hudson, C. E.; Bailey, P. S. Stereospecificity in ozonide and cross-ozonide formation. *J. Am. Chem. Soc.* **1968**, *90*, 1822–1830.
- Becker, E. W. Micro-algae as a source of protein. *Biotechnol. Adv.* **2007**, *25*, 207–210.
- Belgers, M. D. J.; Van Lieverloo, J. R.; Van der Pas, T. J. L.; Van den Brink, J. P. Effects of the herbicide 2,4-D on the growth of nine aquatic macrophytes. *Aquat. Botany*, **2007**, *86*, 260–268.
- Bhattacharya, D.; Price, D.; Chan, C. X.; Qiu, H.; Rose, N.; Ball, S. Genome of the red alga *Porphyridium purpureum*. *Nat. Commun.* **2013**, *4*, 1941.
- Bianchi, G. Plant waxes. In: Hamilton RJ (ed) Waxes: Chemistry, Molecular Biology and Functions, vol 6. The Oily Press, Dundee, **1995**, pp 175–222.
- Bleakley, S.; Hayes, M. Algal proteins: extraction, application, and challenge concerning production. *Foods.* **2017**, *6*, 33.
- Blee, E.; Schuber, F. Regio- and enantioselectivity of soybean fatty acid epoxide hydrolase. *J. Biol. Chem.* **1992**, *286*, 5197–5203
- Bondareva, L.; Mogilnaya, O.; Vlasova, I. Subcellular localization of 241Am in structural 35. components of submerged macrophyte of the River Yenisei *Elodea Canadensis*. *International Aquatic Research.* **2012**, *4*, 13–28.
- Borga, K.; Hop, H.; Skaare, J. U.; Selective bioaccumulation of chlorinated pesticides and metabolites in Arctic seabirds. *Environ. Pollut.* **2007**, *45*, 545–553.
- Breyer, E. D.; Strasters, J. K.; Khaledi, M. G. Quantitative retention-biological activity relationship study by micellar liquid chromatography. *Anal. Chem.* **1991**, *63*, 828–833.
- Briggs, G. G.; Bromilow, R. H.; Evansa, A. A.: Relationships between lipophilicity and

- root uptake and translocation of non-ionised chemicals by barley. *Pestic. Sci.* **1982**, *13*, 495–504.
- Bromilow, R. H.; Chamberlain, K. Principles governing uptake and transport of chemicals. In *Plant Contamination: Modeling and Simulation of Organic Chemical Processes*, ed. S. Trapp J. C. Mc Farlane. *CRC Press, Boca Raton, FL*, **1995**, pp. 37–68.
- Burešová, H.; Crum, S. J. H.; Belgers, J. D. M.; Adriaanse, P. I.; Arts, G. H. P. Effects of linuron on a rooted aquatic macrophyte in sediment-dosed test systems. *Environ. Pollut.* **2013**, *175*, 117–124.
- Burrows, H. D.; Canle, M.; Santaballa, J. A.; Steenken, S. Reaction pathways and mechanisms of photodegradation of pesticides. *J. Photochem. Photobiol. B Biol.* **2002**, *67*, 71–108.
- Cairns, J. R. K.; Esen, A. β -glucosidase. *Cell. Mol. Life Sci.* **2010**, *67*, 3389–3405.
- Campbell, N. A.; Reece, J. B. *Biology*. California: Benjamin Cummings. **2002**, pp. 753–754.
- Caporgno, M. P.; Mathys, A. Trends in microalgae incorporation into innovative food products with potential health benefits. *Front. Nutr.* **2018**, *5*, 58.
- Caquet, T.; Lagadic, L.; Sheffield, S. R. Mesocosms in ecotoxicology (1): Outdoor aquatic systems. *Rev. Environ. Contaminat. Toxicol.* **2000**, *165*, 138.
- Carvalho, de R. F.; Bromilow, R. H.; Greenwood, R. Uptake and translocation of non-ionized pesticides in the emergent aquatic plant parrot feather *Myriophyllum aquaticum*. *Pest Manag. Sci.* **2007**, *63*, 798–8002.
- Carvalho, de R. F.; Bromilow, R. H.; Greenwood, R. Uptake of pesticides from water by curly waterweed *Lagarosiphon major* and lesser duckweed *Lemna minor*. *Pest Manag. Sci.* **2007**, *63*, 789–797.
- Cedergreen, N.; Streibig, C. J.; Spliid, H. N. Sensitivity of aquatic plants to the herbicide metsulfuron-methyl. *Ecotoxicol. Environ. Saf.* **2004b**, *57*, 153–161.
- Chen, J.; Zhang, Z.; Stebbins, J.; Zhang, X.; Hoffman, R.; Moore, A.; Pellecchia, M. A fragment-based approach for the discovery of isoform-specific p38 α inhibitors. *Chem. Bio.* **2007**, *2*, 329–336.
- Cicek, M.; Blanchard, D.; Bevan, D. R.; Esen, A. The aglycone specificity-determining sites are different in 2,4-dihydroxy-7-methoxy-1,4-benzoxazin-3-one (DIMBOA)-

- glucosidase (maize beta-glucosidase) and dhurrinase (sorghum beta-glucosidase). *J. Biol. Chem.* **2000**, *275*, 20002–20011.
- Class, T. J.; Ando, T.; Casida, J. E. Pyrethroid metabolism: microsomal oxidase metabolism of (*S*)-bioallethrin and the six natural pyrethrins. *J. Agric. Food Chem.* **1990**, *38*, 529–537.
- Cole, L. M.; Casida, J. E.; Ruzo, L. O. Comparative degradation of the pyrethroids toralomeethrin, traloccythrin, deltamethrin, and cypermethrin on cotton and bean foliage. *J. Agric. Food Chem.* **1982**, *30*, 916–920.
- Criegee, R. Mechanism of ozonolysis. *Angew. Chem. Internat. Edit.* **1975**, *14*, 745–752.
- Cronin, M. T. D.; Schultz, T. W. Development of quantitative structure–activity relationships for the toxicity of aromatic compounds to *Tetrahymena pyriformis*: comparative assessment of the methodologies. *Chem. Res. Toxicol.* **2001**, *14*, 1284–1295.
- Cupid, B. C.; Holmes, E.; Wilson, I. D.; Lindon, J. C.; Nicholson, J. K. Quantitative structure- metabolism relationships (QSMR) using computational chemistry : pattern recognition analysis and statistical prediction of phase II conjugation reactions of substituted benzoic acids in the rat. *Xenobiotica.* **1999**, *29*, 27–42.
- Day, J. A.; Saunders, F. M. Glycosidation of chlorophenols by *Lemna minor*. *Environ. Toxicol. Chem.* **2004**, *23*, 102–109.
- Denny, P. Solute movement in submerged angiosperms. *Biol. Rev.* **1980**, *55*, 65–92.
- Dettenmaier, E. M.; Doucette, W. J.; Bugbee, B. Chemical hydrophobicity and uptake by plant roots. *Environ. Sci. Technol.* **2009**, *43*, 324–329.
- Diepens, N. J.; Arts, G. H. P.; Focks, A.; Koelmans, A.A. Uptake, translocation, and elimination in sediment-rooted macrophytes: a model-supported analysis of whole sediment test data. *Environ. Sci. Technol.* **2014**, *48*, 12344–12353.
- Dimou, A. D.; Sakkas, V. A.; Albanis, T. A. Trifluralin photolysis in natural waters and under the presence of isolated organic matter and nitrate ions: kinetics and photoproduct analysis. *J. Photochem. Photobiol. A.* **2004**, *163*, 473–480.
- Doucette, W. J.; Shunthirasingham, C.; Dettenmaier, E. M.; Zaleski, R. T.; Fantke P.; Arnot, J. A. Review of measured bioaccumulation data on terrestrial plants for organic chemicals: metrics, variability, and the need for standardized measurement protocols. *Environ Toxicol Chem.* **2018**, *37*, 21–33.

- Duhoux, A.; Carrere, S.; Gouzy, J.; Bonin, L.; Delye, C. RNA-Seq analysis of rye-grass transcriptomic response to an herbicide inhibiting acetolactate-synthase identifies transcripts linked to non-target-site-based resistance. *Plant Mol. Biol.* **2015**, *87*, 473–457.
- EU-Commission, 2013b. Working document on the nature of pesticide residues in fish. SANCO/11187/2013; 31.01.2013 rev.3. http://ec.europa.eu/food/plant/pesticides/guidance_documents/docs/app-j_en.pdf (accessed 5 Dec. 2018).
- Ensley, H. E.; Barber, J. T.; Polito, M. A.; Oliver, A. I. Toxicity and metabolism of 2,4-dichlorophenol by the aquatic angiosperm *Lemna gibba*. *Environ Toxicol Chem.* **1994**, *13*, 325–331.
- Estimation Programs Interface Suite for Microsoft Windows, v. 4.11; United States Environmental Protection Agency: Washington, DC, **2017**. <https://www.epa.gov/tsca-screening-tools/epi-suitetm-estimation-program-interface> (accessed 5 Dec. 2018).
- European Commission: “Working Document Guidance Document on Aquatic Ecotoxicology in the Context of the Directive 91/414/EEC, Sanco/3268/2001 rev.4 (final)” **2002**.
- European Food Safety Authority (EFSA). Conclusion on the peer review of the pesticide risk assessment of the active substance flumioxazin. *EFSA journal.* **2014**, *12*, 3736.
- European Food Safety Authority (EFSA). Conclusion on the peer review of the pesticide risk assessment of the active substance buromuconazole. *EFSA Journal* **2010**, *8*, 1704–1788.
- European Food Safety Authority (EFSA). Conclusion on the peer review of the pesticide risk assessment of the active substance dimethoate. *EFSA Journal* **2017**, *11*, 3233–3269.
- European Food Safety Authority (EFSA). Conclusion on the peer review of the pesticide risk assessment of the active substance tolclofos-methyl. *EFSA Journal* **2018**, *16*, 5130–5155.
- European Food Safety Authority (EFSA). Conclusion on the peer review of the pesticide risk assessment of the active substance mandestrobin. *EFSA Journal* **2015**, *13*, 1–72.
- European Food Safety Authority (EFSA). Guidance on tiered risk assessment for plant

- protection products for aquatic organisms in edge-of-field surface waters. *EFSA Journal*. **2013**, *11*, 3290.
- Ewers, J.; Rubio, A. M.; Knackmuss, H.J.; Freier-Schroder, D. Bacterial metabolism of 2,6-xyleneol. *Appl. Environ. Microbiol.* **1989**, *55*, 2904–2908.
- FAMIC: Risk assessment report of Flumioxazin. <https://www.env.go.jp/council/10dojo/y104-49/sankousiryoushu8.pdf> (accessed 5 Dec. 2018).
- FAO: Triazole fungicide metabolites toxicology. http://www.fao.org/fileadmin/templates/agphome/documents/Pests_Pesticides/JMP_E/Report08/Triazole.pdf (accessed 5 Dec. 2018).
- Field, R. J.; Dastgheib, F. Enhancing uptake and translocation of systemic active ingredients. In: Foy CL, Pritchard DW (eds) Pesticide formulation and adjuvant technology. Formulation Forum '94, Washington, DC. CRC Press, Boca Raton, **1996**, pp 241–295.
- Ford, K.; Casida, J. Comparative metabolism and pharmacokinetics of seven neonicotinoid insecticides in spinach. *J. Agric. Food Chem.* **2008**, *56*, 10168–10175.
- Fritiof, A.; Greger, M. Fate of cadmium in *Elodea Canadensis*. *Chemosphere* **2007**, *67*, 365–375.
- Fu, W.; Franco, A.; Trapp, S. Methods for estimating the bioconcentration factor of ionizable organic chemicals. *Environ. Toxicol. Chem.* **2009**, *28*, 1372–1379.
- Fujisawa, T.; Kurosawa, M.; Katagi T. Uptake and transformation of pesticide metabolites by duckweed (*lemna gibba*). *J. Agric. Food Chem.* **2006**, *54*, 6286–6293.
- Gao, L.; Hou, J; Toney, J.; MacDonald, D.; Huang, Y. Mathematic modeling of the aquatic macrophyte inputs of mid-chain n-alkyl lipids to lake sediments: implications for interpreting compound specific hydrogen isotopic records. *Geochimica et Cosmochimica*. **2011**, *75*, 3781–3791.
- Gaughan, L. C.; Casida, J. E. Degradation of *trans*- and *cis*-permethrin on cotton and bean plants. *J. Agric. Food Chem.* **1978**, *26*, 525–528.
- Geletneky, C.; Berger, S. The mechanism of ozonolysis revised by ¹⁷O-NMR spectroscopy. *Eur. J. Org. Chem.* **1998**, *8*, 1625–1627.
- Geoffroy, L.; Frankart, C.; Eullaffroy, P. Comparison of different physiological parameter responses in *Lemna minor* and *Scenedesmus obliquus* exposed to herbicide

- Flumioxazin. *Environ. Pollut.* **2004**, *131*, 233–241.
- Ghadiri, H.; Rose CW. Degradation of endosulfan in a clay soil from cotton farms of western Queensland. *J. Environ. Manag.* **2001**, *62*, 155–69.
- Ghattas, A. K.; Fischer, F.; Wick, A.; Ternes, T. A.; Anaerobic biodegradation of (emerging) organic contaminants in the aquatic environment. *Water Res.* **2017**, *116*, 268–295.
- Glomski, L. M.; Netherland, M. D. Use of a small-scaled primary screening method to predict effects of flumioxazin and cafentrazone-ethyl on native and invasive, submersed plants. *J. Aquat. Plant Manage.* **2013**, *51*, 45–48.
- Gobas, F. A. P. C.; McNell, E. J.; Lovett-Doust, L.; Haffner, G. D. Bioconcentration of chlorinated aromatic hydrocarbons in aquatic macrophytes. *Environ. Sci. Technol.* **1991**, *25*, 924–929.
- Gramatica, P.; Cassani, S.; Chirico, N. QSARINS-Chem: insubria datasets and new QSAR/QSPR models for environmental pollutants in QSARINS. *J. Comput. Chem.* **2014**, *35*, 1036–1044.
- Griesbaum, K.; Quinkert, R. O.; McCullough, K. J. C-C bond formation at ozonide rings by substitution of chlorinated ozonides. *Eur. J. Org. Chem.* **2004**, *17*, 3657–3662.
- Guengerich, F. P. Common and uncommon cytochrome P450 reactions related to metabolism and chemical toxicity. *Chem. Res. Toxicol.* **2001**, *14*, 611–650.
- Guengerich, F. P. Cytochrom p450 oxidations in the generation of reactive electrophiles: epoxidation and related reactions. *Arch. Biophys. Biochem.* **2003**, *409*, 59–71.
- Gunnarsson, C. C.; Petersen, C. M. Water hyacinths as a resource in agriculture and energy production: a literature review. *Waste Manage.* **2007**, *27*, 117–127.
- Haga, N.; Takayanagi, H. Mechanism of photochemical rearrangement of diphenyl ethers. *J. Org. Chem.* **1996**, *61*, 735–745.
- Haitzer, M.; Höss, S.; Traunspurger, W.; Steinberg, C. Effects of dissolved organic matter (DOM) on the bioconcentration of organic chemicals in aquatic organisms – A review. *Chemosphere.* **1998**, *37*, 1335–1362.
- Hall, D.; Luca, V. D. Mesocarp localization of a bi-functional resveratrol/hydroxycinnamic acid glucosyltransferase of concord grape (*Vitis labrusca*). *The Plant Journal.* **2007**, *49*, 579–591.
- Hansch, C.; Leo, A. J. Substituent constant for analysis in chemistry and biology. Wiley,

- New York, **1979**, 171-319.
- Hayashi, O.; Kameshiro, M.; Satoh, K. Intrinsic bioavailability of ¹⁴C-heptachlor to several plant species. *J. Pestic. Sci.* **2010**, *35*, 107–113.
- He, S.; Withers, S. G. Assignment of sweet almond β-glucosidase as a family 1 glycosidase and identification of its active site nucleophile. *J. Biol. Chem.* **1997**, *272*, 24864–24867.
- Heller, W.; Forkmann, G. Biosynthesis of flavonoids. in: the flavonoids; J. B. Harborne Ed.; Chapman & Hall: London, U.K., **1994**.
- Henrissat, B.; Callebaut, I.; Fabrega, S.; Lehn, P.; Mornon, J.-P.; Davies, G. Conserved catalytic machinery and the prediction of a common fold for several families of glycosyl hydrolases. *Proc. Natl. Acad. Sci. U. S. A.* **1995**, *92*, 7090–7094.
- Hinman, M. L.; Klaine, S. J. Uptake and translocation of selected organic pesticides by the rooted aquatic plant *Hydrilla verticillata* Royle. *Environ. Sci. Technol.* **1992**, *26*, 609–613.
- Hiroto, D.; Ueda, N.; Kiguchi, S.; Hirota, M.; Iwashita, K.; Kodaka, R. Research and development of a novel fungicide ‘Mandestrobin’. *SUMITOMO KAGAKU*, **2016**, 1–16.
- Hopper, D.; Chapman, P. Gentisic acid and its 3- and 4-methyl-substituted homologues as intermediates in the bacterial degradation of m-cresol, 3,5-xylenol and 2,5-xylenol. *Biochem. J.* **1970**, *122*, 19–28.
- Hopper, D.; Kemp, P. Regulation of enzymes of the 3,5-xylenol-degradative pathway in *Pseudomonas putida*: evidence for a plasmid. *J. Bacteriol.* **1980**, *142*, 21–26.
- Hsu, C. F.; Kleier, A. D. Phloem mobility of xenobiotics VIII. A short review. *J. Exp. Botany.* **1996**, *47*, 1265–1271.
- Hsu, C. F.; Marxmiller, R. L.; Yang, A. Y. S. Study of root uptake and xylem translocation of cinmethylin and related compounds in detopped soybean roots using a pressure chamber technique. *Plant Physiol.* **1990**, *93*, 1573–1578.
- Ismail, B.; Hayes, K. β-glucosidase activity toward different glycosidic forms of isoflavones. *J. Agric. Food Chem.* **2005**, *53*, 4918–4924.
- Itoh, K.; Fujita, M.; Kumano, K.; Suyama, K.; Yamamoto, H. Phenolic acids affect transformations of chlorophenols by a *Coriolus versicolor* laccase. *Soil Biol. Biochem.* **2000**, *32*, 85–91.

- Jeffree, C. E. The fine structure of the plant cuticle. In: Riederer, M.; Muller, C. editors. *Biology of the plant cuticle*. Oxford, Blackwell, **2006**, P11–125.
- Jenkins, J.; Lo Leggio, L.; Harris, G.; Pickersgill, R. β -Glucosidase, β -galactosidase, family A cellulases, family F xylanases and two barley glycanases form a superfamily of enzymes with 8-fold β/α architecture and with two conserved glutamates near the carboxyterminal ends of β -strands four and seven. *FEBS Lett.* **1995**, *362*, 281–285.
- Jeppesen, E.; Sondergaard, M.; Kirsten, C. The structuring role of submerged macrophytes in lakes. Springer, New York, **1998**.
- Joseph, I. S. R. Metabolism of azoxystrobin in plants and animals. In *Pesticide Chemistry and Bioscience*; Brooks, G. T., Roberts, T. R., Eds.; The food environment challenge; The Royal Society of Chemistry: Cambridge, U.K., **1999**, pp. 265–278.
- Kaneko, H. Pyrethroid chemistry and metabolism. In: Hayes' handbook of pesticide toxicology, 3rd ed.; Krieger, R., Ed.; Elsevier: Amsterdam, The Netherlands, **2010**, Chapter 76, pp 1635–1663.
- Kasai, F.; Takamura N.; Hatakeyama S. Effects of simetryne on growth of various freshwater algal taxa. *Environ. Pollut.* **1993**, *79*, 77–83.
- Katagi, T. Abiotic hydrolysis of pesticides in the aquatic environment. *Rev. Environ. Contam. Toxicol.* **2002**, *175*, 79–261.
- Katagi, T. Bioconcentration, bioaccumulation, and metabolism of pesticides in aquatic organisms. *Rev. Environ. Contam. Toxicol.* **2010**, *204*, 1–132.
- Katagi, T. Hydrolysis of N-phenylimide herbicide flumioxazin and its anilic acid derivative in aqueous solution. *J. Pestic. Sci.* **2003**, *28*, 44–50.
- Katagi, T. Isomerization of chiral pesticides in the environment. *J. Pestic. Sci.* **2012**, *37*, 1–14.
- Katagi, T. Photodegradation of pesticides on plant and soil surfaces. *Rev. Environ. Contam. Toxicol.* **2004**, *182*, 1–195.
- Katagi, T. Surfactant effects on environmental behavior of pesticides. *Rev. Environ. Contam. Toxicol.* **2008**, *194*, 71–177.
- Kelly, B. C.; Ikonomou, M. G.; Blair, J. D.; Morin, A. E.; Gobas, F. A. P. C. Food web-specific biomagnification of persistent organic pollutants. *Science*. **2007**, *317*, 236–238.

- Kodaka, R.; Sugano, T.; Katagi, T.; Takimoto, Y. Clay-catalyzed nitration of a carbamate fungicide diethofencarb. *J. Agric. Food Chem.* **2003**, *51*, 7730–7737.
- Kodaka, R.; Suzuki, Y.; Sugano, T.; Katagi, T. Aerobic metabolism and adsorption of pyrethroid insecticide metofluthrin in soil. *J. Pestic. Sci.* **2007**, *32*, 393–401.
- Kreuz, K.; Tommasini, R.; Martinoia, E. Old enzymes for a new job. Herbicide detoxification in plants. *PlantPhysiol.* **1996**, *111*, 349–353.
- Kusel, A. C.; Sianoudis, J.; Leibfritz, D.; Grimme, L. H.; Mayer, A. The dependence of the cytoplasmic pH in aerobic and anaerobic cells of the green algae *chlorella fusca* and *chlorella vulgaris* on the pH of the medium as determined by ³¹P in vivo NMR spectroscopy. *Arch. Microbiol.* **1990**, *153*, 254–258.
- Kwon, J. W., Armbrust, K. L.; Grey, L. Hydrolysis and photolysis of flumioxazin in aqueous buffer solutions. *Pest Manag. Sci.* **2004**, *60*, 939–943.
- Lamoureux, G. L.; Rusness, D. G. ‘Xenobiotic conjugation in higher plants. ACS Symposium Series 299, ed. by G. D. Paulson, J. Caldwell, D. H. Huston and J. J. Menn. American Chemical Society, Washington DC, Chap. 4, **1986**, pp. 62–105.
- Lao, S.; Loutre, C.; Brazier, M.; Coleman, J.; Cole, D.; Edward, R.; Theodoulou, F. 3,4-dichloroaniline is detoxified and exported via different pathway in *Arabidopsis* and soybean. *Phytochemistry.* **2003**, *63*, 653–661.
- Laskowski, D. A. Physical and chemical properties of pyrethroids. *Rev. Environ. Contam, toxicol.* **2002**, *174*, 49–170.
- Leahey, J. P. Metabolism and environmental degradation. ed. by J. P. Leahey, Taylor & Francis, London, **1979**, pp. 263–342.
- Lewis, A. L. Use of freshwater plants for phytotoxicity testing: a review. *Environ. Pollut.* **1995**, *87*, 319–336.
- Lim, E-K.; Doucet, C. J.; Li, Y.; Elias, L.; Worrall, D.; Spencer, S. P.; Ross, J.; Bowles, D. J. The activity of *Arabidopsis* glycosyltransferases toward salicylic acid, 4-hydroxybenzoic acid, and other benzoates. *J. Biol. Chem.* **2002**, *277*, 586–592.
- Ma, Y.; Gan, J.; Liu, W. Chiral pesticides and environmental safety. In: Chiral pesticides: stereoselectivity and its consequence. American Chemical Society, Washington, **2011**, pp. 97–106.
- MacKay, D.; Celsie, A. K. D.; Powell, D. E.; Parnis, J. M. Bioconcentration, bioaccumulation, biomagnification and trophic magnification: a modelling

- perspective. *Environ. Sci.: Processes Impacts*, **2018**, *20*, 72–85.
- Macalady, D. L.; Tratnyek, P. G.; Grundl, T. J. Abiotic reduction reactions of anthropogenic organic chemicals in anaerobic systems. *J. Contam. Hydrol.* **1986**, *1*, 1–28.
- Madsen, J. D.; Chambers, P. A.; James, W. F.; Koch, E. W.; Weslake, D. F. The interaction between water movement, sediment dynamics and submerged macrophytes. *Hydrobiologia*, **2001**, *71*, 70–84.
- Maltby, L.; Arnold, D.; Arts, G.; Davies, J.; Heimbach, F.; Pickl, C.; Poulsen, V. “Aquatic macrophyte risk assessment for pesticide,” ed. by J. W. Gorsuch, CRC Press, Boca Raton, FL, **2009**, pp. 5–7.
- Marana, S. R. Molecular basis of substrate specificity in family 1 glycoside hydrolases. *IUBMB Life*. **2006**, *58*, 63–73.
- Marion, L.; Paillisson J. M. A mass balance assessment of the contribution of floating-leaved macrophytes in nutrient stocks in an eutrophic macrophyte-dominated lake. *Aquatic Bot.* **2002**, *73*, 249–260.
- Matsuo, N.; Ujihara, K.; Shono, Y.; Iwasaki, T.; Sugano, M.; Yoshiyama, T.; Uwagawa, S. Discovery and development of a novel pyrethroid insecticide ‘Metofluthrin (SumiOne[®], Eminence[®])’. *SUMITOMO KAGAKU II*, **2005**, 1–15.
- Matsuzawa, T.; Jo, T.; Uchiyama, T.; Manninen, J. A.; Arakawa, T.; Miyazaki, K.; Fushinobu, S.; Yaoi, K. Crystal structure and identification of a key amino acid for glucose tolerance, substrate specificity and transglycosylation activity of metagenomic β -glucosidase Td2F2. *FEBS J.* **2016**, *283*, 2340–2353.
- McFarlane, J. C. Anatomy and physiology of plant conductive systems. in: Trapp S, McFarlane JC (eds) *Plant contamination: modeling and simulation of organic chemical processes*. Lewis, Boca Raton, FL, **1995**, pp 13–34.
- Meier, U. Leaf vegetable (Forming heads). in: *Growth stages of mono- and dicotyledonous plants*. BBCH monograph. Federal Biological Research Centre for Agriculture and Forestry. Berlin, **2001**, pp 120–123.
- Mikami, N.; Baba, Y.; Katagi, T.; Miyamoto, J. Metabolism of the synthetic pyrethroid fenprothrin in plants. *J. Agric. Food Chem.* **1985**, *33*, 980–987.
- Mitsou, K.; Koulianou, A.; Lambropoulou, D.; Pappas, P.; Albanis, T.; Lekka, M. Growth rate effects, responses of antioxidant enzymes and metabolic fate of the herbicide

- propanil in the aquatic *lemna minor*. *Chemosphere*. **2006**, *62*, 275–284.
- Miyamoto, J.; Suzuki, T.; Nakane, C. Metabolism of phenothrin or 3-phenoxybenzyl d-trans-chrysanthemumate in mammals. *Pestic. Biochem. Physiol.* **1974**, *4*, 438–450.
- Modolo, M.; Li, L.; Pan, H.; Blount, J. W.; Dixon, R. A.; Wang, X. Crystal structure of glycosyltransferase UGT78G1 reveal the molecular basis of glycosylation and deglycosylation of (iso) flavonoids. *J. Mol. Biol.* **2009**, *392*, 1292–1302.
- Mohr, H.; Schopfer P. *Pflanzen Physiologie*, 4th ed., Springer, USA, **1992**.
- Murray, R. W.; Youssefeyeh, R. D.; Story, P. R. Ozonolysis. Steric and stereochemical effects in the olefin. *J. Am. Chem. Soc.* **1967**, *89*, 2429–2434.
- Myung, K.; Parobek, P. A.; Godbey, A. J.; Bowling J. A.; Pence, E.H. Interaction of organic solvents with the epicuticular wax layer of wheat leaves. *J. Agric. Food Chem.* **2013**, *61*, 8737–8742.
- Møhlenberg, F.; Petersen. S.; Gustavsson, K.; Lauridsen, T.; Friberg, N. Mesocosm experiments in the approval procedure for pesticides – a literature study on effects of mesocosm characteristics and validity of extrapolation methods to protect sensitive species. Pesticide Research No. 56, Danish Environmental Protection Agency, Denmark, **2001**, pp 107.
- Nambu, K.; Ohkawa, H.; Miyamoto, J. Metabolic fate of phenothrin in plants and soils. *J. Pestic. Sci.* **1980**, *5*, 177–197.
- Nishimura, H.; Suzuki, Y.; Nishiyama, M.; Fujisawa, T.; Katagi, T. Photodegradation of insecticide metofluthrin on soil, clay minerals and glass surface. *J. Pestic. Sci.* **2011**, *36*, 376–38.
- Nishiyama, M.; Suzuki, Y.; Katagi, T. Hydrolysis and photolysis of insecticide metofluthrin in water. *J. Pestic. Sci.* **2010**, *35*, 447–455.
- OECD: Draft guidance for aspects of OECD TG 305 on fish bioconcentration. **2016**. https://www.oecd.org/chemicalsafety/testing/12%20December%202016_OECD%20305%20GD%20revised_clean.pdf (accessed 5 Dec. 2018).
- OECD: “OECD GUIDELINES FOR THE TESTING OF CHEMICALS 201, Freshwater alga and cyanobacteria, growth inhibition test,” **2002**.
- OECD: “OECD GUIDELINES FOR THE TESTING OF CHEMICALS 218, Sediment-water chironomid toxicity test using spiked sediment,” **2004**.
- OECD: “OECD GUIDELINES FOR THE TESTING OF CHEMICALS 221, *Lemna sp.*

- growth inhibition test,” **2006**.
- OECD: “OECD GUIDELINES FOR THE TESTING OF CHEMICALS 238, Sediment-free *Myriophyllum spicatum* toxicity test,” **2014**.
- OECD: “OECD GUIDELINES FOR THE TESTING OF CHEMICALS 239, Water-sediment *Myriophyllum spicatum* toxicity test,” **2014**.
- Perry, S. C.; Charman, A. S.; Pranker, J. R.; Chiu, K. F. Chemical kinetics and aqueous degradation pathways of a new class of ozonide antimalarials. *J. Pharm. Sci.* **2006**, *95*, 737–747.
- Peterson, C. A. Exodermal Casparian bands: their significance for ion uptake by roots. *Physiol. Plantar.* **1988**, *72*, 204–208.
- Petroutsos, D.; Katapodis, P.; Samiotaki, M.; Panayotou, G.; Ketos, D. Detoxification of 2,4-dichlorophenol by de marine microalga *Tetraselmis marina*. *Phytochemistry.* **2008**, *69*, 707–714.
- Pflugmacher, S.; Sandermann Jr, H. Taxonomic distribution of plant glucosyltransferases activity on xenobiotics. *Phytochemistry.* **1998a**, *49*, 507–511.
- Pflugmacher, S.; Schröder, P.; Sandermann Jr, H. Taxonomic distribution of plant glutathione *S*-transferases acting on xenobiotics. *Phytochemistry.* **2000**, *54*, 267–273.
- Pflugmacher, S.; Steinberg, C. Activity of phase I and phase II detoxification enzymes in aquatic macrophytes. *Angew. Bot.* **1997**, *71*, 144–146.
- Pflugmacher, S.; Wiencke, C.; Sandermann Jr, H. Activity of phase I and phase II detoxification in antarctic and arctic macroalgae. *Mar. Environ. Res.* **1999**, *48*, 23–36.
- Pflugmacher, S.; Wiencke, C.; Sandermann, W. H. Activity of phase I and phase II detoxification in antarctic and arctic macroalgae. *Mar. Environ. Res.* **1999**, *48*, 23–36.
- Poh, C.; Bayly, R. Evidence for isofunctional enzymes used in m-cresol and 2,5-xylene degradation via the gentisate pathway in *pseudomonas alcaligenes*. *J. Bacteriol.* **1980**, *143*, 59–69.
- Ponec, R.; Yuzhakov, G.; Hass, Y.; Samuni, U. Theoretical analysis of the stereoselectivity in the ozonolysis of olefins. Evidence for a modified criegee mechanism. *J. Org. Chem.* **1997**, *62*, 2757–2762.
- Pryor, A. W. Can vitamin E protect humans against the pathological effects of ozone in

- smog? *Am. J. Clin. Nutr.* **1991**, *53*, 702–722.
- Pryor, A. W.; Giamalva, D.; Church, D. F. Kinetics of ozonation. 3. Substituent effects on the rates of reaction of alkenes. *J. Am. Chem. Soc.* **1985**, *107*, 2793–2797.
- Bromilow, R. H.; Chamberlain, K.; Evans, A. A. Physicochemical aspects of phloem translation of herbicides. *Weed Sci.* **1990**, *38*, 305–314.
- Reinert, K. H.; Giddings, J. M.; Judd, L. Effects analysis of time-varying or repeated exposures in aquatic ecological risk assessment of agrochemicals. *Environ. Toxicol. Chem.* **2002**, *21*, 1977–1992.
- Remucal, C. K. The role of indirect photochemical degradation in the environmental fate of pesticides: A review. *Environ. Sci.: Processes Impacts.* **2014**, *16*, 628–653.
- Rendal, C.; Kusk, K. O.; Trapp, S. Optimal choice of pH for toxicity and bioaccumulation studies of ionizing organic chemicals. *Environ. Toxicol. Chem.* **2011**, *30*, 2395–2406.
- Rocher, F.; Chollet, J-F.; Legros, S.; Jousse, C.; Lemoine, R.; Faucher, M.; Bush, D. R.; Bonnemain, J-L. Salicylic acid transport in *Ricinus communis* involves a pH-dependent carrier system in addition to diffusion. *Plant Physiol.* **2009**, *150*, 2081–2091.
- Rodrigues, E. T.; Lopes, I.; Pardal, M. A. Occurrence fate and effects of azoxystrobin in aquatic ecosystems: a review. *Environ. Int.* **2013**, *53*, 18–28.
- Rodrigues, F. L.; Dairou, J.; Diaz, C. L.; Rubio, M. C.; Sim, E.; Spaink, H. P.; Dupret, J. M. Cloning, functional expression and characterization of mesorhizobium loti arylamine *N*-acetyltransferases: rhizobial symbiosis supplies leguminous plants with the xenobiotic *N*-acetylation pathway. *Mol. Microbiol.* **2006**, *60*, 505–512.
- Ruzo, L. O.; Kimmel, E. C.; Casida, J. E. Ozonides and epoxides from ozonation of pyrethroids. *J. Agric. Food Chem.* **1986**, *34*, 937–940.
- Ryan, J. A.; Bell, R. M.; Davidson, J. M.; O'Connor, G. A. Plant uptake of non-ionic organic chemicals from soils. *Chemosphere.* **1988**, *17*, 2299–2323.
- Rye, C. S.; Withers, S. G. Glycosidase mechanisms. *Curr. Opin. Chem. Biol.* **2000**, *4*, 573-580.
- Cassani, S.; Kovarich, S.; Papa, E.; Roy, P. P.; Van der Wal, L.; Gramatica, P. Daphnia and fish toxicity of (benzo)triazoles: validated QSAR models, and interspecies quantitative activity–activity modelling. *J. Hazard. Mater.* **2013**, *258–259*, 50–60.
- Saito, S.; Kawabata, J. Effects of electron-withdrawing substituents on DPPH radical

- scavenging reactions of protocatechuic acid and its analogues in alcoholic solvents. *Tetrahedron*. **2005**, *61*, 8101–8108.
- Sandermann Jr., H. Higher plant metabolism of xenobiotics: the “green liver” concept. *Pharmacogenetics*. **1994**, *4*, 225–241.
- Sandermann, H.; Schmitt, R.; Eckey, H.; Bauknecht, T. Plant biochemistry of xenobiotics: isolation and properties of soybean *O*- and *N*-glucosyl and *O*- and *N*-malonyltransferases for chlorinated phenols and anilines. *Arch. Biochem. Biophys.* **1991**, *287*, 341–350.
- Sanderson, H., Thomsen, M., Comparative analysis of pharmaceuticals versus industrial chemicals acute aquatic toxicity classification according to the United Nations classification system for chemicals. Assessment of the (Q)SAR predictability of pharmaceuticals acute aquatic toxicity and their predominant acute toxic mode-of-action. *Toxicol. Lett.* **2009**, *187*, 84–93.
- Sangion, A.; Gramatica, P. Hazard of pharmaceuticals for aquatic environment: prioritization by structural approaches and prediction of ecotoxicity. *Environ. Int.* **2016**, *95*, 131–143.
- Sansanya, S.; Opassiri, R.; Kuaprasert, B.; Chen, C. J.; Cairns, J. R. K. The crystal structure of rice (*Oryza sativa* L.) Os4BGlu12, an oligosaccharide and tuberic acid glucoside-hydrolyzing β -glucosidase with significant thioglucosylase activity. *Arch. Biochem. Biophys.* **2011**, *510*, 62–72.
- Sassman, S. A.; Lee, L. S.; Bischoff, M.; Turco, R. F. Assessing N,N'-dibutylurea (DBU) formation in soils after application of n-butyliocyanate and benlate fungicides. *J. Agric. Food Chem.* **2004**, *52*, 747–754.
- Satchivi, N. M.; Stoller, E. W.; Wax, L. M.; Briskin, D. P. A nonlinear, dynamic, simulation model for transport, and whole plant allocation of systemic xenobiotics following foliar application. IV: Physicochemical properties requirements for optimum absorption and translocation. *Pest, Biochem. Physiol.* **2006**, *84*, 83–97.
- Sauveplane, V.; Kandel, S.; Kastner, P.; Ehling, J.; Compagnon, V.; Wrek, R. D.; Pinot, F. *Arabidopsis thaliana* CYP77A4 is the first cytochrome P450 able to catalyze the epoxidation of free fatty acids in plants. *FEBS J.* **2009**, *276*, 719–735.
- Scheffer, M. *Ecology of Shallow Lakes*. Chapman and Hall, New York, **1998**, pp 357.
- Schlegel, T. K.; Schonherr, J.; Schreiber, L. Size selectivity of aqueous pores in stomatous

- uticles of *Vicia faba* leaves. *Planta*. **2005**, *221*, 648–655.
- Schmitt, R.; Kaul, J.; Trenck, T.V.D.; Schaller, E.; Sandermann, H. β -D-glucosyl and O-malonyl- β -D-glucosyl conjugate of pentachlorophenol in soybean and wheat: identification and enzymatic synthesis. *Pestic. Biochem. Physiol.* **1985**, *24*, 77–85.
- Schreiber, L. Polar paths of diffusion across plant cuticles: new evidence for an old hypothesis. *Plant Cell Environ.* **2002**, *25*, 1087–1094.
- Schönherr, J. A mechanistic analysis of penetration of glyphosate salts across astomatous cuticular membrane, *Pest Manag. Sci.* **2002**, *58*, 343–351.
- Schönherr, J. Calcium chloride penetrates plant cuticles via aqueous pores. *Planta*. **2000**, *212*, 112–118.
- Schönherr, J. Characterization of aqueous pores in plant cuticles and permeation of ionic solutes. *J. Exp. Bot.* **2006**, *57*, 2471–2491.
- Schönherr, J. Water permeability of isolated cuticular membranes: the effect of pH and cations on diffusion, hydrodynamic permeability and size of polar pores in the cutin matrix. *Planta* **1976**, *31*, 159–164.
- Sharma, H. A.; Barber, J. T.; Ensley, H. E.; Polito, M. A. A comparison of the toxicity and metabolism of phenol and chlorinated phenols by *Lemna gibba*, with special reference to 2,4,5-trichlorophenol. *Environ Toxicol Chem.* **1997**, *16*, 346–350.
- Shibata, A.; Kodaka R.; Fujisawa T.; Katagi T. Degradation of flumioxazin in illuminated water-sediment systems. *J. Agric. Food Chem.* **2011**, *59*, 11186–11195.
- Shimabukuro, R. H.; Walsh, W. C. Xenobiotic metabolism in plants. ed. by D. G. Paulson, S. D. Frear and P. E. Marks, ACS Symposium Series, American Chemical Society, Washington, DC, Vol. 97, Chap. 1, **1979**, pp. 3–34.
- Siegel, J. B.; Zanghellini, A.; Lovick, H. M.; Kiss, G.; Lambert, A. R.; St.Clair, J. L.; Gallaher, J. L.; Hilvert, D.; Gelb, M. H.; Stoddard, B. L.; Houk, K. N.; Michael, F. E., Baker, D. Computational design of an enzyme catalyst for a stereoselective bimolecular Diels-Alder reaction. *Science*. **2010**, *392*, 309–313.
- Siminzsky, B. Plant cytochrome P450-mediated herbicide metabolism. *Phytochem. Rev.* **2006**, *5*, 445–458.
- Srivastava, D. S.; Kolasa, J.; Bengtsson, J.; Gonzalez, A.; Lawler, P. S.; Miller, E. T.; Munguia, P.; Romanuk, T.; Schneider, C. D.; Trzenski, K. M. Are natural microcosms useful model systems for ecology? *Trends Ecol. Evol.* **2004**, *19*, 379–

- Stevens, P. J. G.; Baker, E. A.; Anderson, N. H. Factors affecting the foliar absorption and redistribution of pesticides. 2. Physicochemical properties of the active ingredient and the role of surfactant. *Pestic. Sci.* **1988**, *24*, 31–53.
- Strandberg, B.; Strandberg, L.; Berqvist, P. A.; Falandysz, J.; Rappe, C. Concentrations and biomagnification of 17 chlordane compounds and other organochlorines in harbour porpoise (*Phocoena phocoena*) and herring from the southern Baltic sea. *Chemosphere.* **1998**, *37*, 2513–23.
- Sugii, A.; Harada, K.; Ogawa, N. Liquid chromatographic characterization of porous vinylpyridine polymer as a weak anion-exchange column packing. *J. Chromatogr. A.* **1986**, *354*, 211–217.
- Taguchi, G.; Ubukata, T.; Nozue, H.; Kobayashi, Y.; Yamamoto, H.; Hayashida, N. Malonylation is a key reaction in the metabolism of xenobiotic. *Plant J.* **2010**, *63*, 1031–1041.
- Talarico, L. Fine structure and X-ray micoranalysis of a red macrophyte cultured under cadmium stress. *Environ. Pollut.* **2002**, *120*, 813–821.
- Theodoridis, G.; Bhar, T. J.; Hotzman, W. F.; Sehgel, S.; Suarez, P. D. New generation of protox-inhibiting herbicides. *Crop Prot.* **2000**, *19*, 533–535.
- Thies, F.; Backhaus, T.; Bossmann, B.; Grimme, L. H. Xenobiotic biotransformation in unicellular green algae. *Plant physiol.* **1996**, *112*, 361–370.
- Tomigahara, Y.; Onogi, M.; Kaneko, H.; Nakatsuka, I.; Yamane, S. Metabolism of 7-fluoro-6-(3,4,5,6-tetrahydrophthalimido)-4-(2-propynyl)-2H-1,4-benzoxazin-3(4H)-one (S-53482, flumioxazin) in the rat: identification of reduced metabolites. *J. Agric. Food Chem.* **1999**, *47*, 2429–2438.
- Torres, M.; Barros, P. M.; Campos, C. G. S.; Pinto, E.; Rajamani, S.; Sayre, T. R.; Colepicolo, P. Biochemical biomarkers in algae and marine pollution: A review. *Ecotox. Environ. Safe.* **2008**, *71*, 1–15.
- Trapp, S. Fruit tree model for uptake of organic compounds from soil and air. *SAR QSAR. Environ. Res.* **2007**, *18*, 367–387.
- Trapp, S. Modelling uptake into roots and subsequent translocation of neutral and ionisable organic compounds. *Pest Manage. Sci.* **2000**, *56*, 767–778.
- Turgut, C. Uptake and modeling of pesticides by roots and shoots of parrot feather

- (*Myriophyllum aquaticum*). *Environ Sci. Pollut. Res. Int.* **2005**, *12*, 342–346.
- Turgut, C.; Fomin, A. Sensitivity of the rooted macrophyte *Myriophyllum aquaticum* (Vell.) verdcourt to seventeen pesticides determined on the basis of EC₅₀. *Bull. Environ. Contam. Toxicol.* **2002**, *69*, 601–608.
- Tyree, T. M.; Peterson, A. C.; Edginton, V. L. A simple theory regarding ambimobility of xenobiotics with special reference to the nematicide, oxamyl. *Plant Physiol.* **1979**, *63*, 367–374.
- USEPA. Ecological Effects Test Guidelines OCSPP 850.4500: Algal Toxicity. **2012**.
- Van Eerd, L. L.; Hoagland, R. E.; Zablotowicz, R. M.; Hall, J. C. Pesticide metabolism in plants and microorganisms. *Weed Sci.* **2003**, *51*, 472–495.
- Van der Waterbeemd, C. H.; Testa, B. The parametrization of lipophilicity and other structural properties in drug design. *Adv. Drug Res.* **1987**, *16*, 85–225.
- Vasella, A.; Davis, J.G.; Bohm, J. Glycosidase mechanisms. *Curr. Opin. Chem. Biol.* **2002**, *6*, 619–629.
- Vaz, A. D. N.; McGinnity, D. F.; Coon, M. J. Epoxidation of olefins by cytochrome P450: evidence from site-specific mutagenesis for hydroperoxo-iron as an electrophilic oxidant. *Proc. Natl. Acad. Sci. USA.* **1998**, *95*, 3555–3560.
- Verdoucq, L.; Morinie`re, J.; Bevan, D.R.; Esen, A.; Vasella, A.; Henrissat, B.; Czjzek, M. Structural determinants of substrate specificity in family 1 β -glucosidases: novel insights from the crystal structure of sorghum dhurrinase-1, a plant β -glucosidase with strict specificity, in complex with its natural substrate. *J. Biol. Chem.* **2004**, *279*, 31796–31803.
- Vicente, A.; Yolanda, P. Determination of pesticides and their degradation products in soil: critical review and comparison of methods. *Trends Anal. Chem.* **2004**, *23*, 772–89.
- Von Gunten, U. Ozonation of drinking water: Part I oxidation kinetics and product formation. *Water Res.* **2003**, *37*, 1443–1467.
- Wang, C. J.; Liu, A. Q. Foliar uptake o pesticides-present status and future challenge. *Pestic. Biochem. Physiol.* **2007**, *87*, 1–8.
- Wang, F., Yi, X., Qu, H., Chen, L., Liu, D., Wang, P. Enantioselective accumulation, metabolism and phytoremediation of lactofen by aquatic macrophyte *Lemna minor*. *Ecotox. Environ. Saf.* **2017**, *143*, 186–192.

- Wang, W.; Li, R.; Zhu, Q.; Tang, X.; Zhao, Q. Transcriptomic and physiological analysis of common duckweed *Lemna minor* responses to NH₄⁺ toxicity. *BMC Plant Biol.* **2016**, *16*, 92.
- Winkler, R.; Sandermann, H. Plant metabolism of chlorinated anilines: isolation and identification of *N*-glucosyl and *N*-malonyl conjugates. *Pestic. Biochem. Physiol.* **1989**, *33*, 239–248.
- Wolf, S. D.; Lassiter R. R.; Wooten, S. E.; predicting chemical accumulation in shoots of aquatic plants. *Environ. Toxicol. Chem.* **1991**, *10*, 665–680.
- Xu, W.; Di, C.; Zhou, S.; Liu, J.; Li, L.; Liu, F.; Yang, X.; Ling, Y.; Su, Z. Rice transcriptome analysis to identify possible herbicide quinclorac detoxification genes. *Front. Genet.* **2015**, *6*, 306–321.
- Yoshitake, A.; Kanamaru, H.; Shono, F.; Nakatsuka I. ¹⁴C-Labeling of optically active fenvalerate, α -cyano-3-phenoxybenzyl (*S*)-2-(4-chlorophenyl)-3-methylbutyrate (1). *J. Labelled Compd. Radiopharm.* **1981**, *18*, 391–402.
- Yoshitake, A.; Kanamaru, H.; Shono, F.; Nakatsuka, I. Labelled organophosphorous pesticides. III. Synthesis of carbon-14 labelled *O*-(2,6-dichloro-4-methylphenyl) *O,O*-dimethyl phosphorothioate. *J. Label. Compds. Radiopharm.* **1979**, *16*, 477–482.
- Zaikov, G.; Rakovsky, S. Ozonation of organic and polymer compounds. *Smithers Rapra*; Shropshire, UK, **2009**, Chapter 3, pp 179–218.
- Zechel, D. L.; Boraston, A. B.; Gloster, T. M.; Boraston, C. M.; Macdonald, J. M.; Tilbrook, D. M. G.; Stick, R. V.; Davies, G. J. Iminosugar glycosidase inhibitors: structural and thermodynamic dissection of the binding of isofagomine and 1-deoxynojirimycin to β -glucosidases. *J. Am. Chem. Soc.* **2011**, *125*, 14313–14323.
- Zhang, D.; Gersberg, R. M.; Ng, W. J.; Tan, S. K. Removal of pharmaceuticals and personal care products in aquatic plant-based system: *A review.* *Environ. Pollut.* **2014**, *184*, 620–639.

8. Acknowledgement

In the end of the thesis, first and foremost, I would like to express my sincere gratitude to my supervisor Professor Kazuhito Itoh, Dean of The Faculty of Life and Environmental Sciences of Shimane University, who offered me the opportunity to peruse the doctoral degree. I am very grateful to his continuous and great support of my Ph.D. thesis, for motivation, enthusiasm, immense knowledge and insightful comments.

I wish to deeply thank Dr. Toshiyuki Katagi, Research Director of Bioscience Research Laboratory of Sumitomo Chemical Ltd., Dr. Yoshitaka Tomigahara, Research Director of Environmental Health Science Laboratory, and Dr. Takuo Fujisawa, Group Manager of Environmental Science Group, for their scientific guide, expertise, discussion and kind encouragement in executing my researches. I would also like to show my sincere appreciation to colleagues in Environmental Fate and Metabolism Team for kind support in preparing the doctoral thesis.

謝辞

本学位論文の終わりに臨み、学位取得の機会ならびに終始ご懇篤なるご指導、ご鞭撻を賜りました島根大学資源科学部長 井藤 和人 教授に深甚なる謝意を表します。

本研究の遂行にあたり、貴重なご助言およびご指導を頂きました住友化学株式会社 バイオサイエンス研究所 片木 敏行 所長殿、生物環境科学研究所所長 富ヶ原 祥隆 殿、同研究所環境科学グループグループマネージャー 藤澤 卓生 殿に心中より深く感謝申し上げます。

本研究の遂行ならびに本論文の執筆に際し、ご協力頂きました住友化学株式会社 生物環境科学研究所 環境科学グループ環境代謝テーマの皆様へ深く感謝致します。

9. Synopsis

Since pesticides directly sprayed or applied at outdoor environment may unintentionally enter into fresh water aquatic ecosystem by spray drift, run-off, drainage or accidental spills, ecotoxicological risk evaluation for aquatic species is essential. Among the aquatic ecosystem, aquatic plants are very important for production/circulation of oxygen and nutrient which securely provide precious food and shelter for many aquatic biota, and thus, the safety for those species has gained much attention. Since herbicides and plant-growth regulators are designed for plants, they may directly cause damages toward non-target aquatic plants and evaluation for these species are necessary. The pesticide registration/evaluation in EU, the acute toxicity test on algae and duckweed had been required as representatives of aquatic plants. However, these suspended and floating species habit in the limited area to cover entire aquatic flora, and especially, the risk for submerged, sediment-rooted macrophytes, which could potentially be exposed to chemicals not only from the water but additionally from the bottom sediment *via* root uptake, was identified as unconfirmed, unmissable matter. Hence, water milfoil was newly included as an additional test species in 2013.

In water milfoil, pesticides concomitantly taken up by shoot and roots may undergo transportation and metabolism in the plant to show complicated behaviors. Each of these behaviors is a basic information to be correlated to the toxicity mechanism and for detailed risk assessment on water milfoil, however, such knowledge is very limited. In this study, the pesticide behaviors in the exposure on terrestrial and water milfoil were experimentally compared. Then, the experimental system which enables to separately conduct shoot and root exposures and to evaluate shoot/root uptake, translocation and metabolism was established. Successively, using the developed system, kinetics of each behavior observed for simple chemicals were determined, and the fate of a herbicide in water milfoil and other aquatic plants was confirmed/compared.

摘要

圃場で使用された農薬は、散布時のドリフト及び降雨による流亡・排水により自然水域へ移入する可能性が想定されるため、水圏生態系への影響評価が必要である。多様な生物から成る水圏生態系の中でも、光合成や栄養素循環により生態系へ貢献する水生植物への安全性が近年益々注目されている。除草剤及び植物成長調節剤は水生植物への直接影響が懸念されるため、農薬登録基準が厳格な欧州では、従来、藻類及び浮遊植物の毒性試験が必須のデータ要求項目であった。しかし、これらの対象生物は多様な水生植物の中では限定的であり、特に底質へ移行した農薬により沈水有根植物が根経由で暴露されるリスクを評価するため、2013年にフサモが対象種に加わった。フサモは水層から茎葉経由及び底質層から根経由の異なる経路で農薬に同時暴露され、各部位からの取込み後の植物内移行/代謝により複雑な動態を示すと推測される。各挙動は毒性メカニズムの理解及び精緻なリスク評価（各暴露経路の寄与、毒性代謝物などの把握）の基盤となるが、知見は殆ど無い。本研究ではフサモ影響評価の一助として、陸生植物との農薬挙動を比較した後、茎葉及び根からの取込み/移行/代謝を個別に評価可能な試験系を構築し、単純化合物における挙動のキネティクス、除草剤の代謝挙動における水生植物種間差を明らかとした。

10. The List of Published Articles as Base of The Doctoral Thesis

Chapter 2:

Ando, D.; Fukushima, M.; Fujisawa T.; Katagi T. Metabolism of the insecticide metofluthrin in cabbage (*Brassica oleracea*). *J. Agric. Food Chem.* **2012**, *60*, 2607–2616.

Ando, D.; Fujisawa, T.; Katagi, T. Metabolism of the strobilurin fungicide mandestrobin in wheat. *J. Agric. Food Chem.* **2018**, *66*, 10154–10162.

Chapter 3:

Ando, D.; Fujisawa T.; Katagi T. Uptake, translocation and metabolism of 3-phenoxybenzoic acid in the submerged rooted water milfoil (*Myriophyllum elatinoides*). *J. Pestic. Sci.* **2012**, *37*, 342–346.

Chapter 4:

Ando, D.; Fujisawa T.; Katagi T. Uptake, translocation and metabolism of phenols by submerged rooted macrophyte, water milfoil (*Myriophyllum elatinoides*). *J. Agric. Food Chem.* **2015**, *63*, 5189–5195.

Chapter 5:

Ando, D.; Fujisawa T.; Katagi T. Fate of flumioxazin in aquatic plants: two algae (*Pseudokirchneriella subcapitata*, *Synechococcus sp.*), duckweed (*Lemna sp.*), and water milfoil (*Myriophyllum elatinoides*). *J. Agric. Food Chem.* **2017**, *65*, 8813–8822.